Colloidal suspensions responsive to external field variations

Inaugural-Dissertation

zur Erlangung des Doktorgrades
der Mathematisch-Naturwissenschaftlichen Fakultät
der Heinrich-Heine-Universität Düsseldorf

vorgelegt von

Sonja Tarama, geb. Babel
aus Willich

Düsseldorf, September 2019

Institut für Theoretische Physik II: Weiche Materie
der Heinrich-Heine-Universität Düsseldorf

Gedruckt mit der Genehmigung der
Mathematisch-Naturwissenschaftlichen Fakultät der
Heinrich-Heine-Universität Düsseldorf

Referent: Prof. Dr. Hartmut Löwen

Koreferent: Prof. Dr. Stefan U. Egelhaaf

Tag der mündlichen Prüfung: 14.10.2019

Abstract

Colloidal suspensions are comprised of small solid particles suspended in a liquid. The particles are mesoscopic in size, such that they are typically much larger than the surrounding solvent molecules, yet still small compared to a macroscopic length scale. Colloidal suspensions are widely studied since the dynamics of the dispersed colloids can be seen as an upscaled and thus visible analogue of atoms. Additionally, interaction energies are of the order of the thermal energy which renders these suspensions highly sensitive to external fields and makes it easy to drive them out of equilibrium. Thus, they present ideal model systems to methodologically study both equilibrium and non-equilibrium systems. From a more applied viewpoint, it is important to understand the dynamics of colloidal suspensions as they comprise materials that we encounter on a daily basis, e.g., food items such as milk, colorants such as ink or paint and body liquids such as blood. Understanding of such materials is essential to facilitate their production or handling by evading unwanted structural and dynamical properties. Reversely, deeper insight into their characteristics and the underlying physics opens up the path to engineering products with desired properties. In particular, in recent years the field of smart materials has seen growing attention. These systems may adapt their behavior depending on a self-created or external stimulus. They thus enable a broad range of usages and give rise to fascinating behavior such as self-healing or shape-memory.

This thesis aims to contribute to this topic by exploring the characteristics of colloidal suspensions under the influence of two different kinds of external fields which are introduced in the two parts of this thesis. The first part of the thesis considers the case of a charged colloidal suspension under strong confinement and driving. The system is studied via the use of dynamic density functional theory (DDFT) for which existing models were extended to include particle size effects. For a capacitor configuration, a previously unreported optimal alternating voltage frequency was found at which the impedance becomes minimal. This phenomenon appears for systems whose width is comparable to the size of the charged colloidal particles and is independent of the newly-introduced steric interactions. The observed effect could be of relevance in the development of micro-scale capacitive devices since appropriate modification of the system width allows to prescribe a resonance frequency onto the system.

The second part, which is the main focus of this thesis, studies a colloidal suspension under the influence of an external feedback potential as a new form of non-equilibrium system. Here, the external potential takes a system(-history)-dependent form. The

suspension is subject to forces that depend on its current or previous state, rendering the system self-adaptive. In particular, we consider the case in which the system dynamics depends on the particle positions at a delay time prior to the actual time. The effect on the colloidal particles was investigated using analytical calculations, including the derivation of a DDFT equation, and particle-resolved simulations. Generally, two cases can be differentiated when studying the feedback potential: attractive or repulsive coupling to the previous particle positions. The particles are then either drawn back to or pushed away from their past positions. For a single particle, this leads, in the case of an attractive potential, to oscillatory motion with a reduced long-time diffusion coefficient. Contrarily, in the case of repulsive potentials, self-propulsion-like behavior with an increased long-time diffusion is observed. For many particles, the particle propulsion in the repulsive case is further accompanied by a self-ordering into moving bands, provided that the feedback strength is sufficiently high.

The fact that the relatively simple form of the feedback potential considered here already leads to new patterns, indicates the rich dynamics hidden in this new type of non-equilibrium systems. The systems are experimentally accessible. In general, any form of feedback-potential can be externally constructed, e.g., via a laser intensity field, such that there is an unrestricted number of systems to be explored. The experiments can be conducted by continuously repeating three steps: First, the relevant quantities of the system are measured. Second, the desired forces are constructed corresponding to this potential. Last, the externally-programmed potential is introduced onto the system. In this case, by simply changing the externally prescribed feedback rule, that is how the (previous) system state enters the forces, a new system can be created. The experimental realization of this feedback-driven colloidal system is currently in progress as part of an ongoing collaboration with our experimental Soft Matter department. The particular form of the potential considered here may be relevant in biological systems that show autochemotactic behavior.

Kurzfassung

Kolloidale Suspensionen bestehen aus kleinen harten Teilchen, die in einem flüssigen Medium suspendiert sind. Die Teilchen haben eine mesoskopische Größe, typischerweise um einiges größer als die Lösungsmoleküle, andererseits klein gegenüber einer makroskopischen Längenskala. Kolloidale Suspensionen werden oft als ein hoch-skaliertes und somit sichtbares Analogon zu Atomen untersucht. Zudem sind die Wechselwirkungsenergien in diesen Systemen vergleichbar mit der thermischen Energie, sodass die Suspensionen leicht durch externe Felder beeinflussbar und somit ins Nichtgleichgewicht zu bringen sind. Sie stellen daher ideale Modellsysteme zur methodologischen Untersuchung sohwohl von Gleichgewichts- als auch Nichtgleichgewichtssystemen dar.

Von einem mehr anwendungsorientierten Blickpunkt her ist es wichtig, die Dynamik kolloidaler Suspensionen zu verstehen, da diese Materialien einschließen, die uns in unserem täglichen Leben begegnen, z.B. Lebensmittel wie Milch, Verbrauchsgegenstände wie Tinte oder Farbe und Körperflüssigkeiten wie Blut. Verständnis dieser Materialien ist notwendig, um ihre Produktion und Handhabung zu erleichtern sowie ungewollten strukturellen und dynamischen Eigenschaften entgegenzuwirken. Andersherum erlaubt tiefere Einsicht in die Eigenschaften und die ihnen unterliegende Physik, Produkte mit vorgegebenen gewünschten Eigenschaften zu designen. Im Besonderen erhält das Forschungsfeld der intelligenten Materialien zunehmende Aufmerksamkeit. Diese Systeme können ihre Eigenschaften an äußere Gegebenheiten anpassen. Sie können daher in einer breiten Reihe von Verwendungen genutzt werden und zeigen spannende Effekte wie Selbstheilung und Formgedächtnis.

Diese Arbeit stellt einen Beitrag zu diesem Thema dar, indem sie die Eigenschaften kolloidaler Suspensionen unter dem Einfluss zweier verschiedener externer Felder untersucht, die in den beiden Teilen dieser Arbeit vorgestellt werden. Der erste Teil der Arbeit betrachtet den Fall einer Suspension von geladenen kolloidalen Teilchen unter enger räumlicher Einschränkung und starker treibender Kraft. Das System wird mittels dynamischer Dichtefunktionaltheorie (DDFT) untersucht. Hierfür haben wir bisherige Modelle um einen weiteren Term zur Beschreibung der sterischen Teilchen-Abstoßung erweitert. Für eine Kondensator-Anordnung wurde eine bisher nicht berichtete optimale Frequenz der treibenden Wechselspannung gefunden, für die die gemessene Impedanz minimal wird. Dieses Phänomen tritt in Systemen auf, deren Breite vergleichbar zur Größe der Kolloid-Teilchen ist und ist unabhängig von der neu-eingeführten sterischen Wechselwirkung. Der beobachtete Effekt könnte für die Entwicklung von kapazitiven Geräten auf der Mikroskala relevant werden, da eine Änderung der Systemweite ein Aufprägen einer gewünschten Resonanzfrequenz ermöglicht.

Der zweite Teil, auf dem der Hauptfokus dieser Arbeit liegt, beschäftigt sich mit einer kolloidalen Suspension unter dem Einfluss eines externen Feedback-Potentials als einer neuen Form eines Nichtgleichgewicht-Systems. Das externe Potential ist in diesem Fall abhängig von dem aktuellen oder vorherigen System-Zustand, wodurch das System selbst-adaptiv wird. Konkret betrachten wir den Fall, dass die System-Dynamik von den Teilchen-Positionen zu einer vorherigen Zeit abhängt. Der Effekt auf die kolloidalen Teilchen wurde durch analytische Rechnungen, einschließlich der Herleitung einer DDFT Gleichung, und Teilchen-basierten Computer-Simulationen untersucht. Im Allgemeinen lassen sich bei der Betrachtung zwei Fälle unterscheiden: Attraktiver oder repulsiver Einfluss der vorherigen Teilchenpositionen. Die Teilchen werden entweder von den vorherigen Positionen weggetrieben oder dorthin zurück gezogen. Für ein einzelnes Teilchen ergibt sich daraus im Fall eines attraktiven Potentials eine oszillierende Bewegung mit einer reduzierten Langzeit-Diffusionskonstante. Im Fall eines repulsiven Potentials wurde entsprechend eine Art Selbstantrieb mit einer erhöhten Langzeit-Diffusion beobachtet. Der Teilchenantrieb im repulsiven Fall wird darüber hinaus für mehrere Teilchen von einer Selbstorganisation in laufende Bänder begleitet, sofern die Stärke des Feedbacks ausreicht.

Die Tatsache, dass bereits die hier untersuchte einfache Form eines Feedback-Potentials zu neuer Strukturbildung führt, lässt erahnen, welche reiche Dynamik in diesem neuen Typ von Nichtgleichgewichtssystem versteckt liegt. Diese Systeme sind zudem experimentell realisierbar. Generell lässt sich jede Form von Feedback-Potential z.B. über ein Laser-Intensitätsfeld extern erzeugen, sodass eine unbegrenzte Anzahl neuer Systeme erforscht werden kann. Die Experimente können durch kontinuierliche Wiederholung dreier Schritte durchgeführt werden: Zuerst werden die relevanten Größen eines Systems durch Messung bestimmt. Zweitens wird das entsprechende Potential erzeugt. Als Letztes wird das extern erstellte Potential an das System angelegt. In diesem Fall kann durch einfache Änderung des Feedback-Algorithmus, also der Vorgabe, wie der (vorherige) System-Zustand in das Potential eingeht, ein neues System konstruiert werden. Die experimentelle Umsetzung eines Feedback-getriebenen kolloidalen Systems ist Objekt eines fortlaufenden Forschungsprojekts, das wir in Kooperation mit unserem Experimental-Institut für Weiche Materie betreiben. Die spezielle Form des Potentials, die in dieser Arbeit betrachtet wird, könnte zudem für biologische autochemotaktische Systeme relevant sein.

Eidesstattliche Versicherung

Ich versichere an Eides Statt, dass die Dissertation von mir selbständig und ohne unzulässige fremde Hilfe unter Beachtung der „Grundsätze zur Sicherung guter wissenschaftlicher Praxis an der Heinrich-Heine-Universität Düsseldorf“ erstellt worden ist.

Düsseldorf, 16. Oktober Sonja Tarama

Preface

The content of this dissertation is based to a large degree on the following two publications in international peer-reviewed scientific journals to which I contributed during my work at the *Insitute for Theoretical Physics II: Soft Matter* at *Heinrich-Heine-University Düsseldorf* between September 2015 and October 2019.

I. S. Babel, M. H. Eikerling, H. Löwen. *Impedance Resonance in Narrow Confinement.* J. Phys. Chem. C **122**, 21724 (2018)

II. S. Tarama, S. U. Egelhaaf, H. Löwen. *Traveling band formation in feedback-driven colloids.* Phys. Rev. E **100**, 022609 (2019)

An additional Section has been added to the start of Chapter 3 presenting the single-particle equivalent of Publication II which focuses on collective effects in the system.

Danksagung

Zunächst möchte ich mich bei Herrn Prof. Dr. Hartmut Löwen für die Möglichkeit bedanken, an seinem Lehrstuhl zu promovieren. Ebenso bin ich ihm für das spannende Thema und die Betreuung der Arbeit zu Dank verpflichtet. Weiterhin danke ich Herrn Prof. Dr. Stefan U. Egelhaaf für seine Co-Betreuung der Arbeit und die vielen hilfreichen Diskussionen auch hinsichtlich der experimentellen Realisierung des betrachteten Systems. Leider konnten aufgrund von aufgetretenen Schwierigkeiten im Experimentalaufbau diese Experimente nun nicht Teil dieser Arbeit werden. Ich möchte mich an dieser Stelle bei Herrn Dr. Debasish Saha für die bisherige Zusammenarbeit bezüglich einer experimentellen Umsetzung bedanken und hoffe, dass wir diese in naher Zukunft produktiv zu Ende führen werden.

Weiterhin danke ich den Mitarbeitern am Institut für Theoretische Physik II für die produktive Arbeitsatmosphäre und die vielen fachlichen Gespräche und guten Ratschläge. Besonderer Dank gilt zudem Frau Claudia Stader und Herrn Joachim Wenk für die administrative Unterstützung sowie Christian Hoell, Soudeh Jahanshahi und Patrick Laermann für das Korrekturlesen dieser Arbeit.

Zuletzt danke ich meinen Eltern für die emotionale Unterstützung sowie ebenfalls für das Korrekturlesen der Arbeit. Besonderer Dank gilt darüber hinaus meinem Ehemann Mitsusuke, der mich durch fachlichen Rat sowie Korrekturlesen der Arbeit unterstützt hat.

Contents

Chapter 1

Introduction

Colloidal suspensions are part of the field of soft condensed matter [1–5]. The latter is concerned with the physical properties of systems that show structuring on a mesoscopic length scale. Examples of soft matter systems include polymers [6–8], colloidal suspensions [9–12], gels [13–17] and glasses [18–21] as well as biological systems such as single cells and cell tissues [22–25]. The field of *active* soft matter is concerned with intrinsically propelled particles [26–32], e.g., bacteria [33] or sperm [34, 35]. The considered materials share the attribute of being *soft*, i.e., they can be influenced by external fields and compound objects are easy to deform [36, 37].

The sensitivity to external fields may be exploited to tune the system behavior without the need to directly interfere with its internal components. For example, the viscosity of electrorheological [38–41] or magnetorheological fluids [42–44] can be adapted by application of an electric or magnetic external field. In this case, the application of the field causes the suspended charged or magnetic particles to form elongated chains that resist shearing. Thereby the viscosity of the fluids can be tuned over several orders of magnitude [45]. These fluids have found applications in damping systems [46].

Another example is that of ferrogels [47, 48] which can be deformed through an external magnetic field and may even display super-elasticity [49]. Here, magnetic particles embedded in a polymer matrix can be manipulated with an external magnetic field regulating the elastic material response. Ferrogels are used in dampers [50], vibration absorbers [51], or actuators [52, 53].

These systems share the possibility to non-invasively tailor the system behavior after production through the introduction of an external field. This field can also be dynamically changed and the system behavior can thus be matched to the specific needs of the application or the current situation. Such materials are therefore called *smart* [54, 55]. In general, for a material to qualify as smart, it needs at least one property that can be significantly modified in a controlled manner through an external stimulus such as temperature [56, 57], moisture [58, 59], pH [56, 60] and electric [40, 41] or magnetic fields [45, 48]. In particular, this includes pyroelectric [61], magneto- or electro-strictive [62, 63], magneto- or electro-rheologic [41, 44] and piezoelectric [63] materials. Similarly, although less easily accessible, tuning of the system length allows

to prescribe a resonance frequency for the system discussed in Chapter 2 (Publication I). This effect may be exploited in the design of a smart system. Smart systems are typically used as sensors and actuators but applications range broadly including food packaging [64, 65] and drug delivery systems [15, 56, 66].

A stricter definition of smart materials requires the material to not only behave as a sensor or actuator but to have the ability to decide on a proper response and react depending on a measured change in the environment. The material thus needs to act as a sensor, a control and an actuator [55]. More advanced effects can be designed in this case. The materials may heal after mechanical damage [67–71] or may return to a previous system state upon external stimulation. For example, shape-memory alloys return to a default configuration upon heating [55, 72, 73]. Necessarily, such an effect requires knowledge of the system history, i.e., the presence of memory in the system.

A particularly interesting case arises when the stimulus the system reacts to is self-generated. In this case there is no need to manually tune an external field, instead the system becomes self-adaptive. This kind of self-adaptivity is for example seen in cells which are able to sense their local density and adapt their gene expression accordingly leading to the stable formation of tissues [74–76], an effect known as quorum sensing [77–79]. Similarly, it is known that direct contact between cells leads to *contact inhibition of locomotion* (CIL) [80–84] and *contact inhibition of proliferation* (CIP) [85–87], i.e., to a reduction in cell movement or proliferation, respectively. Note that the underlying mechanisms for these two effects are not necessarily related [85, 87]. Moreover, cells also show chemotactic behavior with respect to a concentration field of a chemical substance that may be self-secreted [75, 88, 89]. The cells sense the concentration gradient either through comparison of concentrations over the cell surface [90–95] or via temporal comparison of the experienced concentration [96–100] or rely on collective effects to achieve chemotaxis [101, 102]. These biological systems have further inspired the research topic of self-adaptive programming [103] that tries to mimic the observed adaptiveness for computer programming purposes.

Whenever a smart system displays a more complex response to an external stimulus, a time lag necessarily arises. This time delay can be thought of as a sensory lag, e.g., the time that a cell needs to react to a change in chemical concentration [104, 105]. An example of a self-adaptive system with a time-delayed feedback is presented in Chapter 3 (Publication II). In our model, a repulsion from past positions is prescribed as for example given for autochemorepulsive particles [89, 106]. This feedback-mechanism leads to self-organized dynamic structure formation [107, 108]. The system develops a specific traveling direction via symmetry breaking.

In the following, the properties of colloidal suspensions are introduced in more detail and the behavior under different forms of external potential is discussed. Additionally, microswimmers [109, 110] are introduced as a form of internally driven colloidal matter. Afterwards, methods for a mathematical description of these systems are presented.

1.1 Colloidal suspensions

Colloidal suspensions are constituted of mesoscopic particles suspended in a liquid medium. The particles are typically large enough such that quantum effects can be neglected ($\gtrsim$ 1nm), yet small enough ($\lesssim 1\mu$m) to show *Brownian motion* [2,36,111,112], i.e., thermal (random) motion due to collisions with the liquid molecules, an effect named after Robert Brown who was the first to observe it for plant pollen in water [113]. Due to the colloidal size, for typical systems, the *Reynolds number*, describing the strength of inertia relative to viscous forces in the system, is small and inertia is usually negligible.

In a stable colloidal suspension particles do not sediment over an appreciable amount of time. However, the particles will tend to coagulate due to van-der-Waals attraction, also termed *dispersion forces*, arising in case of a difference in the refractive index for light between the suspended particles and the solution. Spontaneous inhomogeneities in the charge distribution of one molecule induces an electric dipole in its neighbors, in sum leading to an attraction between the particles [114]. A strategy to counteract this effect by introducing an additional repulsive interaction must be devised [36]. In general, two strategies exist: The first one is to introduce a charge onto the colloidal particles [115–117]. This *charge stabilization* results in Coulomb repulsion between the colloid particles of like charges, preventing coagulation. The repulsion between the particles is screened by free counterions that exist as free ions in the liquid. The effective interaction between the particles then takes the form of a screened Coulomb potential

$$V_{\mathrm{Yuk}}(r) = \frac{V_0}{r}\mathrm{e}^{-\kappa r}\,, \tag{1.1}$$

which is also referred to as the *Yukawa potential*. The potential describes the screened interaction between two charges with an inverse screening length κ. This length depends on the concentration of free ions in the solution and can thus be altered by adding salt to it. The potential form can be derived from the linear screening theory of Derjaguin and Landau as well as Verwey and Overbeek which is named after its authors, Derjaguin-Landau-Verwey-Overbeek (DLVO) theory [118–122]. The Yukawa potential is assumed in Chapter 3 (Publication II) for the direct interactions between the colloid particles.

The second method of stabilization is by coating the colloidal particles with polymer chains [111, 120, 123]. Despite being referred to as *steric stabilization*, the particle repulsion does not exclusively rely on steric interaction between the polymer hairs but to a large degree originates from entropic effects. Having particles at a close distance to each other leads to a reduced number of states accessible to the attached polymers, thus reducing the entropy and thereby increasing the energy of the system. The energy increase generates a repulsion between the particles [31, 124] of radius R,

which can be described by a hard-core potential

$$V_{\mathrm{HS}}(r) = \begin{cases} 0\,, & \text{for } r > 2R \\ \infty\,, & \text{for } r \leq 2R \end{cases} . \tag{1.2}$$

In this case the potential energy is zero for non-overlapping particles and infinity in the case of overlap. This interaction is assumed in Chapter 2 (Publication I) with an additional unscreened Coulomb term. The additional unscreened Coulomb term arises for charged colloidal particles in a solvent prepared at low counterion concentration. Such a system can be prepared for organic solvents [125,126]. In the system considered, the suspension is in total charge neutral and the charged particles are considered as hard spheres, a description referred to as the *restricted primitive model* [127].

1.2 Driven colloidal suspensions

Due to their sensitivity to external fields, colloidal suspensions can easily be driven out of equilibrium [128–133]. Moreover, on the same length scale, systems of bacteria [26, 27, 33], amoebae [134], sperm [135] and plankton [136, 137] are inherently out of equilibrium due to their self-propulsion. These microswimmers consume energy from their surroundings in order to generate a forward motion [32]. A feedback potential can be employed to produce a similar driving effect for passive colloidal particles. The difference between the two systems is discussed in the following by means of comparing the single-particle dynamics in the two cases. Furthermore, feedback potentials can be created that reproduce complex behavior observed in biological systems, such as quorum sensing [138–140]. The potential in this case becomes state- or history-dependent, rendering the system self-adaptive. Examples of these three types of non-equilibrium systems are discussed in more detail in this Section.

1.2.1 External driving

The most well-studied case of driven colloidal suspensions is the one of simple external potentials, i.e., instantaneous potentials that do not take a state-dependent input parameter. External potentials may include electric [131, 141–143], magnetic [132, 144–146], and optical fields [133, 147, 148] as well as shear forces [130, 149] and confinement [150, 151]. The responsiveness to the external forcing can be exploited as an analogy of non-equilibrium atomic systems but at a higher length and time-scale, thus rendering the involved processes observable [152, 153]. Already for a single colloidal particle an external field acting on the particle will lead to modified observed dynamics. The effect can be characterized by the mean square displacement (MSD) $\langle (x(t'+t) - x(t'))^2 \rangle_{t'}$, i.e., the squared (in this case one-dimensional) distance that a colloid particle travels on average within a time t. Here, $\langle \cdots \rangle_{t'}$ indicates an average

over the reference time t' for a dependent quantity $B(t')$ in the form

$$\langle B \rangle_{t'} = \frac{1}{T} \int_{t_{\mathrm{eq}}}^{t_{\mathrm{eq}}+T} B(t') \mathrm{d}t' \,, \tag{1.3}$$

where t_{eq} is an equilibration time at which effects due to the initial turning-on of the potential have subsided. Considering a constant external force $\mathrm{F}_{\mathrm{ext}}$ on the particle, the MSD is given by

$$\langle (x(t'+t) - x(t'))^2 \rangle_{t'} = 2Dt + \left(\frac{\mathrm{F}_{\mathrm{ext}}}{\gamma} \right)^2 t^2 \,, \tag{1.4}$$

where the first term, $2Dt$, is the squared distance that the particle travels by diffusion. The diffusion constant D relates to the thermal energy $k_B T$ of the system via the *fluctuation-dissipation theorem* $D = k_B T/\gamma$, where γ denotes the friction coefficient. A constant deterministic force $\mathrm{F}_{\mathrm{ext}}$ changes the observed time proportionality from $\propto t$ to $\propto t^2$ behavior for times $t \gtrsim 2D\gamma^2/{\mathrm{F}_{\mathrm{ext}}}^2$ leading to an increase in the MSD, see also Fig. 1.1.

For many particles, external fields may lead to self-assembly [154–157] or pattern formation [158–160] in colloidal systems. For example, introducing a DC electric field onto a binary suspension of oppositely-charged colloidal particles can lead to the formation of lanes [131, 158, 161–163] in the direction of the field. For oscillating (AC) electric fields, axial segregation into sheets perpendicular to the driving direction and tilted bands are observed [159] while rotating electric fields may cause crystallization [160]. The case of an AC voltage is considered in Chapter 2 (Publication I) under the additional constraint of high confinement in the direction of the electric field, constituting a colloidal capacitor analogue. Similarly to electric fields, magnetic fields can be used to drive magnetic [164] or magnetizable [146] colloidal particles out of equilibrium. The applied field may lead to chain formation [132, 165] and for oscillating fields to flocking and global rotation [164]. Shear forces may induce freezing or melting [130, 149] while confinement may lead to a modified crystal structure [150, 151].

Electric and magnetic fields have the disadvantage that the fields are in general applied to the system as a whole, apart from some simple field inhomogeneities that can be realized [166]. Contrarily, a light field can easily be varied spatially. Gradient forces can be used to trap a single particle in the intensity maximum of a highly-focused laser beam, a technique known as *optical tweezers* [167–169]. The optical tweezers setup can be extended by a computer-controlled diffractive optical element (DOE) to produce *holographic optical tweezers*. By providing a holographic mask of the desired potential as an input, the corresponding light intensity landscape can be realized [169] such that space-dependent potentials can be produced in a controlled way. Even the most simple case, a random potential energy landscape [170–173], which is a constant intensity with a random perturbation, results in interesting effects

in the particle dynamics, showing subdiffusive behavior on intermediate time-scales due to localization in local potential minima.

By appropriate programming of the hologram, the dynamics of colloidal particles in structured environments such as periodic potentials [133, 174, 175] can be investigated. Further, the light field does not need to be kept the same over time. By introducing a computer control that dynamically changes the input hologram according to a prescribed algorithm, time-varying potentials can be realized [176, 177]. The computer control may take additional parameters, which may even depend on the system state, as inputs to create the hologram, thus imposing a feedback onto the system [140]. Employing such a feedback loop allows to create feedback potentials like the one considered in Chapter 3 (Publication II).

1.2.2 Internal driving: microswimmers

Microswimmers can be understood as colloids with an additional internal driving mechanism [29, 31, 110]. In the low Reynolds number regime of negligible inertia, swimming, i.e., self-propulsion, can be hard because symmetric time-reversible motion cannot cause any net motion [178, 179]. Typical microswimmers such as bacteria and plankton evade this problem by using rotation or other types of non-reciprocal beating motion of their flagella or cilia to self-propel [26, 27, 33, 135, 180–182].

Artificial analogues to biological microswimmers have been produced [183–187] that take up energy from external fields to produce forward motion in a particle-fixed propulsion direction [188–190]. These artificial microswimmers exploit effects such as self-thermophoresis [191, 192] or self-diffusiophoresis [193, 194] upon illumination or use external acoustic [187] or magnetic [183] fields to generate a forward motion. Further, droplets [185, 195, 196] can propel based on a self-sustained Marangoni flow. While this dynamics is usually referred to as self-propulsion, in a stricter sense these systems are not truly *self*-propelled as an external field is necessary to drive the process. The propelling colloid particles may thus be more carefully referred to as *active Brownian particles* (ABPs) and there exists some ambiguity between externally-driven and internally self-propelled objects.

Nevertheless, independent of the precise origin of the self-propulsion, the motion is often simplistically described as an *effective* self-propulsion force [28, 197, 198] despite the fact that, due to the intrinsic nature of the propulsion, the actual system has to be force- and torque-free. More precise descriptions consider the self-propulsion force as a pair of two oppositely orientated forces on the swimmer body that are slightly displaced with respect to each other [199–203]. The swimmer experiences a propulsion due to the displaced forces. In contrast to a propulsion force however, this self-propulsion leads to a different hydrodynamic flow-field which is given by a *force dipole* at far distances [202–206]. Nevertheless, for our purposes, the description via an effective force is sufficient and hydrodynamic interactions are neglected. The propulsion force is further often assumed to be of constant magnitude [28, 33]. For a

single particle moving in two dimensions the self-propulsion is then described with a constant effective force $\mathrm{F_s}\hat{\mathbf{u}}$, where $\hat{\mathbf{u}} = (\cos(\phi), \sin(\phi))^T$ denotes the self-propulsion orientation which is fixed to the particle. The orientation is fully determined by the angle ϕ to a fixed reference axis. This angle undergoes rotational Brownian motion characterized by the rotational diffusion constant D_r. The effective self-propulsion force modifies the mean square displacement compared to the freely-diffusing case, cf. Fig. 1.1. Averaging over the initial propulsion orientation, the one-dimensional MSD is given by [198]

$$\begin{aligned}\langle (x(t'+t) - x(t'))^2 \rangle_{t'} &= 2Dt + \left(\frac{\mathrm{F_s}}{\gamma D_\mathrm{r}}\right)^2 \left[D_\mathrm{r} t - \left(1 - \mathrm{e}^{-D_\mathrm{r} t}\right)\right] \\ &= 2Dt + \left(\frac{\mathrm{F_s}}{\gamma}\right)^2 t^2 + \mathcal{O}(t^3)\,. \end{aligned} \tag{1.5}$$

The correction term in the MSD is proportional to the square of the force such that the self-propulsion always leads to an increase in the square displacement. At small times a microswimmer shows diffusive behavior due to thermal motion, the same as for passive particles. This is followed by a transient propelled regime (for $t \gtrsim 2D\gamma^2/\mathrm{F_s^2}$) due to the self-propulsion force. In the MSD, this is similar to the case of external pulling. However, in the case of self-propulsion the long time ($t > 1/D_r$) behavior is again diffusive because rotational diffusion changes the direction of the propulsion force and an initial orientation is lost on the time scale $1/D_r$. The diffusion coefficient at long times is always larger compared to the first diffusive regime, $D_\mathrm{L} > D$, due to the additional distance traveled via self-propulsion. The long-time diffusion coefficient is then defined by

$$\frac{D_\mathrm{L}}{D} = \lim_{t\to\infty} \frac{1}{2t} \langle (x(t'+t) - x(t'))^2 \rangle_{t'} = 1 + \frac{1}{2} \frac{\mathrm{F_s^2}}{\gamma^2 D_\mathrm{r} D} = 1 + \frac{1}{2}\,\mathrm{Pe}^2 \tag{1.6}$$

and can be written in terms of the unitless *Péclet number* $\mathrm{Pe} = \frac{\mathrm{F_s}}{\gamma\sqrt{D_\mathrm{r} D}}$ which quantifies the strength of the internal propulsion [32]. The prefactor of this quantity may vary depending on its exact definition but generally the number gives the ratio of the strength of the active particle movement due to self-propulsion and diffusion. It may take values as low as 10^{-2} [207] or as high as 10^6 [208] with typical values in the range 100 to 1000 [209, 210].

For many particles, self-propulsion may cause pattern formation in systems of microswimmers [211–216]. Motility-induced phase separation (MIPS) [29, 31, 109, 216, 217] is observed even in the absence of any attractive interaction between the particles. The underlying process is solely based on collisions between swimmers and the involved reorientation time. Two swimmers that have collided take approximately a time $1/D_\mathrm{r}$ to reorient their propulsion directions away from each other. If within this time span additional particles collide with the swimmer pair, particle clusters will

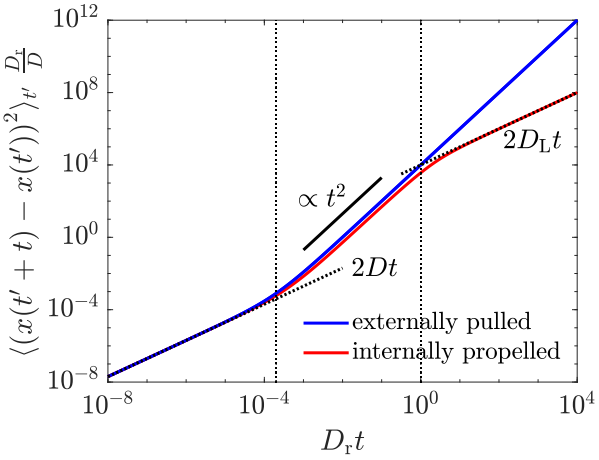

Figure 1.1: MSD for a colloidal particle pulled by an external force $\mathrm{F}_{\mathrm{ext}}$ or propelled via an effective internal driving force F_{s} with $\mathrm{F}_{\mathrm{ext}} = \mathrm{F}_{\mathrm{s}} = \mathrm{F}$. The strength of the propulsion is given by the Péclet number $\mathrm{Pe} = \mathrm{F}/\gamma\sqrt{D_{\mathrm{r}}D} = 100$. The vertical lines indicate the time $t = 2D\gamma^2/\mathrm{F}^2$ at which the effect of the respective force starts to dominate, resulting in a $\propto t^2$-regime, as well as the cross-over time $t = 1/D_{\mathrm{r}}$ at which diffusive behavior is recovered for a microswimmer.

grow. This is the case for sufficiently high particle density and propulsion velocity. Furthermore, "living crystals" [189] and swarming phases [218] have been observed. Additionally, external fields may be used to steer microswimmers, such as temperature gradients [219], gravitation [220], magnetic [221], light fields [222] and chemical gradient fields [223, 224]. In particular, responsiveness to chemical gradients is not limited to externally-created fields but may also be exploited by microorganisms through self-created chemical fields [89, 106]. This *autochemotaxis* was investigated for artificial swimmers, showing clustering [225, 226] as well as complex static and dynamic patterns such as stationary density patterns and traveling waves [216, 227]. A more elaborate response to self-created chemical fields may result in quorum sensing behavior [228, 229] and can even cause memory effects in the system [29, 195, 196] constituting different forms of feedback.

1.2.3 Feedback driving

Feedback may arise naturally in systems that show autochemotactic behavior such as observed for a range of artificial [195, 196, 216, 228] and biological [75, 88, 89, 106, 230] microswimmers. The effect of feedback in biological systems [77, 140, 231] is of particular interest: Bacterial quorum sensing may pose a target point for the therapy of infections [232–234] and failure of inter-cell communication such as contact inhibition

of locomotion is involved in the invasion of cancerous cells into healthy tissue [82, 235].

Feedback potentials can also be produced artificially as external potentials that include a system-state dependent parameter [140, 231]. This can for example be realized through programming of an external trap. The simplest form of feedback is realized by turning-on or off of a potential dependent on the system state [236, 237]. A slightly more elaborate feedback mechanism is the anti-Brownian electrophoretic trap (ABEL trap) [238, 239] which was used to trap a charged particle via an electric field. Here, the strength of the field is adapted depending on the position of the particle, moving it back to a target position. However, such a setup only works for charged particles and also cannot easily be extended to simultaneous trapping of multiple particles.

Another example of an artificial feedback system are gold colloid particles in a polymer solution [240]. The particles can be selectively heated through laser irradiation, leading to a local reduction in viscosity that follows the particle positions with a certain delay.

Furthermore, feedback experiments have also been conducted on a larger length scale with robots that were equipped with both lamps to produce a light intensity field around themselves and sensors to measure the incident light in their surrounding caused by other robots. In this case, an algorithm to produce a desired response to the measurement result can be prescribed [241, 242]. A microscopic analogue of this system can be created through the use of holographic optical tweezers [133, 140, 169, 243–247]. These can be used to generate a feedback potential in the form of a light field which can easily be varied spatially [238, 239, 248] and is not limited to specific potential forms. The feedback may be used for the guided transport of active or passive particles [236, 249–251], stabilization of otherwise unstable dynamic states [252] or structures [243, 253] and trapping of particles [238, 239]. It can also cause pattern formation [140, 231, 254, 255]. Moreover, artificial feedback potentials can be used to mimic quorum sensing in biologic microswimmers [140].

For feedback systems the equation of motion can, in general, not be reduced to an instantaneous form. The particle dynamics at any time depends on the history of the particle positions as this determines the potential seen by the particles. Solving the equation of motion in the case of feedback analytically is difficult, even for a single particle and a simple dependence on a single previous position with a constant time-shift to the actual time. This *delay time* τ between the signal and the reaction of the system is an important feature of feedback systems and may lead to qualitative changes in the behavior of a suspension of microswimmers [241, 256]. A time delay also arises in biological systems in the sensing of chemical gradients [105, 257] and may be prescribed when externally creating a feedback [242].

Unlike an external driving or the internally-driven microswimmers, the lowest-order correction to the MSD of a single particle is linear in the feedback force, see also Chapter 3. As an important consequence, feedback potentials can be used for efficient trapping of particles [239, 251]. They may also result in dynamic structure formation

for many particles, see Chapter 3 (Publication II).

1.3 Mathematical description

In this Section, I introduce the mathematical background needed to understand the work presented in the following Chapters. In particular, for my purposes these are a particle-based and a density-based description of the colloidal suspension [112, 258]. For both of these descriptions, the difference in size between the solvent molecules and the colloid particles allows to treat the solution as a continuous background. The problem is then reduced to solving the dynamics of the suspended colloid particles. The first description tracks the positions of the individual particles via a force-balance equation, the Langevin equation. The result is a *stochastic differential equation* (SDE) for the temporal evolution of the particle positions. In the case of a feedback potential with a history-dependence, the system is rendered *non-Markovian* and the governing equation of motion becomes a stochastic *delay* differential equation (SDDE) [259–262].

The second description considers the probability density of finding the particles at specified positions. The resulting Fokker-Planck equation is called the Smoluchowski equation and constitutes a drift-diffusion equation for the probability density. For the case of feedback, it has been shown that the non-Markovian system can be treated as a Markovian system with an expanded phase space [263] and a corresponding Fokker-Planck equation for the particle's probability density can be formulated. However, a general solution to this SDDE has not yet been found [259]. The obstacle in finding a solution is that the system dynamics at time t depends on the past state at time $t-\tau$ which in turn depends on the system state at $t-2\tau$ and so on. Finding a solution for the probability density thus involves a hierarchy of dependent equations. Nevertheless, the Fokker-Planck equation has been the starting point for some approximative solutions. Solutions have been derived for the steady-state probability density of the particles in the case of small delay times [264] and for a linear approximation of the feedback forces in the case of an additional static sinusoidal or double-well potential [261]. Further, a perturbation strategy has been employed to systems in which the influence of an additional feedback potential on the stationary problem is small [265].

Furthermore, from the Smoluchowski equation, an evolution equation for the one-particle density can be derived which can be rewritten in terms of the density-field dependent free energy of the system. The resulting description is referred to as dynamic density functional theory (DDFT) [266–269].

The first approach via a Langevin equation may be more intuitive as it describes a single set of particle trajectories. However, the resulting equations become difficult to solve in the case of interacting particles due to the nonlinearity of the interaction potential. Contrarily, DDFT can easily be extended to account for interactions between the particles, including hard core repulsions which are difficult to realize in a Langevin picture. Additionally, DDFT can readily be extended to include hydrodynamic fields

for both colloidal particles [270] and microswimmers [202]. Particle mixtures [271, 272] and arbitrarily shaped particles can also be described [273, 274]. DDFT can further be employed to describe large systems and thus rule out finite size effects.

1.3.1 Langevin equation

The Langevin equation is a stochastic differential equation describing the movement of the colloidal particles. The time scale of this movement, the *Brownian timescale* is large compared to the molecular timescale on which the molecules of the suspension move. The surrounding liquid is therefore considered as an equilibrated continuous background. Further, for the *overdamped* dynamics considered here, inertia can be neglected. The equation of motion for the position of the ith particle, $\mathbf{r}_i$, is then simply given by the force-balance equation

$$\gamma \frac{\mathrm{d}\mathbf{r}_i}{\mathrm{d}t} = \sum_{\substack{j=1 \\ j\neq i}}^{N} \mathbf{F}_{\mathrm{int}}\left(\mathbf{r}_i - \mathbf{r}_j\right) + \mathbf{F}_{\mathrm{ext}}\left(\mathbf{r}_i, t\right) + \mathbf{f}_i(t)\,, \tag{1.7}$$

which equates the friction force $\gamma \frac{\mathrm{d}\mathbf{r}_i}{\mathrm{d}t}$ (on the left) with the remaining forces acting on particle i in a suspension of in total N colloidal particles. Here, the systematic force $\mathbf{F}_{\mathrm{int}}\left(\mathbf{r}_i - \mathbf{r}_j\right)$ describes the direct pair interaction between particles i and j. This force depends only on the relative distance of the particles. The next term, $\mathbf{F}_{\mathrm{ext}}\left(\mathbf{r}_i, t\right)$, gives the force on particle i due to a (time-dependent) external potential. Furthermore, the effect of diffusion is included via a stochastic force $\mathbf{f}_i(t)$. This force is a Gaussian random variable and is characterized by its first two moments, $\langle \mathbf{f}_i(t) \rangle = 0$ and $\langle \mathbf{f}_i(t) \otimes \mathbf{f}_j(t') \rangle = 2D\gamma^2 \mathbb{1} \delta\left(t - t'\right) \delta_{ij}$. Here, $\delta\left(t\right)$ is the Dirac delta function and δ_{ij} denotes the Kronecker delta. The random forces only depend on time but not on the particle position. They are uncorrelated for different particles and distinct times such that there is no memory in the dynamics of the solvent.

Equation (1.7) can be extended to include a feedback force as considered in Chapter 3 in a straight-forward manner. Adding a feedback force $\mathbf{F}_{\mathrm{fb}}$ to the right side of the equation leads to the Langevin equation in the case of feedback,

$$\gamma \frac{\mathrm{d}\mathbf{r}_i(t)}{\mathrm{d}t} = \sum_{j=1}^{N} \mathbf{F}_{\mathrm{fb}}\left(\mathbf{r}_i(t) - \mathbf{r}_j(t-\tau)\right) + \sum_{\substack{j=1 \\ j\neq i}}^{N} \mathbf{F}_{\mathrm{int}}\left(\mathbf{r}_i(t) - \mathbf{r}_j(t)\right) + \mathbf{F}_{\mathrm{ext}}\left(\mathbf{r}_i(t), t\right) + \mathbf{f}_i(t)\,. \tag{1.8}$$

In this definition, the feedback-force only depends on the distance of the current particle positions to the previous ones $\mathbf{F}_{\mathrm{fb}}\left(\mathbf{r}_i(t) - \mathbf{r}_j(t-\tau)\right)$. The time argument was added to the other terms for clarity.

Chapter 3 investigates the effect of a feedback potential on a colloidal suspension confined to two dimensions. The protocol for creating the feedback is shown in

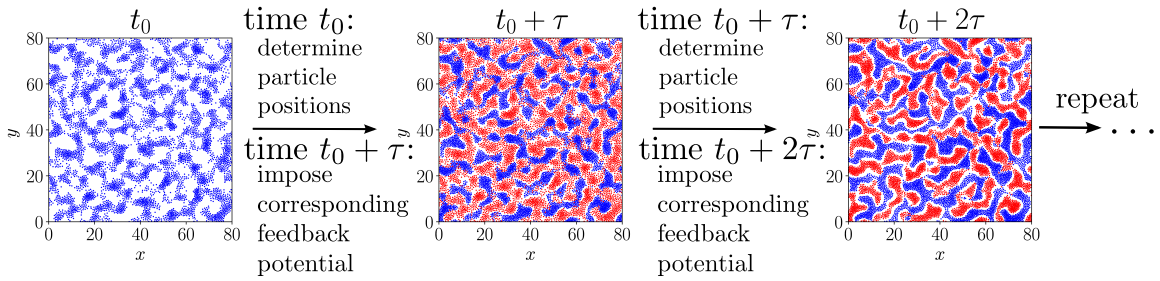

Figure 1.2: Visualization of the feedback potential construction. Particle positions at the specified times are shown in blue. The imposed potential is constructed from the particle positions at a previous time, preceding the current time by a time shift τ and shown in red. Continuous updates $t_0 \in [-\tau, 0)$ or discrete updates $t_0 = -\tau$ of the potential are possible.

Fig. 1.2: The potential imposed at time $t+\tau$ takes the particle position at time t as an input. The feedback system thus requires knowledge of the particle positions in a time window $t \in [-\tau, 0]$ in order to define the potential at all following times. An alternative approach is to prescribe discrete update times at which the potential is updated. After an update the same potential is imposed until the next renewal. This case only requires the particle positions at time $t = -\tau$ as an input and can be considered as an approximation to the continuous update. A similar situation to this case will also arise in an experimental setup using holographic optical tweezers, for which updates of the potential are limited by the rate at which the positions of the particles can be tracked. Additionally, high update rates create a huge computational load in producing the necessary input holograms. Indeed, the feedback potential update can therefore only be performed at discrete times, leading to the same protocol. In Chapter 3, the feedback is considered for the single-particle case (Sec. 3.1) for an attractive and a repulsive nature of the potential. For the case $N = 1$ and linear forces with discrete update times, the associated Langevin equation (1.8) can be solved analytically and the results for the particle position and the mean square displacement are given. For many particles (Publication II), we employ Brownian dynamics simulations according to eq. (1.8) with a continuous potential update to study the collective dynamics of the system. In this case, self-organization into traveling bands is observed.

1.3.2 Smoluchowski equation

The Langevin equation has a counterpart formulation in terms of the probability density of finding particles at a set of given positions. This equivalent description is called the Smoluchowski equation, which is a Fokker-Planck equation for the distribution of the particle positions in the large friction limit [268]. The Smoluchowski equation equivalent to Langevin eq. (1.7) describes the many-body probability density

$w(\mathbf{r}^N = \mathbf{r}_1, \ldots, \mathbf{r}_N)$ to have N particles at positions $\mathbf{r}_1, \ldots, \mathbf{r}_N$ and reads

$$\frac{\partial w\left(\mathbf{r}^N, t\right)}{\partial t} = \frac{1}{\gamma} \sum_{i=1}^{N} \nabla_i \left[k_B T \nabla_i - \sum_{\substack{j=1 \\ j \neq i}}^{N} \mathbf{F}_{\text{int}}\left(\mathbf{r}_i - \mathbf{r}_j\right) - \mathbf{F}_{\text{ext}}\left(\mathbf{r}_i, t\right) \right] w\left(\mathbf{r}^N, t\right) . \quad (1.9)$$

The first term describes diffusion of the particles, while the following terms take into account the effects of interactions between the particles and external forces. The equation thus constitutes a convection-diffusion equation for the probability density of the particle positions.

For the Smoluchowski equation, the inclusion of feedback forces is not as trivial as the case of the Langevin equation due to the dependence on the past particle positions. However, it can be shown [265] that the same equation holds now for the conditional probability density, i.e., for a specified set of past positions. The corresponding equation for a subset of ensembles $w\left(\mathbf{r}^N, t | \mathbf{r}_\tau^N, t_\tau\right)$ under the condition that the particles were at positions $\mathbf{r}_\tau^N = \mathbf{r}_{\tau_1}, \ldots, \mathbf{r}_{\tau_N}$ at time $t_\tau = t - \tau$ then reads

$$\begin{aligned} \left.\frac{\partial w\left(\mathbf{r}^N, t | \mathbf{r}_\tau^N, t_\tau\right)}{\partial t}\right|_{t_\tau = t-\tau} = & \frac{1}{\gamma} \sum_{i=1}^{N} \nabla_i \left[k_B T \nabla_i - \sum_{j=1}^{N} \mathbf{F}_{\text{fb}}\left(\mathbf{r}_i - \mathbf{r}_{\tau_j}\right) \right. \\ & \left. - \sum_{\substack{j=1 \\ j \neq i}}^{N} \mathbf{F}_{\text{int}}\left(\mathbf{r}_i - \mathbf{r}_j\right) - \mathbf{F}_{\text{ext}}\left(\mathbf{r}_i, t\right) \right] w\left(\mathbf{r}^N, t | \mathbf{r}_\tau^N, t_\tau\right) \end{aligned} \quad (1.10)$$

with the time-derivative on the left only acting on t but not t_τ. This equation can then be used to derive a DDFT equation for the dynamics of the particle density, which is usually the actual quantity of interest. This is done for the feedback case in Chapter 3 (Publication II) and in the following for the simpler case without feedback, eq. (1.9).

1.3.3 Dynamic density functional theory (DDFT)

The Smoluchowski equation can be used to derive an equation for the one-particle density [268]. The DDFT equation [266–269, 275] can be obtained by integrating out all but one particle position with the resulting one-particle density defined by

$$\rho\left(\mathbf{r}_1, t\right) = N \int \mathrm{d}\mathbf{r}_2 \cdots \int \mathrm{d}\mathbf{r}_N \; w\left(\mathbf{r}^N, t\right) \quad (1.11)$$

with the additional factor N originating from the indistinguishability between the particles. Analogously, the two-particle density is given by

$$\rho^{(2)}\left(\mathbf{r}_1, \mathbf{r}_2, t\right) = N\left(N-1\right) \int \mathrm{d}\mathbf{r}_3 \cdots \int \mathrm{d}\mathbf{r}_N \; w\left(\mathbf{r}^N, t\right) . \quad (1.12)$$

In the case of externally-driven interacting particles, integration of eq. (1.9) with $N \int \mathrm{d}\mathbf{r}_2 \cdots \mathrm{d}\mathbf{r}_N$ leads to

$$\begin{aligned}\frac{\partial \rho\left(\mathbf{r}_1, t\right)}{\partial t} =& D \Delta_1 \rho\left(\mathbf{r}_1, t\right) - \frac{1}{\gamma} \int \mathrm{d}\mathbf{r}_2 \nabla_1 \left[\rho^{(2)}\left(\mathbf{r}_1, \mathbf{r}_2, t\right) \mathbf{F}_{\mathrm{int}}(\mathbf{r}_1 - \mathbf{r}_2)\right] \\ & - \frac{1}{\gamma} \nabla_1 \left[\rho\left(\mathbf{r}_1, t\right) \mathbf{F}_{\mathrm{ext}}(\mathbf{r}_1)\right] . \end{aligned} \tag{1.13}$$

This can be rewritten (dropping the index) in the form

$$\gamma \frac{\partial \rho\left(\mathbf{r}, t\right)}{\partial t} = \nabla \left[\rho\left(\mathbf{r}, t\right) \nabla \frac{\delta \mathcal{F}\left[\rho\left(\mathbf{r}, t\right)\right]}{\delta \rho\left(\mathbf{r}, t\right)}\right] \tag{1.14}$$

as the functional derivative of the free energy

$$\mathcal{F}\left[\rho\left(\mathbf{r}, t\right)\right] = k_B T \int \mathrm{d}\mathbf{r} \rho\left(\mathbf{r}, t\right) \left(\ln\left(\Lambda^2 \rho\left(\mathbf{r}, t\right)\right) - 1\right) + \mathcal{F}^{\mathrm{exc}}\left[\rho\left(\mathbf{r}, t\right)\right] + \int \mathrm{d}\mathbf{r} \rho\left(\mathbf{r}, t\right) V_{\mathrm{ext}}\left(\mathbf{r}\right) . \tag{1.15}$$

Here, the first term $\mathcal{F}^{\mathrm{id}} = k_B T \int \mathrm{d}\mathbf{r} \rho\left(\mathbf{r}, t\right) \left(\ln\left(\Lambda^2 \rho\left(\mathbf{r}, t\right)\right) - 1\right)$ is the *ideal* contribution giving the energy in the case of non-interacting particles and leading to particle diffusion in eq. (1.14). The argument of the logarithm is decorated with a factor Λ^2 for a two-dimensional density, where Λ denotes the thermal de Broglie wavelength. Note that this factor is solely introduced to obtain a unitless expression and has no consequence for the temporal evolution of $\rho(\mathbf{r}, t)$. The second term $\mathcal{F}^{\mathrm{exc}}$ gives the interaction energy in *excess* of the first one. Rewriting the particle interactions with this energy term uses the *adiabatic approximation* of DDFT. This approximation requires that the relations valid for equilibrium systems, connecting the interaction potential to the direct correlation function $c^{(1)}\left(\mathbf{r}_1\right)$,

$$\int \mathrm{d}\mathbf{r}_2 \rho^{(2)}\left(\mathbf{r}_1, \mathbf{r}_2\right) \nabla_1 V_{\mathrm{int}}(|\mathbf{r}_1 - \mathbf{r}_2|) = -k_B T \rho\left(\mathbf{r}_1\right) \nabla_1 c^{(1)}\left(\mathbf{r}_1\right) , \tag{1.16}$$

and the direct correlation function to the excess free energy of the system,

$$c^{(1)}\left(\mathbf{r}\right) = -\frac{1}{k_B T} \frac{\delta \mathcal{F}_{\mathrm{exc}}\left[\rho(\mathbf{r})\right]}{\delta \rho\left(\mathbf{r}\right)} , \tag{1.17}$$

also hold for non-equilibrium systems [268]. In eq. (1.16), $V_{\mathrm{int}}(r)$ denotes the interaction potential between the particles related to the interaction forces by $\mathbf{F}_{\mathrm{int}}(\mathbf{r}) = -\nabla V_{\mathrm{int}}(r)$. Here, an orientationally-symmetric potential form that only depends on the magnitude r of the distance $\mathbf{r}$ is assumed. Finally, the last term of eq. (1.15) denotes the energy contribution due to an external potential, from which the external forces derive via $\mathbf{F}_{\mathrm{ext}}\left(\mathbf{r}\right) = -\nabla V_{\mathrm{ext}}\left(\mathbf{r}\right)$. An analogous equation for the case of a feedback-driven system

is derived in Chapter 3 (Publication II) and used to examine the stability of a colloidal feedback-driven system.

Equation (1.14) shifts the problem of finding the density distribution of the particles to the problem of knowing the free energy of an arbitrary system state as a functional of the density. The obstacle here is that the excess free energy is in general not known exactly with the only exceptions of the ideal gas (for which the term vanishes) and rods in one dimension [276–278]. For other systems, approximative functionals are used. One very good approximation is known for hard interactions between the particles. The *fundamental measure theory* (FMT) rewrites the excess free energy in terms of weighted densities (measures). The original formulation by Rosenfeld [279], which was unable to reproduce freezing, has been modified several times since, resulting in the white bear (WBI) [280] and white bear II (WBII) [271] versions of the functional which cover the exact low density limit [281] and are able to account for freezing.

Another frequently-used approximation is given by the *mean-field* functional [282],

$$\mathcal{F}^{\mathrm{exc}}[\rho(\mathbf{r}_1,t)] \approx \frac{1}{2}\int \mathrm{d}\mathbf{r}_1 \int \mathrm{d}\mathbf{r}_2 V_{\mathrm{int}}(|\mathbf{r}_1-\mathbf{r}_2|)\rho(\mathbf{r}_1,t)\rho(\mathbf{r}_2,t)\,, \tag{1.18}$$

which is the same as putting

$$\rho^{(2)}\left(\mathbf{r}_1,\mathbf{r}_2,t\right) \approx \rho(\mathbf{r}_1,t)\rho(\mathbf{r}_2,t) \tag{1.19}$$

in eq. (1.13). This approximative scheme becomes asymptotically exact at high densities for penetrable potentials [276].

Chapter 2 (Publication I) considers a suspension of charged colloidal particles for which the steric interaction is taken into account via FMT and charge interactions are considered on a mean-field level. The advantage of the mean-field approximation is that it can be used in a straight-forward manner for any interaction potential. Also, it does not require additional knowledge of a reference system as other approximations may.

Chapter 2

Colloidal capacitor

Publication I Impedance Resonance in Narrow Confinement

Sonja Babel, Michael Eikerling, and Hartmut Löwen,
Impedance Resonance in Narrow Confinement,
J. Phys. Chem. C, **122**, 21724 (2018),
published by *American Chemical Society*.

Digital Object Identifier (DOI): 10.1021/acs.jpcc.8b05559

Link to version of record:
https://pubs.acs.org/doi/full/10.1021/acs.jpcc.8b05559

Link to supplementary information:
https://pubs.acs.org/doi/suppl/10.1021/acs.jpcc.8b05559

Statement of contribution

M.E. and H.L. developed the project. I implemented the numerical code for the DDFT and produced all data and figures presented in the publication. All authors contributed to interpreting the results and writing the manuscript.

Copyright and license notice

Appendix

An appendix was added after the publication giving intermediate steps of the calculations involved.

THE JOURNAL OF PHYSICAL CHEMISTRY C

Article

Cite This: *J. Phys. Chem. C* 2018, 122, 21724−21734

pubs.acs.org/JPCC

Impedance Resonance in Narrow Confinement

Sonja Babel,[†] Michael Eikerling,[‡] and Hartmut Löwen*[,†]

[†]Institut für Theoretische Physik II: Weiche Materie, Heinrich-Heine-Universität Düsseldorf, Universitätsstraße 1, D-40225 Düsseldorf, Germany

[‡]Department of Chemistry, Simon Fraser University, 8888 University Drive, Burnaby, British Columbia, Canada V5A 1S6

Supporting Information

ABSTRACT: The article explores the ion flux response of a capacitor configuration to an alternating voltage. The model system comprises a symmetric binary electrolyte confined between plan-parallel capacitor plates. The alternating current response is investigated for the sparsely studied albeit practically important case of a large amplitude voltage applied across a narrow capacitive device, with the distance between the two plates amounting to a few ion diameters. Dynamic density functional theory is employed to solve for the spatiotemporal ion density distribution as well as the transient ion flux and complex impedance of the system. The analysis of these properties reveals a hitherto hidden impedance resonance. A single ion analogue of the capacitor, which is equivalent to neglecting all interactions between the ions, is employed for a physical interpretation of this phenomenon. It explains the resonance as a consequence of field-induced ion condensation at the capacitor plates and coherent motion of condensed ions in response to the field variation.

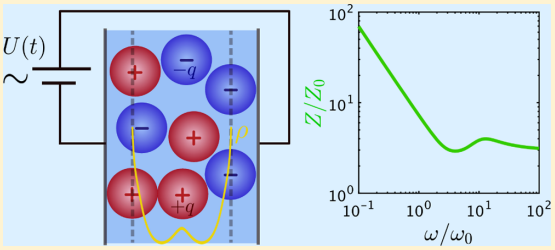

INTRODUCTION

There is a growing interest in understanding capacitive phenomena in narrowly confined ionic systems.[1−4] Obviously, the topic is of fundamental importance in electrochemistry. Besides, it is of practical utility for analyzing the dynamic response of charged colloidal systems[5−7] as well as nanoelectrochemical systems[8,9] to a varying electric field, as encountered for instance in electroactuators[10,11] or capacitive deionization systems.[12−14] The size of ions in relation to the size of the confining systems is a crucial consideration in such systems. Specifically, for ionic systems confined to lengths on the order of the ion diameter, steric effects become important.

The archetypal capacitive system consists of a liquid electrolyte or ionic liquid that is confined by rigid walls made of a metallic conductor insulated against the electrolyte, as depicted in Figure 1. The model system used here is infinite in lateral direction, rendering the problem effectively one-dimensional. Note that there is thus no bulk from which ions are taken or to which ions can leave nor are charges transferred from the ions to the walls. Ions only move back and forth within the gap. The primordial scientific interest lies in understanding the response of such a system to a modulation of the applied metal-phase potential, which is a topic of central interest in physical chemistry. The response function in question is the result of a complex interplay between variations in metal surface charge density, electrolyte potential, and ion density distribution.

In this work, classical dynamic density functional theory (DDFT)[15−18] is used to study the ion dynamics in a narrow electrolyte slab, whose thickness equals a few ionic diameters. The ionic system is exposed to a dynamic voltage between the capacitor plates with harmonic (sinusoidal) time dependence determined by the angular frequency ω and the amplitude ΔU.

The motivation to study this model is threefold: first of all, the model is best applied to the mesoscopic scale for oppositely charged colloids.[5,6] Using organic solvents, these can be prepared even at low concentrations of dissolved ionic countercharges such that the microion concentration is small.[19] These dispersions have been exposed to direct current[20] and alternating current (AC)[21] electric fields that gave rise to strong spatiotemporal responses. The presented model system resembles the configuration considered in ref 21 though in our case the electrolyte-filled slit between the walls is only a few colloidal layers wide. Apparent issues in applying our model to colloids lie in ignoring the residual microion concentration, which however can be kept to small (micromolar) concentrations in organic solvents, and neglecting the hydrodynamic interactions mediated by the solvent, which can be justified by using particles whose hydrodynamic radius is much smaller than their interaction radius, as is the case for solvent-permeable particles.[22,23] The mentioned problems are also mitigated by the fact that the responses of the microions and solvent molecules on the one hand and the colloidal ions on the other hand are separated in the frequency domain. The colloidal system can of course be scaled down in size toward charged micelles and nanocolloids.

Received: June 11, 2018
Revised: September 4, 2018
Published: September 5, 2018

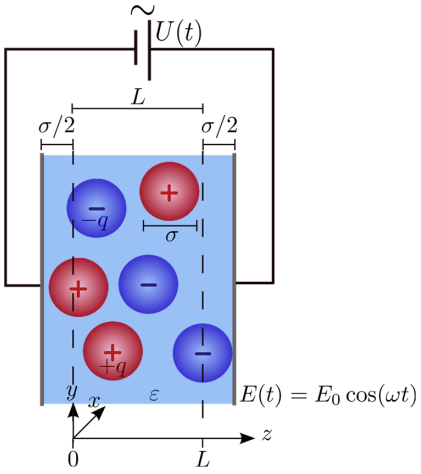

Figure 1. Sketch of the system. Balanced numbers of equally sized ions with diameter σ and charge $q_\pm = \pm q$ are kept in a slab between two plan-parallel insulating capacitor plates in an electrolyte of relative dielectric constant ε. The width L denotes the accessible length in z-direction. For simplicity, the system is assumed to be infinitely extended in xy-direction. An alternating external voltage $U(t)$ with amplitude ΔU produces an oscillating electric field $E(t)$ acting on the ions.

Secondly, one can think about a molecular realization in nanogap electrodes with the capacitor walls electrically isolated from the electrolyte in order to prevent any ion oxidation at the walls. The peculiar geometry has not yet been exploited experimentally but is in principle feasible.[24] It should be noted though that applying our model to this case implies neglecting any specific solvent contributions to the AC electric field response as well as any structural details of the walls.[25]

Thirdly, the considered model logically extends basic model studies of capacitor configurations that can be traced back to classical works of Gouy (1910)[26] and Chapman (1913).[27] From these early works, problems of electrified interfaces and confined electrolytes were approached using continuum theories based on Poisson−Boltzmann and Poisson−Nernst−Planck (PNP) equations. Later on, these continuum theories were modified to account for steric effects induced by finite ion size[28−36] and specific solvent polarization effects.[37]

Our model system is similar to those considered in recent theoretical studies by Beunis et al.,[38] Olesen et al.,[39] and Feicht et al.[40] However, in contrast to those works, we consider a case of more narrow ion confinement, wherein the width of the electrolyte slab, L, is on the order of several ion diameters, σ, that is, $\sigma \leq L \leq 4\sigma$, and we focus entirely on the limit of large electric fields. We employ classical dynamic density functional theory[15−18] (DDFT), including the steric repulsion between the ions. A similar model has been used before in refs 35, 36 to consider the charging kinetics of an electric double layer in response to a voltage step.

Here, we apply this approach to study the capacitive response of the ionic system to a transient electric field. Our system is smaller than the one that was considered in refs 35, 36, and we are interested in the ion flux response to an AC voltage signal with large amplitude. This response function should be amenable to experimental study by electrochemical impedance spectroscopy.

DDFT is known to be computationally highly efficient and it allows geometric parameters like ion diameter and slab thickness to be tuned widely. With DDFT, the system response can be studied under large amplitude, $\Delta U \gg U_T$, with the thermal voltage $U_T = k_B T/q$, where k_B is the Boltzmann constant, T is the temperature, and q is the ion charge, and over a wide range of ω. It is thus an ideal tool to explore ion dynamics in a capacitor configuration in the limit of strong ion confinement[1−4] where the full interplay of steric correlation effects, electrostatic interactions, as well as ion transport by diffusion and migration unfolds.

In the following section, we introduce the model system and describe the physical-computational methodology based on dynamic density functional theory. Equations are non-dimensionalized and typical parameter sets are discussed. In the results section, we analyze and discuss the dynamic density profiles of ions and the impedance response of the microscopic model system. A single-ion capacitor model is presented to explain the observed resonance effect in the impedance.

MODEL

An electroneutral mixture of colloidal cations and anions with equal charge magnitude q and equal diameter σ is kept in a stagnant fluid with dielectric constant ε. This ionic system[30,41−49] is confined between two infinitely extended plan-parallel capacitor plates;[38−40,50−56] see Figure 1. The plates are polarized with an external alternating voltage $U(t)$ that creates an oscillating electric field $E(t)$ across the electrolyte slab. The ions are modeled within the restricted primitive model[57−66] as hard charged spheres of diameter σ interacting via steric and Coulomb interactions. The capacitor plates are introduced as hard insulating walls leading to a no-flow condition for the ions. The outermost possible position of the ion centers is then situated at a distance $\sigma/2$ away from the physical walls. L denotes the accessible width perpendicular to the capacitor plates. The system is considered in the highly confined limit where L is on the order of σ.

We solve the model for the time- and space-dependent densities of the two ion species using DDFT,[15−18] which is the time-dependent variant of classical DFT.[67−79] From the densities, we also obtain the charge flux in the system. The linear response part of the current is used to further calculate a quantity that is analogous to a local impedance of the capacitor configuration. Subsequently, we will therefore refer to it as the local impedance.

Theory. *Dynamic Density Functional Theory (DDFT).* Dynamic density functional theory relates the time evolution of the density to the functional derivative of the free energy of the system in the form

$$\frac{\partial \rho_\pm(\vec{r}, t)}{\partial t} = \beta D \nabla \left[\rho_\pm(\vec{r}, t) \nabla \left(\frac{\delta \mathcal{F}[\rho_+(\vec{r}, t), \rho_-(\vec{r}, t)]}{\delta \rho_\pm(\vec{r}, t)} \right) \right] \tag{1}$$

where $\rho_\pm(\vec{r}, t)$ stands for the density of the ions with either positive ρ_+ or negative charge ρ_- as a function of position $\vec{r}$ and time t; $\beta = 1/k_B T$ is the inverse thermal energy, and D is the diffusion coefficient of the ions, which, for simplicity, is taken to be the same for both ion species $D_+ = D_- \equiv D$. $\mathcal{F}$ denotes the free energy of the system, which is a functional of the two densities ρ_+ and ρ_-, and $\frac{\delta}{\delta \rho_\pm}$ is the functional derivative[80,81] with respect to the density. By connecting the time derivative

DOI: 10.1021/acs.jpcc.8b05559
J. Phys. Chem. C 2018, 122, 21724−21734

of the density to the functional derivative of the system's energy, DDFT shifts the problem of determining the time evolution of the densities to the problem of knowing the energy of the system for any given density distribution. If we know the energy of all states, we can determine the time evolution of the system from this knowledge. Thus, we first need to construct an expression for the energy of the system. We consider a free energy functional of the form

$$\mathcal{F} = \mathcal{F}^{\mathrm{id}} + \mathcal{F}^{\mathrm{HS}} + \mathcal{F}^{\mathrm{Coul}} + \int \mathrm{d}\vec{r}\, \rho_{\pm}(\vec{r}, t) V_{\mathrm{ext},\pm}(\vec{r}, t) \tag{2}$$

The ideal part $\mathcal{F}^{\mathrm{id}}$ gives the free energy of an ideal gas. The remaining terms describe the interaction of the particles due to steric hard-sphere $\mathcal{F}^{\mathrm{HS}}$ and charge effects $\mathcal{F}^{\mathrm{Coul}}$ (Coulomb) as well as the effect of the external potential $V_{\mathrm{ext},\pm}(\vec{r}, t) = -q_{\pm}E(t)z$ with the electric field

$$E(t) = E_0 \cos(\omega t) \tag{3}$$

The amplitude E_0 is related to the voltage amplitude ΔU and the accessible system length L by

$$E_0 = \Delta U / L \tag{4}$$

The ideal part $\mathcal{F}^{\mathrm{id}}$ is known exactly, the hard-sphere (HS) part is described by fundamental measure theory (FMT),[14,82−86] introduced in the next paragraph, while the Coulomb interaction is taken into account with a mean-field approach,[56,85] such that for the ions within a volume V we obtain

$$\begin{aligned}
\mathcal{F}^{\mathrm{id}}[\rho_+, \rho_-] &= k_{\mathrm{B}}T \sum_{\pm} \int_V \mathrm{d}\vec{r}\, \rho_{\pm}(\vec{r}, t) \ln(\Lambda^3 \rho_{\pm}(\vec{r}, t)) \\
\mathcal{F}^{\mathrm{HS}}[\rho_+, \rho_-] &= \mathcal{F}^{\mathrm{FMT}}[\rho_+ + \rho_-] \\
\mathcal{F}^{\mathrm{Coul}}[\rho_+, \rho_-] &= \frac{1}{8\pi\epsilon\epsilon_0} \int_V \mathrm{d}\vec{r} \int_V \mathrm{d}\vec{r}\,' \frac{\rho_{\mathrm{c}}(\vec{r}, t)\rho_{\mathrm{c}}(\vec{r}\,', t)}{|\vec{r} - \vec{r}\,'|}
\end{aligned} \tag{5}$$

with charge density $\rho_{\mathrm{c}}(\vec{r}, t) = q(\rho_+(\vec{r}, t) - \rho_-(\vec{r}, t))$. ε_0 denotes the vacuum and ε denotes the relative permittivity. Λ is the de Broglie wavelength. As a remark, an extension of this functional to account for short-range electrostatic correlations between the ions was recently derived in ref 74.

Fundamental Measure Theory (FMT). We use the White Bear II version of the fundamental measure theory in tensor[87] form[84,85] to write the hard-sphere contribution to the free energy functional as

$$\mathcal{F}^{\mathrm{FMT}} = \int_V \mathrm{d}\vec{r}\, \Phi(\{n_\alpha\}) \tag{6}$$

where $\Phi = \Phi_1 + \Phi_2 + \Phi_3$ is the free energy density with

$$\begin{aligned}
\Phi_1 &= -\frac{n_2}{4\pi R^2} \ln(1 - n_3) \\
\Phi_2 &= \frac{1}{4\pi R}(n_2^2 - \vec{n}_2 \cdot \vec{n}_2) \frac{1 + \frac{1}{3}\psi_2(n_3)}{1 - n_3} \\
\Phi_3 &= \left(n_2^3 - 3n_2 \vec{n}_2 \cdot \vec{n}_2 + \frac{9}{2}(\vec{n}_2 \vec{n}_{m_2} \vec{n}_2 - \mathrm{Tr}(\vec{n}_{m_2}^3))\right) \\
&\quad \times \frac{1 - \frac{1}{3}n_3\psi_3(n_3)}{24\pi(1 - n_3)^2}
\end{aligned} \tag{7}$$

using the functions

$$\begin{aligned}
\psi_2 &= \frac{1}{n_3}(2n_3 - n_3^2 + 2(1 - n_3)\ln(1 - n_3)) \\
\psi_3 &= \frac{1}{n_3^2}(2n_3 - 3n_3^2 + 2n_3^3 + 2(1 - n_3)^2 \ln(1 - n_3))
\end{aligned} \tag{8}$$

These expressions are solely dependent on a set of functions n_α, referred to as weighted densities, which are obtained from convolutions of the particle density ρ with weight functions $\omega^{(\alpha)}$ such that

$$n_\alpha(\vec{r}, t) = \int_V \rho(\vec{r}\,', t)\omega^{(\alpha)}(\vec{r} - \vec{r}\,')\mathrm{d}\vec{r}\,' \tag{9}$$

where

$$\begin{aligned}
\omega^{(2)}(\vec{r}) &= \delta(R - |\vec{r}|) \\
\omega^{(3)}(\vec{r}) &= \theta(R - |\vec{r}|) \\
\vec{\omega}^{(2)}(\vec{r}) &= \frac{\vec{r}}{|\vec{r}|}\delta(R - |\vec{r}|) \\
\vec{\vec{\omega}}^{(m_2)}(\vec{r}) &= \left(\frac{\vec{r} \cdot \vec{r}^{\,t}}{|\vec{r}|^2} - \frac{\vec{\vec{\mathbb{I}}}}{3}\right)\delta(R - |\vec{r}|)
\end{aligned} \tag{10}$$

are the weights in the case of spherical particles. Here, $R = \sigma/2$ denotes the hard-sphere radius. δ is the Dirac delta function, θ is the heavyside step function, $\vec{r}^{\,t}$ is the transpose of the vector $\vec{r}$, and $\vec{\vec{\mathbb{I}}}$ is the unit matrix. Arrows indicate vectors, while the double-headed arrow denotes a matrix. Tr in eq 7 is the trace of the matrix, that is, the sum of its diagonal elements. In particular, the weighted density $n_3(\vec{r}, t)$ gives the number of particles within a sphere of radius R around $\vec{r}$ at time t. Term Φ_1 of eq 7 ensures, via divergence of the logarithm, that this value does not become unphysical, that is, larger than one, thus accounting for the particle size.

System Parameters and Nondimensionalization. We will present parameterizations for the model on two different length scales. For a microscale realization, we consider low-charged colloidal particles of charge $q = |q_{\pm}| = 5e$, where e is the elementary charge, and of diameter $\sigma = 2.61\ \mu$m, which serves as the length scale. We further assume the ions to be partially solvent permeable with a hydrodynamic radius of $R_{\mathrm{h}} = \frac{\sigma}{20}$. The relative permittivity of the organic electrolyte is assumed as $\varepsilon = 2.3$, corresponding for instance to the relative permittivity of a decalin−tetrachloroethylene mixture as discussed in ref 88. The energy scale is set by the thermal energy at standard temperature ($T = 298$ K), $k_{\mathrm{B}}T = 4.11 \times 10^{-21}$ J, that can be used to define a thermal voltage $U_{\mathrm{T}} = k_{\mathrm{B}}T/$

DOI: 10.1021/acs.jpcc.8b05559
J. Phys. Chem. C 2018, 122, 21724−21734

The Journal of Physical Chemistry C Article

Table 1. Summary of the System Parameters[a]

dimensional property	symbol	definition	normalized value	typical value nanoscale	typical value microscale
ion diameter	σ		1	3 nm	2.61 μm
accessible system length	L		L/σ	10 nm	8.70 μm
Bjerrum length	λ_B	$q^2/(4\pi\epsilon\epsilon_0 k_B T)$	$q^2/(4\pi\epsilon\epsilon_0 k_B T\sigma)$	0.70 nm	0.61 μm
Debye length	λ_D	$\frac{\sigma}{2}\sqrt{\frac{\sigma}{\lambda_B}\frac{1}{6\phi}}$	$\frac{1}{2}\sqrt{\frac{\sigma}{\lambda_B}\frac{1}{6\phi}}$	2.07 nm	1.80 μm
self-diffusion time	τ_0	σ^2/D_0	1	5.50×10^{-8} s	5.25 s
driving period	T		TD_0/σ^2		
transit time	τ_{tr}	$\pi L^2 k_B T/(2qUD_0)$	$\pi L^2/(2\sigma^2 U^*)$	2.47×10^{-9} s	2.35 s
diffusion time	τ_{diff}	L^2/D_0	L^2/σ^2	6.12×10^{-7} s	58.3 s
self-diffusion frequency	ω_0	$2\pi D_0/\sigma^2$	2π	1.14×10^{8} s^{-1}	1.20 s^{-1}
driving frequency	ω		$\omega\sigma^2/2\pi D_0$		
transit frequency	ω_{tr}	$4qUD_0/(L^2 k_B T)$	$4\sigma^2 U^*/L^2$	2.54×10^{9} s^{-1}	2.67×10^{-1} s^{-1}
diffusion frequency	ω_{diff}	$2\pi D_0/L^2$	$2\pi\sigma^2/L^2$	1.03×10^{8} s^{-1}	0.11×10^{-1} s^{-1}
current scale	j_0	$q/(\sigma^2\tau_0)$	1	3.23×10^{5} A m^{-2}	2.24×10^{-8} A m^{-2}
current harmonics	j_n	$\frac{2}{T}\int_{-T/2}^{T/2} dt\, j(\vec{r}, t)\, e^{-in\omega t}$	j_n/j_0		
thermal voltage	U_T	$k_B T/q$	1	25.7 mV	5.14 mV
external voltage	ΔU	$\Delta U = E_0 L$	$\Delta U/U_T = U^*$	1 V	0.2 V
impedance scale	Z_0	$k_B T\tau_0/q^2$	1	8.8×10^{9} Ω	3.36×10^{16} Ω
impedance	Z	$U/(j_1\sigma^2)$	$U^* j_0/j_1$		
relative permittivity	ϵ			80	2.3
particle charge	q		q/e	1e	5e

[a]Typical values are given for the two possible realizations constituted by a system of relatively large monovalent ions (nanoscale) with L = 10 nm, σ = 3 nm, $q = e$, $D_0 = 1.63 \times 10^{-10}$ m^2 s^{-1}, $k_B T = 4.11 \times 10^{-21}$ J, and ΔU = 1.0 V and a system of low-charged partially solvent-permeable colloidal particles (microscale) where L = 8.70 μm, σ = 2.61 μm, $q = 5e$, $D_0 = 1.30 \times 10^{-12}$ m^2 s^{-1}, $k_B T = 4.11 \times 10^{-21}$ J, and ΔU = 0.2 V, both leading to the same normalized system parameters.

q = 5.14 mV. The viscosity of the electrolyte at room temperature is $\eta = 1.29 \times 10^{-3}$ Pa s, such that the diffusion constant of macroions is $D_0 = \frac{k_B T}{6\pi\eta R_h} = 1.30 \times 10^{-12}$ m^2 s^{-1}. We define a characteristic time scale $\tau_0 = \sigma^2/D_0 = 5.25$ s that corresponds to a characteristic angular frequency $\omega_0 = \frac{2\pi}{\tau_0} = 1.20$ s^{-1}.

On the other hand, a nanoscale system of monovalent ions at the same temperature with $q = e$, σ = 2, R_h = 3 nm, ε = 80, and $U_T = k_B T/q$ = 25.7 mV leads to the same reduced system parameters. With the viscosity of water at room temperature, $\eta_{water} = 8.9 \times 10^{-4}$ Pa s, the diffusion coefficient in this case is $D_0 = 1.63 \times 10^{-10}$ m^2 s^{-1} and the time and frequency scales are now given by $\tau_0 = 5.5 \times 10^{-8}$ s and $\omega_0 = 1.14 \times 10^{8}$ s^{-1}, respectively. The following calculation can thus be considered in either of these cases. A summary of the system parameters can be found in Table 1.

The dimensionless amplitude of the applied voltage is given by

$$U^* = \frac{\Delta U}{U_T} \tag{11}$$

As a baseline parameter for this amplitude, we use U^* = 38.9.

In addition to the ion diffusion and self-diffusion time, $\tau_{diff} = \frac{L^2}{D_0}$ and $\tau_0 = \frac{\sigma^2}{D_0}$, respectively, we introduce the ion transit time, τ_{tr}, which corresponds to the time that an ion needs to cross the thickness of the device when the electric field is not screened. The latter is given by the ratio of the system length L and the mean velocity of the particles in the unscreened case, $\bar{v} = \frac{qE}{\gamma}\frac{2}{T}\int_{-T/4}^{T/4} dt\, \cos(\omega t) = \frac{2}{\pi}\frac{U^* D}{L}$, as $\tau_{tr} = \frac{L}{\bar{v}} = \frac{\pi}{2}\frac{U_T}{\Delta U}\frac{L^2}{D_0}$. All time scales are normalized to the self-diffusion time τ_0, such that the dimensionless ion transit time becomes

$$\frac{\tau_{tr}}{\tau_0} = \frac{\pi}{2}\frac{L^2}{\sigma^2 U^*} \tag{12}$$

and the dimensionless diffusion time of ions in the electrolyte is

$$\frac{\tau_{diff}}{\tau_0} = \frac{L^2}{\sigma^2} \tag{13}$$

The corresponding dimensionless angular frequencies are given by

$$\frac{\omega_{tr}}{\omega_0} = \frac{2}{\pi}\frac{U^*\sigma^2}{L^2} \tag{14}$$

and

$$\frac{\omega_{diff}}{\omega_0} = \frac{\sigma^2}{L^2} \tag{15}$$

The free parameters of the model, varied in simulations, are ΔU and L.

The dimensionless thickness L/σ should be evaluated in relation to two common characteristic length scales of ionic systems: Bjerrum length λ_B and Debye length λ_D, which are given in the dimensionless form as

DOI: 10.1021/acs.jpcc.8b05559
J. Phys. Chem. C 2018, 122, 21724−21734

$$\frac{\lambda_B}{\sigma} = \frac{1}{4\pi\varepsilon}\frac{q^2}{\varepsilon_0 k_B T \sigma}$$

$$\frac{\lambda_D}{\sigma} = \sqrt{\frac{\varepsilon\varepsilon_0 k_B T}{\sigma^2 \sum_\pm n_\pm q_\pm^2}} = \sqrt{\frac{\varepsilon}{\frac{q^2}{\varepsilon_0 k_B T \sigma}}\frac{\pi}{6\phi}} = \frac{1}{2}\sqrt{\frac{\sigma}{\lambda_B}\frac{1}{6\phi}} \tag{16}$$

where n_+ and n_- is the number density of cations and anions, respectively, and $\phi = \frac{\pi}{6}\sigma^3(n_+ + n_-)$ is the volume fraction occupied by ions, each defined on the accessible region of width L. We fix $\phi = 0.375$ such that we obtain $\lambda_B/\sigma = 0.23$ and $\lambda_D/\sigma = 0.69$ for the (macro-)ions. Thus, both of the lengths, λ_B and λ_D, are smaller than the particle diameter σ, and a strong effect of the hard-sphere interactions is expected.

Quantities of Interest. At the start, the system is equilibrated without applied potential to reach a steady state, at which point the transverse oscillating voltage $U(t)$ is introduced. The latter causes an electric field $E(t)$ and thus an ion flux in z-direction. The resulting ion flux density $\vec{j}_{p,\pm}(\vec{r}, t)$ is a periodic function in time and can easily be derived from eq 1 together with the continuity equation $\frac{\partial\rho_\pm(\vec{r},t)}{\partial t} = -\nabla\cdot\vec{j}_{p,\pm}(\vec{r}, t)$ as

$$\vec{j}_{p,\pm}(\vec{r}, t) = -\beta D\left[\rho_\pm(\vec{r}, t)\nabla\left(\frac{\delta\mathcal{F}[\rho_+(\vec{r}, t), \rho_-(\vec{r}, t)]}{\delta\rho_\pm(\vec{r}, t)}\right)\right] \tag{17}$$

The ionic current density in z-direction is then given as

$$j(\vec{r}, t) = \sum_\pm q_\pm \vec{j}_{p,\pm}(\vec{r}, t)\cdot\hat{e}_z \tag{18}$$

Analogously, we can define contributions to the ion flux density that stem from different energy terms

$$\vec{j}^{\,k}_{p,\pm}(\vec{r}, t) = -\beta D\left[\rho_\pm(\vec{r}, t)\nabla\left(\frac{\delta\mathcal{F}^k[\rho_+(\vec{r}, t), \rho_-(\vec{r}, t)]}{\delta\rho_\pm(\vec{r}, t)}\right)\right] \tag{19}$$

where $k \in \{\text{id, HS, Coul, ext}\}$ and the ionic current density contribution is then again given by eq 18 replacing $\vec{j}_{p,\pm}$ with $\vec{j}^{\,k}_{p,\pm}$. Note that considering the contributions due to the external potential, $\mathcal{F}^{\text{ext}}$, and the ideal term, $\mathcal{F}^{\text{id}}$, the equation is identical to the Nernst–Planck equation. Adding also the Coulomb interaction term, $\mathcal{F}^{\text{Coul}}$, we obtain the Poisson–Nernst–Planck (PNP) description. The additional hard-sphere interaction term, $\mathcal{F}^{\text{HS}}$, is a nontrivial extension to this model accounting for the finite ion size, an essential contribution due to the small system width.

The current response is nondimensionalized relative to $j_0 = e/\sigma^2\tau_0$ and can, due to its periodicity, be decomposed into different harmonic contributions of amplitude j_n with $n = 1, 2, 3, \ldots$ The harmonics are obtained as

$$j_n(\vec{r}) = \frac{2}{T}\int_{-T/2}^{T/2} \mathrm{d}t\, j(\vec{r}, t)\, \mathrm{e}^{-in\omega t} \tag{20}$$

with $T = 2\pi/\omega$. Plots of the current will always show j while we use j_1, the amplitude of the first harmonic of the current density, to define the complex impedance Z given by

$$\frac{Z}{Z_0} = U^*\frac{j_0}{j_1}\,\mathrm{e}^{\mathrm{i}(\phi_U - \phi_{j_1})} \tag{21}$$

The scale of this quantity is set by $z_0 = k_B T\tau_0/e^2$. Higher harmonic contributions to the current (j_n with $n \geq 2$) will be discussed in the Supporting Information.

RESULTS AND DISCUSSION

Density Profiles and Current Response. First, we investigate the effect of the system width on the density distribution and current induced in the system. In Figure 2, the effect of the hard-sphere interaction is reflected in the increased values of the particle densities at the walls and at multiples of σ. Counterion accumulation at the walls is enhanced with the application of a finite voltage difference and for larger system widths, when ions are attracted to walls of opposite charge. The effect is preserved but weakens as the frequency increases. Thus, lower frequencies correspond to higher amounts of localized ions at the walls. Further, while at high frequencies the current is harmonic and in phase with the driving voltage, the low-frequency current shows anharmonicity and a phase shift; see Figure 3. For a stronger electric field (smaller system width), the current becomes increasingly

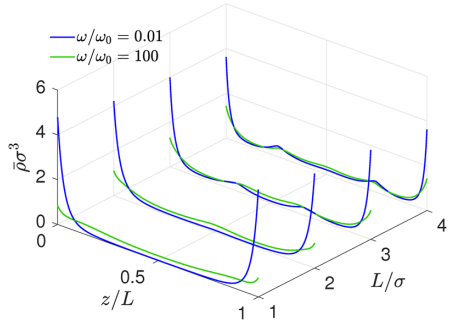

Figure 2. Mean density distribution $\bar{\rho} \equiv \bar{\rho}_+ = \bar{\rho}_-$ averaged over one period for different widths, $L/\sigma = 1$, $L/\sigma = 2$, $L/\sigma = 3$, and $L/\sigma = 4$. Layering at the walls and at multiples of σ is observed. The effect is stronger for smaller frequencies.

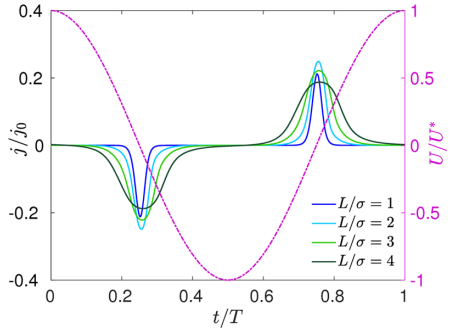

Figure 3. Time dependence of current density at the center position ($z = L/2$) at small frequency ($\omega/\omega_0 = 0.01$). The resulting current shows strong anharmonicity and a phase shift with respect to the driving voltage $U(t)$, which is also plotted for reference (purple dash-dot line).

DOI: 10.1021/acs.jpcc.8b05559
J. Phys. Chem. C 2018, 122, 21724–21734

The Journal of Physical Chemistry C Article

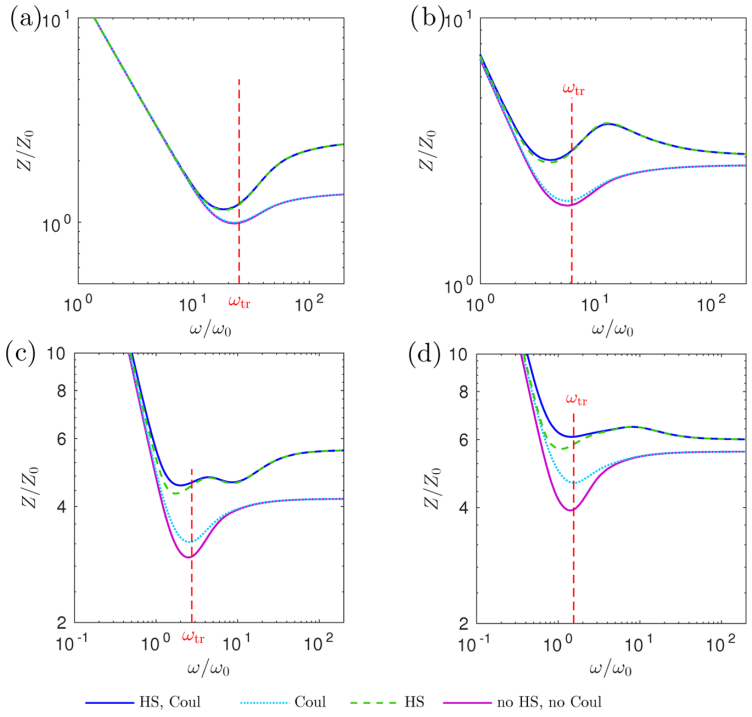

Figure 4. Impedance with respect to angular frequency of the driving voltage ω for systems of lengths (a) $L/\sigma = 1$, (b) $L/\sigma = 2$, (c) $L/\sigma = 3$, and (d) $L/\sigma = 4$. The impedance values in the large frequency limit are reached from below for system lengths that are odd multiples of σ and from above for even ones. The analytical result for the position of the minimum in the impedance ω_{tr} according to eq 14 is also indicated.

peaked and the system response is nonlinear. The effect of short-range electrostatic correlations on the density profile based on the usage of the more sophisticated density functional from ref 74 is discussed in the Supporting Information.

Impedance Response. To examine the effect of the hard-sphere character of the ions, eq 1 was solved, for reference, with and without hard-sphere (HS) and Coulomb (Coul) interaction terms, and the impedance corresponding to the ion flux at the capacitor midplane was calculated; see Figure 4. Hard-sphere interactions lead to a large increment of this impedance at medium and high frequencies, whereas the effect of Coulomb interactions in determining the impedance is much less pronounced.

The hard-sphere contribution is responsible for a maximum in the impedance at $\omega > \omega_{tr}$. This feature vanishes when the hard-sphere contribution is switched off. We conjecture that the maximum is thus related to the additional structure in the density distribution induced by hard-sphere interactions.

Another peculiar feature in Figure 4 is the impedance minimum seen at $\omega \approx \omega_0$. This feature is independent of the hard-sphere character of ions and also independent of their Coulomb interaction. It represents a resonance phenomenon that should be common to all systems of confined ions exposed to an oscillating external potential. While overdamped particles in a continuous environment do not show resonance behavior, it is the confinement in combination with the ion oscillation that leads to the resonance effect. However, observation of this phenomenon depends critically on system parameters. It is a peculiar signature of the pronounced wall effects, which prevail in strongly confined systems upon application of an AC voltage with large amplitude. Under normal conditions in planar capacitive devices, the resonance should be quenched by thermal diffusion.[38−40,50,54] Diffusion causes a melting or dephasing of the highly coherent ion motion induced by wall effects. Since the occurrence of the impedance resonance is not affected by hard-sphere or Coulombic interaction terms, the phenomenon can be illustrated and explained using a highly simplified model, which will be presented next.

Resonance Effect. *Single-Ion Capacitor Model.* The origin of the minimum in Figure 4 must be universal and can thus be understood for the simple case of a noninteracting gas of ions with charge q confined between two charged plates. For simplicity, we neglect thermal motion. In the non-interacting case, every ion can be considered individually. The equation of motion for each ion is equivalent to the case of a capacitor configuration with just one ion between the plates and is given by

$$\dot{z}(t) = \frac{qE_0}{\gamma}\cos(\omega t) \tag{22}$$

with the friction coefficient γ and the angular frequency ω. The ion position is then

$$z(t) = z_0 + \frac{qE_0}{\omega\gamma}\sin(\omega t) \tag{23}$$

with arbitrary starting position z_0. During one oscillation period, an ion will transfer through a total transverse distance $d_{tr} = 2qE_0/\omega\gamma$ between the plates.

DOI: 10.1021/acs.jpcc.8b05559
J. Phys. Chem. C 2018, 122, 21724−21734

In terms of the distance d_{tr} and frequency ω, we can distinguish three regimes. In the regime of small amplitude, $d_{tr} < L/2$, and high frequency, $\omega > 4qE_0/\gamma L$, ions that cross the midplane and contribute to j and Z at this plane perform full harmonic oscillations with zero phase shift to the applied AC voltage. The resulting ionic current density is easily obtained as

$$j(z = L/2, t) = q\dot{z}(t)\rho_0 = \frac{q^2 E_0 \rho_0}{\gamma}\cos(\omega t) \tag{24}$$

in the case of negligible thermal motion.

In the regime of large amplitude, $d_{tr} > L$, and small frequency, $\omega < 2qE_0/\gamma L$, all ions will accumulate at either one of the surface planes during a half-period. Therefore, under ideal conditions, as considered with this simple model, cations and anions will perform a highly coherent motion and cross the midplane as two condensed and oppositely directed layers; see also Figure 3. In this regime, all ions will contribute to current and impedance responses determined at this plane. The ionic current density, averaged over a half-period, will thus be proportional to the frequency of the applied field; it will be highly anharmonic and exhibit a monotonically decreasing phase shift with decreasing ω, approaching $-\frac{\pi}{2}$ in the zero frequency limit. The solutions of eq 22 in this and the following case are given in the Supporting Information.

In the intermediate regime with $L/2 \leq d_{tr} \leq L$ and $\frac{4qE_0}{\gamma L} \geq \omega \geq \frac{2qE_0}{\gamma L}$, all ions in the system contribute to current density and impedance at the midplane; however, a fraction d_{tr}/L of these ions forms a condensed layer at the walls, whereas the remaining fraction of ions remains distributed uniformly in between and follows the applied field harmonically and with zero phase shift. The transition that gives rise to the impedance resonance occurs at $\omega_{tr} = \frac{4qE_0}{\gamma L}$: slightly above this frequency, only 50% of ions (corresponding to d_{tr}/L) contribute to the ion flux at the midplane, and as the frequency increases, this fraction diminishes with the decrease of d_{tr}/L. In the frequency range at and below ω_{tr}, 100% of ions contribute to the midplane current as a consequence of the ion condensation at the walls. Thus, the resonance seen in Figure 4 has a simple geometric interpretation.

A necessary condition for observing this resonance at finite temperature is that diffusional dephasing of the coherent ion motion will take place on a time scale that is much larger than the ion transit time, that is, $\tau_{diff} \gg \tau_{tr}$ or $\omega_{diff} \ll \omega_{tr}$. The critical parameter that decides this condition is U^*, which should be much larger than 1 for the ion condensation effect to be discernible.

Further, the preceding small amplitude or high frequency case, eq 24, can be adopted to determine the high frequency limit behavior of nonuniform distributions of interacting particles by interpreting ρ as a local density, which we understand as the mean density over the length that particles oscillate, d_{tr}. Then, if the local density has a maximum at the plane of interest, j grows for smaller d_{tr}, that is, for larger ω, and the impedance $Z \propto 1/j$ declines toward its high frequency value. For a minimum in the density, the opposite is true and we approach the constant high-frequency impedance from below. This effect is also visible in Figure 4 for interacting particles (HS, Coul). For system lengths that are even multiples of σ, there is a maximum in the density at the center position when hard-sphere interactions are included and the high frequency limit of the impedance is approached from above. For odd multiples of σ, the center position is at a density minimum and the high frequency limit of the impedance is approached from below. Similarly, density inhomogeneities in the vicinity of the considered plane also appear in the impedance response at the corresponding frequencies, leading to additional extrema at medium frequencies.

Rescaled Resonance. We use the one-particle model to further investigate the emerging resonance. Defining the current averaged over a period of the driving signal $\bar{j} = \frac{1}{T}\int_0^T \mathrm{d}t j(t)$, we determine the corresponding time-averaged impedance $\tilde{Z} = \Delta U/\bar{j}\sigma^2$. For high frequencies, j is given by eq 24 in the athermal case. At finite temperature, we find that even though the condensed particles at the walls do not contribute to the current directly, diffusion from the condensed part into the gap center will lead to a density higher than the equilibrium density ρ_0 there. This effect is particularly dominant for medium frequencies where the fraction of condensed particles, d_{tr}/L, is expected to be high. As a next-order improvement, we correct for this effect by neglecting the peaked structure altogether. The numerical results for the density show that this is a valid approximation as the ion density peaks account for only about 10% of all ions. Considering only the uniform distribution part, the leftmost ions reach the extremal position d_{tr}, while the rightmost are pushed against the wall at position L. The effective width available to the ions is thus reduced to $L - d_{tr}$. The density, assuming again a constant distribution but now over the reduced region, is given by

$$\rho = \rho_0 L/(L - d_{tr}) \tag{25}$$

From eqs 24 and 25, we thus obtain

$$\bar{j} = \frac{2}{\pi}\frac{q^2 E_0}{\gamma}\frac{\rho_0 L}{L - d_{tr}} \tag{26}$$

and the high frequency limit, $\omega \to \infty$, as $j^\infty = \frac{2}{\pi}\frac{q^2 E_0 \rho_0}{\gamma}$. Normalizing the frequencies to the transit frequency ω_{tr} and the impedance to the high frequency limit $Z^\infty = U^* j_0/j^\infty$, we find that the result is solely depending on the value of U^*; see Figure 5. An approximate analytic result in the limit of negligible thermal motion compared to the driving force is given by eq 26 for $\omega > \omega_{tr}$ and $\bar{j} = q\rho_0 L\omega/\pi$ for $\omega \leq \omega_{tr}$ when all ions are passing the midplane.

The resonance becomes more pronounced for higher values of U^*. However, it cannot exceed a factor of 2 between the resonance value and the high frequency limit of the impedance. High values of U^* may appear unphysical but could be realized by using multivalent ions rather than higher voltages.

Effect of Condensed Layer. *Impedance.* So far we have only considered the impedance corresponding to the current at the system center at $z = L/2$. However, it is intuitive to expect the local impedance response, that is, the impedance associated with the time-dependent current at a fixed point between the capacitor plates, to be highly dependent on the position. The current response in the ion layer at the wall should significantly differ from the current in the system center. As a next step, we therefore consider the dependence of the local impedance on the position between the two capacitor plates. In Figure 6, the case $z/\sigma = 2$ corresponds to the center of the system. The

DOI: 10.1021/acs.jpcc.8b05559
J. Phys. Chem. C 2018, 122, 21724−21734

The Journal of Physical Chemistry C Article

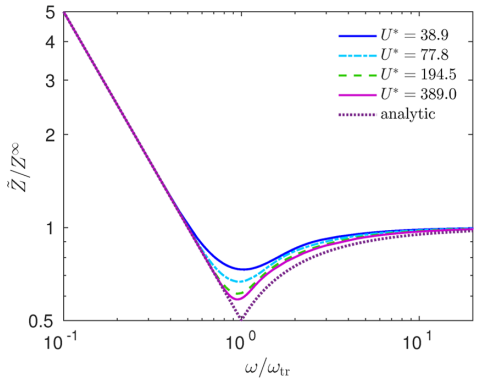

Figure 5. Impedance $\tilde{Z}$ for different values of the external voltage U^* and for the approximative analytic result with respect to angular frequency ω. The results are rescaled to the transition frequency ω_{tr} and the high frequency impedance limit Z^∞. The observed resonance at $\omega/\omega_{tr} = 1$ becomes more pronounced for higher U^*.

system response here is as expected, with a $1/\omega$ decay to the high frequency constant value in the impedance amplitude and the phase changing from $-\pi/2$ to 0. Approaching the wall, the position of $z/\sigma = 0.5$ corresponds to a density minimum and the large frequency limit of the impedance is approached from below. The rise in Z toward the high frequency limit is accompanied by a maximum in the phase with the system response even becoming inductive ($\varphi > 0$) for a limited frequency range. The phase behavior is caused by ion condensation at the wall. These ions lead to a temporal shift of the maximum in the current response toward the time at which they pass the plane. The resulting phase shift increases with ω and may even become positive. Upon further increasing ω, ions from the wall no longer reach the plane and the effect abates.

Decreasing the distance to the wall, we find that the low frequency phase value approaches zero as we enter the region of condensed ions. If we now consider again the time the ions condensed at the wall take to reach the plane at which we determine the impedance, we find that some of these ions are already present at the considered plane, reducing the phase shift toward zero. The effect becomes stronger the more ions are present at the plane, so the closer we are to the wall. At large frequencies, the oscillation amplitude is very small and the current is constituted by the ions freely oscillating in the field; thus, also in this limit the phase grows toward zero.

A discussion of the effect of short-range electrostatic correlations on the impedance response based on the usage of the more sophisticated density functional from ref 74 is included in the Supporting Information.

Current Components. To better understand the effect of ion interaction on the current, we separate the flow into contributions corresponding to the different energy terms in eq 2. In Figure 7, the flows caused by the external electric field, j_{el}, by the hard-sphere, j_{HS}, and Coulomb interaction, j_{Coul}, and the one due to diffusion of the ions, j_{diff}, are shown together with the total flow, j_{tot}, as a function of time for two different frequencies.

At the center (right column), the largest contribution to the total flow is always given by the flow due to the external electric field. Owing to the moderate density at this position, the hard-sphere interaction term is negligible. At high frequencies, the ions are freely following the electric field with a small amplitude oscillation around their position. The oscillation is in phase with the external electric field and the effect of the interaction terms is minute. For lower frequencies, however, the amplitude of the oscillatory motion becomes larger and the ions feel their neighbors via their Coulomb potential. Together with the diffusive flow, the Coulomb effect counteracts the particle oscillation induced by the electric field, resulting in a phase-shifted total flow j_{tot}.

Close to the wall, and at low frequencies, there are three main components that enter the total flow. These are given by hard-sphere interaction, diffusion, and external field term. The external electric field causes high densities near the walls for which the hard-sphere interaction becomes important. Additionally, the high-density gradient close to the walls causes a strong diffusive flow. The electric field and hard-sphere terms lead to charge flows in the same direction, pushing the ions against the wall. This flow is countered by the diffusive flow, which works against the formation of the accompanying density gradient. The different contributions show large anharmonicity, and the resulting current is tiny. At high frequencies, the current contributions are harmonic and the hard-sphere flow term is reduced due to the smaller oscillation amplitude.

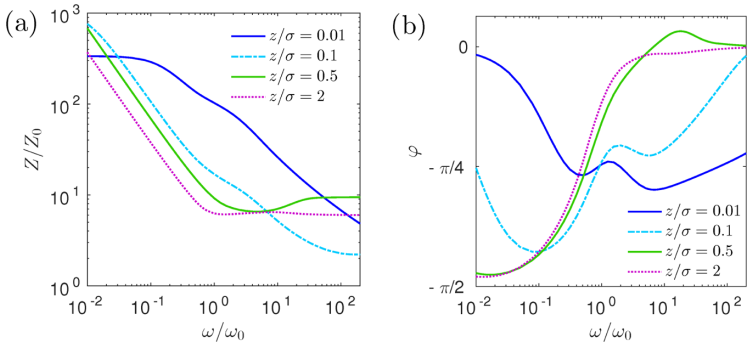

Figure 6. Impedance Z (a) and phase φ (b) as functions of frequency for different positions z between the plates. The frequency-dependent impedance changes qualitatively when approaching the wall. The parameters are $L/\sigma = 4$, $U^* = 38.9$.

DOI: 10.1021/acs.jpcc.8b05559
J. Phys. Chem. C 2018, 122, 21724−21734

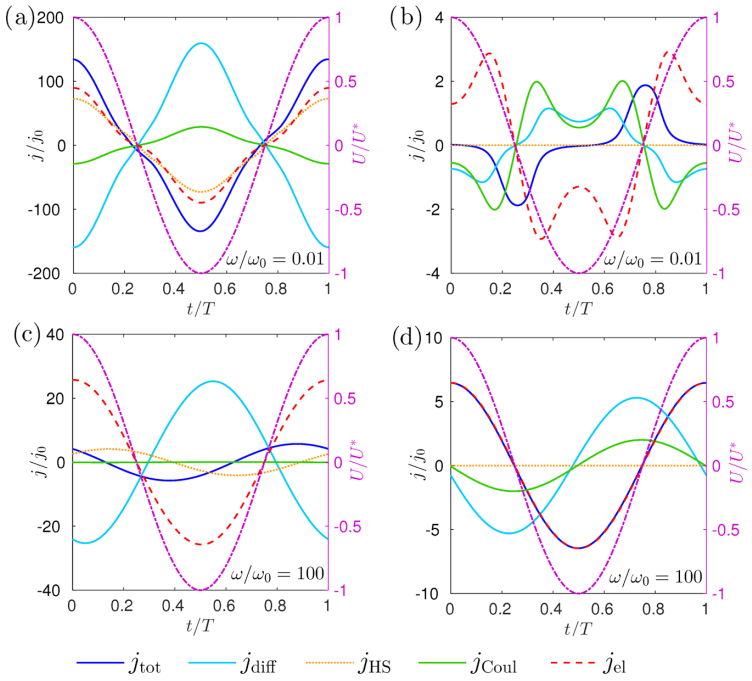

Figure 7. Contributions of the different flow terms to the system response for a system of length $L/\sigma = 4$ near the wall (a, c) ($z/\sigma = 0.01$) and at the center (b, d) ($z/\sigma = 2$). The contributions to the currents show considerable anharmonicity at small frequencies (upper row), which disappears at high frequencies (lower row). The effect of particle interaction grows for high densities close to the wall as well as for small frequencies. For better visibility, the current components have been scaled in (a) $j_{tot} \times 1000$, $j_{Coul} \times 10$, (b) $j_{tot} \times 10$, and (d) $j_{diff} \times 100$, $j_{HS} \times 100$, $j_{Coul} \times 100$. For reference, the voltage $U(t)$ is plotted against the right y axis.

CONCLUSIONS

We have explored by dynamic density functional theory the effect of an alternating voltage on a symmetric binary electrolyte confined between plan-parallel capacitor plates. This nonlinear theory provides a unifying framework to include steric interactions between ions and their drift dynamics induced by the AC electric field. It thus significantly generalizes previous approaches based on Poisson−Nernst−Planck theory. Besides the dynamical layering of the driven ions near the confining walls, we predict a resonance effect of the impedance, which can be traced back to a simple single-ion effect, but is modified by Coulomb and steric interactions. This effect becomes relevant in strong confinement and allows one to tune the electric response by confinement spacing, temperature, and external voltage applied. It was explored for two different realizations, both of vital importance to physical chemistry, namely, charged colloids and microions of nanometric size.

Future work should concentrate on the molecular details of the solvent as well as specific substrate properties like surface charges and roughness. In particular, reorientation and polarization effects of the liquid molecules and the impact of these effects on the capacitive ion response discussed here should be considered. Density functional theory can in fact be generalized toward solvent-ion mixtures[89,90] and more general external potentials. Modeling of electrode details can in principle be incorporated as well.

ASSOCIATED CONTENT

Supporting Information

The Supporting Information is available free of charge on the ACS Publications website at DOI: 10.1021/acs.jpcc.8b05559.

Comparison with modified functional from ref 74; current form for medium and low frequencies; contributions of higher harmonics in the current (PDF)

AUTHOR INFORMATION

Corresponding Author

*E-mail: hlowen@thphy.uni-duesseldorf.de. Phone: +49-211-81-11377. Fax: +49-211-81-10776.

ORCID

Sonja Babel: 0000-0002-7633-1493

Notes

The authors declare no competing financial interest.

ACKNOWLEDGMENTS

We thank Alexei A. Kornyshev and Andreas Härtel for helpful discussions. We gratefully acknowledge financial support by the DFG grant LO 418/19-1.

REFERENCES

(1) Jiang, D.-e.; Jin, Z.; Wu, J. Oscillation of Capacitance inside Nanopores. *Nano Lett.* **2011**, *11*, 5373−5377.

(2) Kornyshev, A. A. The Simplest Model of Charge Storage in Single File Metallic Nanopores. *Faraday Discuss.* **2013**, *164*, 117−133.

DOI: 10.1021/acs.jpcc.8b05559
J. Phys. Chem. C 2018, 122, 21724−21734

(3) Rochester, C. C.; Kondrat, S.; Pruessner, G.; Kornyshev, A. A. Charging Ultrananoporous Electrodes with Size-Asymmetric Ions Assisted by Apolar Solvent. *J. Phys. Chem. C* **2016**, *120*, 16042−16050.
(4) Kong, X.; Wu, J.; Henderson, D. Density Functional Theory Study of the Capacitance of Single File Ions in a Narrow Cylinder. *J. Colloid Interface Sci.* **2015**, *449*, 130−135.
(5) Leunissen, M. E.; Christova, C. G.; Hynninen, A.-P.; Royall, C. P.; Campbell, A. I.; Imhof, A.; Dijkstra, M.; van Roij, R.; van Blaaderen, A. Ionic Colloidal Crystals of Oppositely Charged Particles. *Nature* **2005**, *437*, 235−240.
(6) Demirörs, A. F.; Stiefelhagen, J. C. P.; Vissers, T.; Smallenburg, F.; Dijkstra, M.; Imhof, A.; van Blaaderen, A. Long-Ranged Oppositely Charged Interactions for Designing New Types of Colloidal Clusters. *Phys. Rev. X* **2015**, *5*, No. 021012.
(7) Würger, A. Transport in Charged Colloids Driven by Thermoelectricity. *Phys. Rev. Lett.* **2008**, *101*, No. 108302.
(8) Aricò, A. S.; Bruce, P.; Scrosati, B.; Tarascon, J.-M.; van Schalkwijk, W. Nanostructured Materials for Advanced Energy Conversion and Storage Devices. *Nat. Mater.* **2005**, *4*, 366−377.
(9) Montelongo, Y.; Sikdar, D.; Ma, Y.; McIntosh, A. J. S.; Velleman, L.; Kucernak, A. R.; Edel, J. B.; Kornyshev, A. A. Electrotunable Nanoplasmonic Liquid Mirror. *Nat. Mater.* **2017**, *16*, 1127−1135.
(10) Baughman, R. H.; Cui, C.; Zakhidov, A. A.; Iqbal, Z.; Barisci, J. N.; Spinks, G. M.; Wallace, G. G.; Mazzoldi, A.; De Rossi, D.; Rinzler, A. G.; et al. Carbon Nanotube Actuators. *Science* **1999**, *284*, 1340−1344.
(11) Kornyshev, A. A.; Twidale, R. M.; Kolomeisky, A. B. Current-Generating Double-Layer Shoe with a Porous Sole: Ion Transport Matters. *J. Phys. Chem. C* **2017**, *121*, 7584−7595.
(12) Porada, S.; Zhao, R.; van der Wal, A.; Presser, V.; Biesheuvel, P. Review on the Science and Technology of Water Desalination by Capacitive Deionization. *Prog. Mater. Sci.* **2013**, *58*, 1388−1442.
(13) Biesheuvel, P. M.; Bazant, M. Z. Nonlinear Dynamics of Capacitive Charging and Desalination by Porous Electrodes. *Phys. Rev. E* **2010**, *81*, No. 031502.
(14) Härtel, A.; Janssen, M.; Samin, S.; van Roij, R. Fundamental Measure Theory for the Electric Double Layer: Implications for Blue-Energy Harvesting and Water Desalination. *J. Phys.: Condens. Matter* **2015**, *27*, No. 194129.
(15) Evans, R.; Oettel, M.; Roth, R.; Kahl, G. New Developments in Classical Density Functional Theory. *J. Phys.: Condens. Matter* **2016**, *28*, No. 240401.
(16) Archer, A. J.; Evans, R. Dynamical Density Functional Theory and Its Application to Spinodal Decomposition. *J. Chem. Phys.* **2004**, *121*, 4246−4254.
(17) Español, P.; Löwen, H. Derivation of Dynamical Density Functional Theory Using the Projection Operator Technique. *J. Chem. Phys.* **2009**, *131*, No. 244101.
(18) Marconi, U. M. B.; Tarazona, P. Dynamic Density Functional Theory of Fluids. *J. Chem. Phys.* **1999**, *110*, 8032−8044.
(19) Royall, C. P.; Leunissen, M. E.; van Blaaderen, A. A New Colloidal Model System to Study Long-Range Interactions Quantitatively in Real Space. *J. Phys.: Condens. Matter* **2003**, *15*, S3581−S3596.
(20) Vissers, T.; Wysocki, A.; Rex, M.; Lowen, H.; Royall, C. P.; Imhof, A.; van Blaaderen, A. Lane Formation in Driven Mixtures of Oppositely Charged Colloids. *Soft Matter* **2011**, *7*, 2352−2356.
(21) Vissers, T.; van Blaaderen, A.; Imhof, A. Band Formation in Mixtures of Oppositely Charged Colloids Driven by an ac Electric Field. *Phys. Rev. Lett.* **2011**, *106*, No. 228303.
(22) Saunders, B. R.; Vincent, B. Microgel Particles as Model Colloids: Theory, Properties and Applications. *Adv. Colloid Interface Sci.* **1999**, *80*, 1−25.
(23) Holmqvist, P.; Mohanty, P. S.; Nägele, G.; Schurtenberger, P.; Heinen, M. Structure and Dynamics of Loosely Cross-Linked Ionic Microgel Dispersions in the Fluid Regime. *Phys. Rev. Lett.* **2012**, *109*, No. 048302.
(24) Lemay, S. G.; Kang, S.; Mathwig, K.; Singh, P. S. Single-Molecule Electrochemistry. *Acc. Chem. Res.* **2013**, *46*, 369−377.
(25) Catalano, J.; Biesheuvel, P. AC-Driven Electro-Osmotic Flow in Charged Nanopores 2018, arXiv:1805.10845. arXiv.org e-Printarchive. https://arxiv.org/abs/1805.10845 (accessed May 28, 2018).
(26) Gouy, M. Sur la Constitution de la Charge Electrique à la Surface d'un Electrolyte. *J. Phys. Theor. Appl.* **1910**, *9*, 457−468.
(27) Chapman, D. L. LI. A Contribution to the Theory of Electrocapillarity. *London, Edinburgh Dublin Philos. Mag. J. Sci.* **1913**, *25*, 475−481.
(28) Bikerman, J. XXXIX. Structure and Capacity of Electrical Double Layer. *London, Edinburgh Dublin Philos. Mag. J. Sci.* **1942**, *33*, 384−397.
(29) Borukhov, I.; Andelman, D.; Orland, H. Steric Effects in Electrolytes: A Modified Poisson-Boltzmann Equation. *Phys. Rev. Lett.* **1997**, *79*, 435−438.
(30) Kornyshev, A. A. Double-Layer in Ionic Liquids: Paradigm Change? *J. Phys. Chem. B* **2007**, *111*, 5545−5557.
(31) Burger, M.; Schlake, B.; Wolfram, M.-T. Nonlinear Poisson-Nernst-Planck Equations for Ion Flux through Confined Geometries. *Nonlinearity* **2012**, *25*, 961−990.
(32) Siddiqua, F.; Wang, Z.; Zhou, S. A Modified Poisson-Nernst-Planck Model with Excluded Volume Effect: Theory and Numerical Implementation 2017, arxiv:1801.00751. arXiv.org e-Printarchive. https://arxiv.org/abs/1801.00751 (accessed Nov 2, 2013).
(33) Meng, D.; Zheng, B.; Lin, G.; Sushko, M. L. Numerical Solution of 3D Poisson-Nernst-Planck Equations Coupled with Classical Density Functional Theory for Modeling Ion and Electron Transport in a Confined Environment. *Commun. Comput. Phys.* **2014**, *16*, 1298−1322.
(34) Qiao, Y.; Liu, X.; Chen, M.; Lu, B. A Local Approximation of Fundamental Measure Theory Incorporated into Three Dimensional Poisson-Nernst-Planck Equations to Account for Hard Sphere Repulsion Among Ions. *J. Stat. Phys.* **2016**, *163*, 156−174.
(35) Jiang, J.; Cao, D.; en Jiang, D.; Wu, J. Time-Dependent Density Functional Theory for Ion Diffusion in Electrochemical Systems. *J. Phys.: Condens. Matter* **2014**, *26*, No. 284102.
(36) Lian, C.; Zhao, S.; Liu, H.; Wu, J. Time-Dependent Density Functional Theory for the Charging Kinetics of Electric Double Layer Containing Room-Temperature Ionic Liquids. *J. Chem. Phys.* **2016**, *145*, No. 204707.
(37) Gongadze, E.; Iglič, A. Asymmetric Size of Ions and Orientational Ordering of Water Dipoles in Electric Double Layer Model - an Analytical Mean-Field Approach. *Electrochim. Acta* **2015**, *178*, 541−545.
(38) Beunis, F.; Strubbe, F.; Marescaux, M.; Beeckman, J.; Neyts, K.; Verschueren, A. R. M. Dynamics of Charge Transport in Planar Devices. *Phys. Rev. E* **2008**, *78*, No. 011502.
(39) Olesen, L. H.; Bazant, M. Z.; Bruus, H. Strongly Nonlinear Dynamics of Electrolytes in Large AC Voltages. *Phys. Rev. E* **2010**, *82*, No. 011501.
(40) Feicht, S. E.; Frankel, A. E.; Khair, A. S. Discharging Dynamics in an Electrolytic Cell. *Phys. Rev. E* **2016**, *94*, No. 012601.
(41) Levin, Y. Electrostatic Correlations: From Plasma to Biology. *Rep. Prog. Phys.* **2002**, *65*, 1577−1632.
(42) Fisher, M. E.; Levin, Y. Criticality in Ionic Fluids: Debye-Hückel Theory, Bjerrum, and Beyond. *Phys. Rev. Lett.* **1993**, *71*, 3826−3829.
(43) van Roij, R.; Hansen, J.-P. Van der Waals−Like Instability in Suspensions of Mutually Repelling Charged Colloids. *Phys. Rev. Lett.* **1997**, *79*, 3082−3085.
(44) Kornyshev, A. A.; Vilfan, I. Phase Transitions at the Electrochemical Interface. *Electrochim. Acta* **1995**, *40*, 109−127.
(45) Kornyshev, A. A.; Qiao, R. Three-Dimensional Double Layers. *J. Phys. Chem. C* **2014**, *118*, 18285−18290.
(46) Messina, R.; Holm, C.; Kremer, K. Strong Attraction between Charged Spheres due to Metastable Ionized States. *Phys. Rev. Lett.* **2000**, *85*, 872−875.

DOI: 10.1021/acs.jpcc.8b05559
J. Phys. Chem. C 2018, 122, 21724−21734

(47) Lobaskin, V.; Dünweg, B.; Medebach, M.; Palberg, T.; Holm, C. Electrophoresis of Colloidal Dispersions in the Low-Salt Regime. *Phys. Rev. Lett.* **2007**, *98*, No. 176105.
(48) Fennell, C. J.; Bizjak, A.; Vlachy, V.; Dill, K. A. Ion Pairing in Molecular Simulations of Aqueous Alkali Halide Solutions. *J. Phys. Chem. B* **2009**, *113*, 6782−6791.
(49) Girotto, M.; dos Santos, A. P.; Levin, Y. Simulations of Ionic Liquids Confined by Metal Electrodes Using Periodic Green Functions. *J. Chem. Phys.* **2017**, *147*, No. 074109.
(50) Bazant, M. Z.; Thornton, K.; Ajdari, A. Diffuse-Charge Dynamics in Electrochemical Systems. *Phys. Rev. E* **2004**, *70*, No. 021506.
(51) Bazant, M. Z.; Kilic, M. S.; Storey, B. D.; Ajdari, A. Towards an Understanding of Induced-Charge Electrokinetics at Large Applied Voltages in Concentrated Solutions. *Adv. Colloid Interface Sci.* **2009**, *152*, 48−88.
(52) Härtel, A.; Kohl, M.; Schmiedeberg, M. Anisotropic Pair Correlations in Binary and Multicomponent Hard-Sphere Mixtures in the Vicinity of a Hard Wall: A Combined Density Functional Theory and Simulation Study. *Phys. Rev. E* **2015**, *92*, No. 042310.
(53) Härtel, A.; Samin, S.; van Roij, R. Dense Ionic Fluids Confined in Planar Capacitors: On- and Out-of-Plane Structure from Classical Density Functional Theory. *J. Phys.: Condens. Matter* **2016**, *28*, No. 244007.
(54) Härtel, A. Structure of Electric Double Layers in Capacitive Systems and to what Extent (Classical) Density Functional Theory Describes It. *J. Phys.: Condens. Matter* **2017**, *29*, No. 423002.
(55) Gillespie, D. A Review of Steric Interactions of ions: Why Some Theories Succeed and Others Fail to Account for Ion Size. *Microfluid. Nanofluid.* **2015**, *18*, 717−738.
(56) Härtel, A.; Janssen, M.; Weingarth, D.; Presser, V.; van Roij, R. Heat-to-Current Conversion of Low-Grade Heat from a Thermocapacitive Cycle by Supercapacitors. *Energy Environ. Sci.* **2015**, *8*, 2396−2401.
(57) Orkoulas, G.; Panagiotopoulos, A. Z. Phase behavior of the Restricted Primitive Model and Square-Well Fluids from Monte Carlo Simulations in the Grand Canonical Ensemble. *J. Chem. Phys.* **1999**, *110*, 1581−1590.
(58) Luijten, E.; Fisher, M. E.; Panagiotopoulos, A. Z. Universality Class of Criticality in the Restricted Primitive Model Electrolyte. *Phys. Rev. Lett.* **2002**, *88*, No. 185701.
(59) Yan, Q.; de Pablo, J. J. Hyper-Parallel Tempering Monte Carlo: Application to the Lennard-Jones Fluid and the Restricted Primitive Model. *J. Chem. Phys.* **1999**, *111*, 9509−9516.
(60) Hynninen, A.-P.; Leunissen, M. E.; van Blaaderen, A.; Dijkstra, M. CuAu Structure in the Restricted Primitive Model and Oppositely Charged Colloids. *Phys. Rev. Lett.* **2006**, *96*, No. 018303.
(61) Panagiotopoulos, A. Z. Critical Parameters of the Restricted Primitive Model. *J. Chem. Phys.* **2002**, *116*, 3007−3011.
(62) Caillol, J.-M.; Levesque, D.; Weis, J.-J. Critical Behavior of the Restricted Primitive Model Revisited. *J. Chem. Phys.* **2002**, *116*, 10794−10800.
(63) Valleau, J.; Torrie, G. Heat Capacity of the Restricted Primitive Model near Criticality. *J. Chem. Phys.* **1998**, *108*, 5169−5172.
(64) de Carvalho, R. J. F. L.; Evans, R. Criticality of Ionic Fields: The Ginzburg Criterion for the Restricted Primitive Model. *J. Phys.: Condens. Matter* **1995**, *7*, L575−L583.
(65) Smit, B.; Esselink, K.; Frenkel, D. Solid-Solid and Liquid-Solid Phase Equilibria for the Restricted Primitive Model. *Mol. Phys.* **1996**, *87*, 159−166.
(66) Alts, T.; Nielaba, P.; D'Aguanno, B.; Forstmann, F. A Local Density Functional Approximation for the Ion Distribution Near a Charged Electrode in the Restricted Primitive Model Electrolyte. *Chem. Phys.* **1987**, *111*, 223−240.
(67) Hansen, J.-P.; Löwen, H. Effective Interactions Between Electric Double Layers. *Annu. Rev. Phys. Chem.* **2000**, *51*, 209−242.
(68) Evans, R. The Nature of the Liquid-Vapour Interface and Other Topics in the Statistical Mechanics of Non-Uniform, Classical Fluids. *Adv. Phys.* **1979**, *28*, 143−200.
(69) Gillespie, D.; Nonner, W.; Eisenberg, R. S. Coupling Poisson-Nernst-Planck and Density Functional Theory to Calculate Ion Flux. *J. Phys.: Condens. Matter* **2002**, *14*, 12129.
(70) Gillespie, D.; Nonner, W.; Eisenberg, R. S. Density Functional Theory of Charged, Hard-Sphere Fluids. *Phys. Rev. E* **2003**, *68*, No. 031503.
(71) Gillespie, D.; Valiskó, M.; Boda, D. Density Functional Theory of the Electrical Double Layer: The RFD Functional. *J. Phys.: Condens. Matter* **2005**, *17*, 6609−6626.
(72) Gillespie, D. Free-Energy Density Functional of Ions at a Dielectric Interface. *J. Phys. Chem. Lett.* **2011**, *2*, 1178−1182.
(73) Roth, R.; Gillespie, D. Physics of Size Selectivity. *Phys. Rev. Lett.* **2005**, *95*, No. 247801.
(74) Roth, R.; Gillespie, D. Shells of Charge: A Density Functional Theory for Charged Hard Spheres. *J. Phys.: Condens. Matter* **2016**, *28*, No. 244006.
(75) Patra, C. N.; Ghosh, S. K. A Nonlocal Density Functional Theory of Electric Double Layer: Symmetric Electrolytes. *J. Chem. Phys.* **1994**, *100*, 5219−5229.
(76) Patra, C. N.; Ghosh, S. K. A Nonlocal Density-Functional Theory of Electric Double Layer: Charge-Asymmetric Electrolytes. *J. Chem. Phys.* **1994**, *101*, 4143−4149.
(77) Patra, C. N.; Ghosh, S. K. Density functional Approach to the Structure of Uniform Fluids. *J. Chem. Phys.* **1997**, *106*, 2762−2770.
(78) Patra, C. N.; Yethiraj, A. Density Functional Theory for the Distribution of Small Ions around Polyions. *J. Phys. Chem. B* **1999**, *103*, 6080−6087.
(79) Kierlik, E.; Rosinberg, M. L. Density-Functional Theory for Inhomogeneous Fluids: Adsorption of Binary Mixtures. *Phys. Rev. A* **1991**, *44*, 5025−5037.
(80) Hansen, J.; McDonald, I. *Theory of Simple Liquids*; Elsevier Science, 2006.
(81) Lipkowitz, K.; Boyd, D. *Reviews in Computational Chemistry*; Wiley, 2009.
(82) Tarazona, P. Density Functional for Hard Sphere Crystals: A Fundamental Measure Approach. *Phys. Rev. Lett.* **2000**, *84*, 694−697.
(83) Rosenfeld, Y. Free-Energy Model for the Inhomogeneous Hard-Sphere Fluid Mixture and Density-Functional Theory of Freezing. *Phys. Rev. Lett.* **1989**, *63*, 980−983.
(84) Roth, R. Fundamental Measure Theory for Hard-Sphere Mixtures: A Review. *J. Phys.: Condens. Matter* **2010**, *22*, No. 063102.
(85) Härtel, A. *Density Functional Theory of Hard Colloidal Particles: From Bulk to Interfaces*; Shaker: Aachen, 2013.
(86) Oettel, M.; Görig, S.; Härtel, A.; Löwen, H.; Radu, M.; Schilling, T. Free Energies, Vacancy Concentrations, and Density Distribution Anisotropies in Hard-Sphere Crystals: A Combined Density Functional and Simulation Study. *Phys. Rev. E* **2010**, *82*, No. 051404.
(87) Tyldesley, J. *An Introduction to Tensor Analysis for Engineers and Applied Scientists*; Longman, 1975.
(88) Chaudhuri, M.; Allahyarov, E.; Löwen, H.; Egelhaaf, S. U.; Weitz, D. A. Triple Junction at the Triple Point Resolved on the Individual Particle Level. *Phys. Rev. Lett.* **2017**, *119*, No. 128001.
(89) Oleksy, A.; Hansen, J.-P. Microscopic Density Functional Theory of Wetting and Drying of a Solid Substrate by an Explicit Solvent Model of Ionic Solutions. *Mol. Phys.* **2009**, *107*, 2609−2624.
(90) Medasani, B.; Ovanesyan, Z.; Thomas, D. G.; Sushko, M. L.; Marucho, M. Ionic Asymmetry and Solvent Excluded Volume Effects on Spherical Electric Double Layers: A Density Functional Approach. *J. Chem. Phys.* **2014**, *140*, No. 204510.

DOI: 10.1021/acs.jpcc.8b05559
J. Phys. Chem. C 2018, 122, 21724−21734

Supporting Information

Impedance Resonance in Narrow Confinement

Sonja Babel, Institut für Theoretische Physik II: Weiche Materie, Heinrich-Heine-Universität Düsseldorf, Universitätsstraße 1, D-40225 Düsseldorf, Germany

Michael Eikerling, Department of Chemistry, Simon Fraser University, 8888 University Drive, Burnaby, British Columbia, Canada V5A 1S6

Hartmut Löwen, Institut für Theoretische Physik II: Weiche Materie, Heinrich-Heine-Universität Düsseldorf, Universitätsstraße 1, D-40225 Düsseldorf, Germany

S1 Comparison with modified functional

Here, we discuss the change in our data for the density profiles and impedance upon using the more sophisticated functional proposed in Ref. [74]. The density profile for the two different implementations of the functional are shown in fig. S1 with only minor discrepancies between the two curves. Fig. S2 shows the effect of the modified functional on the impedance response in the system. While some differences are found for small frequencies of the applied AC voltage and close to the confining walls, no qualitative changes are observed.

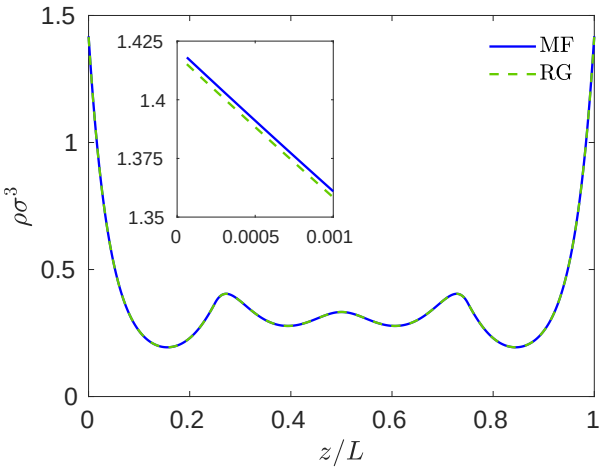

Figure S1: Density profile in the case of no external voltage for the Coulomb mean-field approach (MF) used here and the modified functional introduced by Roth and Gillespie (RG) in Ref. [74].

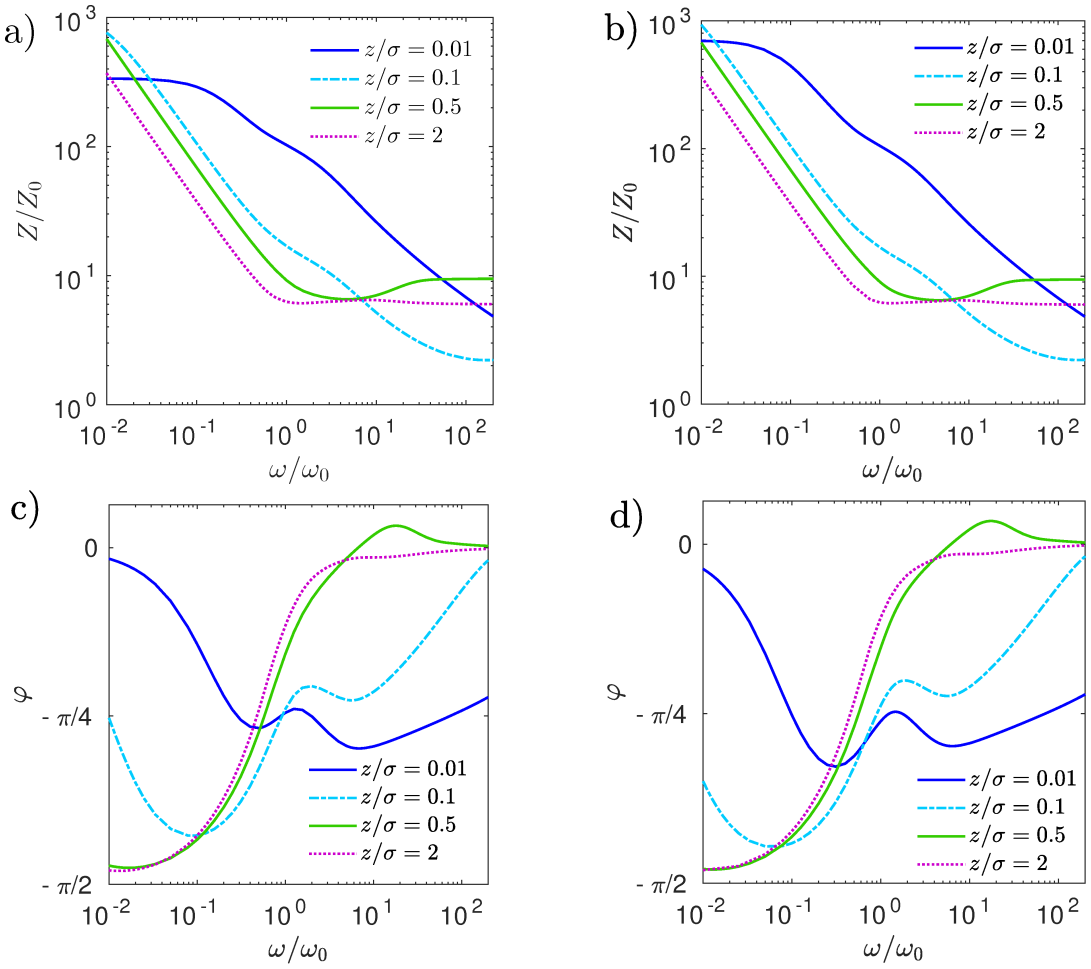

Figure S2: Impedance response as given in fig. 6 for the Coulomb mean-field approach used here (left) and the modified functional introduced in Ref. [74] (right).

S2 Non-interacting ions for negligible thermal motion: Low and medium frequency current

Here, we discuss the ion motion at low and medium frequencies. The position of the ions in the case without walls is

$$z(t) = z_0 + \frac{qE_0}{\omega\gamma}\sin(\omega t)\,. \tag{S1}$$

In the low frequency limit the length that the ions travel is larger than the system length, $d_{\mathrm{tr}} = 2qE_0/\omega\gamma > L$, and the effect of the walls needs to be taken into account. All ions hit the wall at some time and stay there until the field reverses. Though all ions may start at different points z_0, during the first oscillation all get stuck at the wall and start moving away from it at the same time, thus ending up in the same oscillation mode. The equation for this mode over

one period $T = 2\pi/\omega$ is given by

$$z(t) = \begin{cases} \frac{d_{\mathrm{tr}}}{2}\left(\sin\left(\omega t\right)+1\right) & \text{for } t_0 \le t < t_1 \\ L & \text{for } t_1 \le t < t_2 \\ L + \frac{d_{\mathrm{tr}}}{2}\left(\sin\left(\omega t\right)-1\right) & \text{for } t_2 \le t < t_3 \\ 0 & \text{for } t_3 \le t < t_0 + T \end{cases} \tag{S2}$$

with $t_0 = -T/4$, $t_1 = \arcsin\left(2L/d_{\mathrm{tr}} - 1\right)/\omega$, $t_2 = T/4$ and $t_3 = t_1 + T/2$. The current density in the middle of the system produced by the ions is then

$$j(z = L/2, t) = q\omega L\rho_0\left[\delta\left(\omega\left(t - t'\right)\right) - \delta\left(\omega\left(t - t''\right)\right)\right] \propto \omega \tag{S3}$$

with the two times $t' = \left(\arcsin\left(\frac{L}{d_{\mathrm{tr}}} - 1\right)\right)/\omega$ and $t'' = t' + T/2$ at which the ions cross the centre of the system. From this we can also extract the phase of the impedance

$$\varphi = 2\pi\frac{t'}{T} = \arcsin\left(\frac{L}{d_{\mathrm{tr}}} - 1\right) \tag{S4}$$

which is limited by the two cases $\varphi = -\pi/2$ for $d_{\mathrm{tr}} \to \infty$ or $\omega \to 0$ and $\varphi = 0$ for $d_{\mathrm{tr}} = L$ or $\omega = 2qE_0/\gamma L$. The peaked current form of eq. (S3) is broadened due to diffusion and interaction but still persists, see fig. 3.

At medium frequencies, where $L/2 \le d_{\mathrm{tr}} \le L$ and $\frac{4qE_0}{\gamma L} \ge \omega \ge \frac{2qE_0}{\gamma L}$, both the ions stuck at the wall and the freely oscillating ones reach the midplane of the system. The complete current given as a superposition of these two contributions is

$$\begin{aligned} j(L/2, t) = \frac{q^2E_0}{\gamma}\rho_0\Bigg[& \cos\left(\omega t\right)\left[\theta\left(t + t'\right)\theta\left(t' - t\right) + \theta\left(t - \tilde{t}''\right)\theta\left(T - \tilde{t}'' - t\right)\right] \\ & + \delta\left(\omega\left(t + t'\right)\right) + \delta\left(\omega\left(t' - t\right)\right) - \delta\left(\omega\left(t - \tilde{t}''\right)\right) - \delta\left(\omega\left(T - \tilde{t}'' - t\right)\right)\Bigg] \end{aligned} \tag{S5}$$

for $-T/4 \le t < 3T/4$ and the new second passing time $\tilde{t}'' = T/2 - t'$. The current in this simplified picture is thus a cut-off (with respect to time) oscillatory part with four additional peaks. While the ions that oscillate freely in the middle of the system without hitting the wall constitute the oscillatory part, ions that hit the wall all cross the plane at the same time and thus appear as current peaks at the passage time t' and return time $\tilde{t}''$ or times $-\tilde{t}''$ and $-t'$ respectively for the opposite wall. In between the passing and returning, there are no more ions left that could cross and thus there is no current.

S3 Higher harmonics

Here, we consider the effect of non-linearity in the system. From the time-dependent current, see fig. 7, we find a considerable amount of anharmonicity especially at small frequencies. To quantify this effect, we compare the amplitude of the main signal j_1 with the higher frequency contributions to j. From the symmetry of the system, which is composed of equal concentrations of oppositely charged identically sized particles, we find that $j(t + T/2) = -j(t)$ must hold. A direct consequence of this constraint is that only odd harmonics exist. Fig. S3 shows the amplitudes of the first, third and fifth harmonics. The contribution of the first harmonic is always dominating though the third harmonic rises to as much as ten percent of its value. For high frequencies the amplitude of the higher harmonics drops to less than one percent.

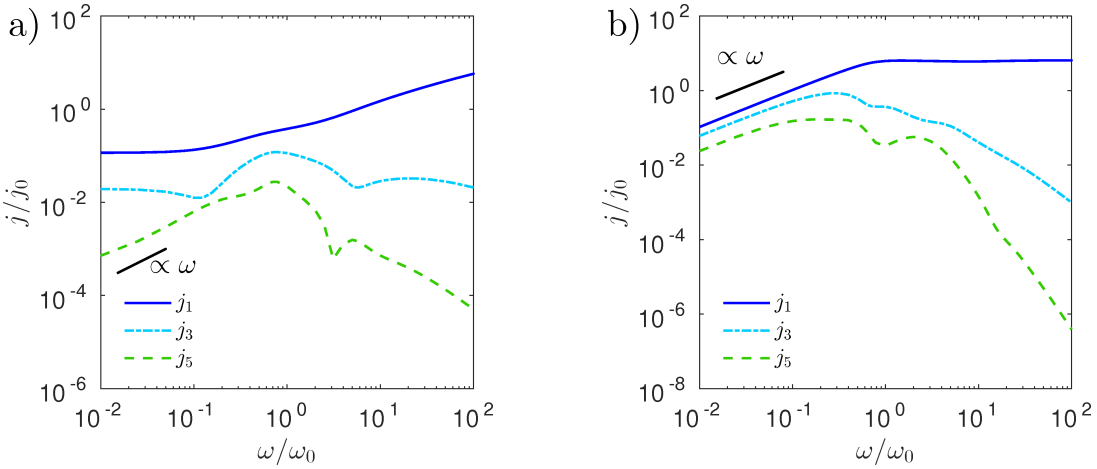

Figure S3: Amplitudes of the first (j_1), third (j_3) and fifth (j_5) harmonic close to the wall (a) ($z/\sigma = 0.01$) and at the centre (b) ($z/\sigma = 2.$). While at the centre of the system all harmonics show the expected proportionality to the frequency for small ω, close to the wall, the first two harmonics take a constant value. The parameters are $L/\sigma = 4$, $U^* = 38.9$.

References

[74] Roth, R.; Gillespie, D. Shells of Charge: A Density Functional Theory for Charged Hard Spheres. *J. Phys. Condens. Matter* **2016**, *28*, 244006

Appendix

Weight functions in effective 1D

The system considered in Chapter 2 (Publication I) is described as an effectively one-dimensional system. Since in this case $\rho(\mathbf{r},t) \equiv \rho(z,t)$, eq. (9) can be further simplified by integrating out the additional spatial directions. The involved volume integral can thereby be reduced to a one-dimensional integral over one particle diameter, considerably lightening the numerical effort. The weighted densities can be rewritten as

$$\begin{aligned} n_\alpha(\mathbf{r},t) &= \int \mathrm{d}\mathbf{r}\,'\rho(\mathbf{r}\,')\,\omega^{(\alpha)}(\mathbf{r}-\mathbf{r}') \\ &= \int \mathrm{d}z'\rho(z')\int \mathrm{d}x'\int \mathrm{d}y'\omega^{(\alpha)}(\mathbf{r}-\mathbf{r}') = \int_{z-R}^{z+R}\mathrm{d}z' W_i^{(\alpha)}(z-z')\,\rho(z') \end{aligned} \tag{2.1}$$

with the modified weight functions [283] given by

$$W_i^{(2)} = 2\pi R\,, \tag{2.2}$$

$$W_i^{(3)} = \pi\left(R^2-(z-z')^2\right)\,, \tag{2.3}$$

$$\mathbf{W}_i^{(2)} = (z-z')\,2\pi\hat{e}_z\,, \tag{2.4}$$

$$\overleftrightarrow{W}_i^{(2)} = 2\pi R\begin{pmatrix} \frac{1}{6}-\frac{(z-z')2}{2R^2} & 0 & 0 \\ 0 & \frac{1}{6}-\frac{(z-z')2}{2R^2} & 0 \\ 0 & 0 & -\frac{1}{3}+\frac{(z-z')2}{R^2} \end{pmatrix}\,. \tag{2.5}$$

$$\tag{2.6}$$

Derivatives of the energy functional

For completeness, the derivatives of the energy functional are also given. These are necessary for the calculation of the temporal evolution of the density field and read

$$\begin{aligned} \frac{\partial\Phi_1^{\mathrm{WBII}}}{\partial n_2} &= -\frac{1}{4\pi R^2}\ln(1-n_3) \\ \frac{\partial\Phi_1^{\mathrm{WBII}}}{\partial n_3} &= -\frac{n_2}{4\pi R^2}\frac{1}{1-n_3} \\ \frac{\partial\Phi_2^{\mathrm{WBII}}}{\partial n_2} &= \frac{n_2}{2\pi R}\frac{1+\frac{1}{3}\phi_2(n_3)}{1-n_3} \\ \frac{\partial\Phi_2^{\mathrm{WBII}}}{\partial n_3} &= \frac{1}{4\pi R}\left(n_2^2-\mathbf{n}_2\cdot\mathbf{n}_2\right)\frac{1}{1-n_3}\left[\frac{1+\frac{1}{3}\phi_2(n_3)}{1-n_3}+\frac{1}{3}\frac{\partial\phi_2}{\partial n_3}\right] \\ \frac{\partial\Phi_2^{\mathrm{WBII}}}{\partial \mathbf{n}_2} &= -\frac{1}{4\pi R}\left(-2\mathbf{n}_2^t\right)\frac{1+\frac{1}{3}\phi_2(n_3)}{1-n_3} \end{aligned}$$

$$
\begin{aligned}
\frac{\partial \Phi_3^{\mathrm{WBII}}}{\partial n_2} &= \left(3n_2^2 - 3\mathbf{n}_2 \cdot \mathbf{n}_2\right) \frac{1 - \frac{1}{3} n_3 \phi_3\left(n_3\right)}{24\pi \left(1 - n_3\right)^2} \\
\frac{\partial \Phi_3^{\mathrm{WBII}}}{\partial n_3} &= \left(n_2^3 - 3n_2 \mathbf{n}_2 \cdot \mathbf{n}_2 + \frac{9}{2}\left(\mathbf{n}_2 \overleftrightarrow{n}_2 \mathbf{n}_2 - \mathrm{Tr}\left(\overleftrightarrow{n}_{m_2}^3\right)\right)\right) \\
&\qquad \times \left[\frac{1 - \frac{1}{3} n_3 \phi_3\left(n_3\right)}{12\pi \left(1 - n_3\right)^3} - \frac{\left(\phi_3\left(n_3\right) + n_3 \frac{\partial \phi_3\left(n_3\right)}{\partial n_3}\right)}{72\pi \left(1 - n_3\right)^2}\right] \\
\frac{\partial \Phi_3^{\mathrm{WBII}}}{\partial \mathbf{n}_2} &= \left(-6n_2 \mathbf{n}_2^t + 9\left(\overleftrightarrow{n}_{m_2} \mathbf{n}_2\right)^t\right) \frac{1 - \frac{1}{3} n_3 \phi_3\left(n_3\right)}{24\pi \left(1 - n_3\right)^2} \\
\frac{\partial \Phi_3^{\mathrm{WBII}}}{\partial \overleftrightarrow{n}_{m_2}} &= \left(\frac{9}{2}\left(\mathbf{n}_2 \mathbf{n}_2^t - 3\left(\overleftrightarrow{n}_{m_2}\right)^2\right)\right) \frac{1 - \frac{1}{3} n_3 \phi_3\left(n_3\right)}{24\pi \left(1 - n_3\right)^2},
\end{aligned}
$$

where

$$
\begin{aligned}
\frac{\partial \phi_2}{\partial n_3} &= -1 - \frac{2}{n_3}\left(1 + \frac{1}{n_3}\ln\left(1 - n_3\right)\right) \\
\frac{\partial \phi_3}{\partial n_3} &= 2 + \frac{2}{n_3} - \frac{4}{n_3^2} - 4\frac{1 - n_3}{n_3^2} - 4\frac{1 - n_3}{n_3^3}\ln\left(1 - n_3\right).
\end{aligned}
$$

Chapter 3

Feedback-driven colloids

In this Chapter, the effect of a feedback potential on a single colloidal particle (Sec. 3.1) and a suspension of N colloidal particles (Publication II) confined to two dimensions is investigated. The case of a single colloidal particle is first considered for a harmonic feedback potential. The harmonic potential form has the advantage of allowing for analytic solutions, although the exact full solution of the time evolution is currently beyond reach [259] and is investigated numerically here. Previous studies have focused on finding stationary solutions to the delayed harmonic potential [284, 285] but additional approximations are needed such as assuming a small delay time [264] or an additional confining potential [261]. Other studies have found solutions for special cases: For a feedback force depending solely on the delayed position, a solution can be formulated in terms of the Laplace transform [286]. Alternatively, in the case of vanishing noise, a simple expression can be obtained [287].

In addition, the case of a Gaussian feedback potential is investigated numerically for the one-particle case. The same feedback potential form is used for the many-particle system in Publication II. In this publication, we show that delay in systems of passive building blocks can lead to propulsion and traveling-band formation.

3.1 Single-particle dynamics

To gain some insight into the effect of the feedback potential, the system is first investigated on the basis of Langevin eq. (1.8) for the dilute limit, i.e., $N = 1$. Without any additional external potential $\mathbf{F}_{\text{ext}} = 0$, the equation of motion for the particle is then simply given by

$$\gamma \frac{\mathrm{d}\mathbf{r}(t)}{\mathrm{d}t} = \mathbf{F}_{\text{fb}}\left(\mathbf{r}(t) - \mathbf{r}(t-\tau)\right) + \mathbf{f}(t)\,. \tag{3.1}$$

In Sec. 3.1.1, the effect of a harmonic feedback potential is considered, such that

$$\mathbf{F}_{\text{fb}}\left(\mathbf{r}\right) = \lambda \mathbf{r}\,. \tag{3.2}$$

However, to solve this case analytically, a further approximation with regard to the force updates is necessary. Two types of approximations are presented here: The

first one treats the forces as force kicks at discrete times that are multiples of the delay time τ. This picture leads to an anomalous effective short-time diffusion in the time-averaged MSD. However, in the opposite limit of long times, it reproduces the same long-time diffusion constant as the exact equation of motion. The second approximation considers continuous feedback forces but prescribes again discrete update times as multiples of τ, cf. also Fig. 1.2. Finally, as a third case, the exact solution of eq. (3.1) is obtained numerically and compared to the approximative analytic solutions.

While the harmonic potential is convenient for finding analytic solutions and allows to study the qualitative change in behavior due to the feedback, it is not a feasible scenario in experiments as it requires an infinitely increasing potential at farther distances. As a more realistic case, a numerical study of the case of a Gaussian feedback potential with continuous potential update leading to feedback forces

$$\mathbf{F}_{\mathrm{fb}}\left(\mathbf{r}\right) = \frac{A\mathbf{r}}{b^2}\mathrm{e}^{-r^2/2b^2}\,. \tag{3.3}$$

is presented in Sec. 3.1.2. This Gaussian shape is the default potential when using optical tweezers [169,288]. Moreover, in chemotactic systems, the concentration field of a diffusing chemo-attractant or chemo-repellent may also lead to a Gaussian potential profile [88].

3.1.1 Harmonic feedback potential

The harmonic potential form considered here allows for analytic solutions and constitutes a suitable approximation of more realistic potentials such as the Gaussian potential if the particle shows only small displacements from the potential minimum within a feedback time τ. The directional components of the particle position are independent in this case. The following discussion thus focuses on the one-dimensional problem

$$\gamma\frac{\mathrm{d}x(t)}{\mathrm{d}t} = \mathrm{F}_{\mathrm{fb}}\left(x(t) - x(t-\tau)\right) + \mathrm{f}(t)\,. \tag{3.4}$$

Force kicks at discrete times

The first approximation considers the driving force as force kicks at discrete times which are given by multiples of the feedback time τ. The time shift between the actual position and the past position used in the feedback forces is then always τ but the force is not always present. The force can be written as a summation over force kicks at times $n\tau$, where n is an integer number $n = 0, 1, 2, \ldots$, in the form

$$\mathrm{F}_{\mathrm{fb}}(t) = \sum_{n=-\infty}^{+\infty} \tilde{\mathrm{F}}(n\tau)\,\tau\,\delta\left(t - n\tau\right) \tag{3.5}$$

with the force-kick amplitude

$$\tilde{\mathrm{F}}(n\tau) = \lambda \left[x(n\tau^-) - x((n-1)\tau^-) \right] . \tag{3.6}$$

The superscript minus sign in eq. (3.6) indicates that the values should be taken before the force kick. The particle displacement between two times t_1 and t_2, with $t_1 \leq t_2$, is readily obtained by integration of eq. (3.4) as

$$x(t_2) - x(t_1) = \frac{1}{\gamma} \int_{t_1}^{t_2} \mathrm{d}t' \, \mathrm{F}_{\mathrm{fb}}(t') + \frac{1}{\gamma} \int_{t_1}^{t_2} \mathrm{d}t' \, \mathrm{f}(t') \, . \tag{3.7}$$

The required value of the feedback force peaks can be retrieved by recursive solution

$$\begin{aligned} \tilde{\mathrm{F}}(n\tau) = \lambda \left[x(n\tau^-) - x\left((n-1)\tau^-\right) \right] &= \frac{\lambda}{\gamma} \left[\int_{(n-1)\tau}^{n\tau} \mathrm{d}t \, \mathrm{f}(t) + \tau \, \tilde{\mathrm{F}}\left((n-1)\tau\right) \right] \\ = \cdots = \frac{1}{\tau} \sum_{i=1}^{\infty} \left(\frac{\lambda\tau}{\gamma} \right)^i \int_{(n-i)\tau}^{(n-i+1)\tau} \mathrm{d}t \, \mathrm{f}(t) &= \frac{1}{\tau} \sum_{i=1}^{\infty} \alpha^i \int_{(n-i)\tau}^{(n-i+1)\tau} \mathrm{d}t \, \mathrm{f}(t) \, , \end{aligned} \tag{3.8}$$

where $\alpha = \lambda\tau/\gamma$ is the dimensionless potential strength which is restricted to sensible cases $|\alpha| < 1$. Otherwise, the particle becomes increasingly fast ($\alpha > 1$) or overshoots its old position ($\alpha < -1$) and the dynamics is non-local in time. The expression for the force kicks, eq. (3.8), is independent of the particle positions and together with eqs. (3.5), (3.7) defines the solution for the particle trajectory.

All terms in the particle displacement then depend linearly on the Brownian noise $\mathrm{f}(t)$ such that the mean displacement vanishes,

$$\langle x(t_2) - x(t_1) \rangle = 0 \, , \tag{3.9}$$

where $\langle \cdots \rangle$ indicates a noise average over the random force $\mathrm{f}(t)$. Furthermore, since the displacement is given by a linear combination of Gaussian-distributed quantities (the random forces $\mathrm{f}(t)$), it is itself described by a Gaussian distribution [7]. In the case of linear feedback forces, the mean displacement and the mean square displacement thus fully determine the distribution. Here, the latter is given by

$$\begin{aligned} \left\langle \left(x(t_2) - x(t_1) \right)^2 \right\rangle = &\frac{1}{\gamma^2} \int_{t_1}^{t_2} \mathrm{d}t' \int_{t_1}^{t_2} \mathrm{d}t'' \langle \mathrm{f}(t') \mathrm{f}(t'') \rangle \\ &+ \frac{1}{\gamma^2} \int_{t_1}^{t_2} \mathrm{d}t' \int_{t_1}^{t_2} dt'' \langle \mathrm{F}_{\mathrm{fb}}(t') \mathrm{F}_{\mathrm{fb}}(t'') \rangle \\ &+ \frac{2}{\gamma^2} \int_{t_1}^{t_2} \mathrm{d}t' \int_{t_1}^{t_2} \mathrm{d}t'' \langle \mathrm{F}_{\mathrm{fb}}(t') \mathrm{f}(t'') \rangle \, . \end{aligned} \tag{3.10}$$

In systems subject to an instantaneous force that does not depend on the past position, the third term on the right vanishes. The peculiar nature of the feedback system,

i.e., the dependence of $\mathrm{F_{fb}}$ on the past position and thus on the noise $\mathrm{f}(t)$, leads to a non-vanishing third term and thereby to a linear correction $\propto \alpha$ in the square displacement. The respective terms are determined in the following. The first term

$$\int_{t_1}^{t_2} \mathrm{d}t' \int_{t_1}^{t_2} \mathrm{d}t'' \langle \mathrm{f}(t')\mathrm{f}(t'')\rangle = 2D\gamma^2 \int_{t_1}^{t_2} \mathrm{d}t' \int_{t_1}^{t_2} \mathrm{d}t'' \delta\left(t'-t''\right) = 2D\gamma^2\left(t_2-t_1\right) \quad (3.11)$$

describes the diffusion of the particle. The second term can be written as

$$\begin{aligned}\int_{t_1}^{t_2} \mathrm{d}t' \int_{t_1}^{t_2} \mathrm{d}t'' \langle \mathrm{F_{fb}}(t')\mathrm{F_{fb}}(t'')\rangle &= \tau^2 \sum_{n=k}^{l-1}\sum_{m=k}^{l-1} \langle \tilde{\mathrm{F}}(n\tau)\tilde{\mathrm{F}}(m\tau)\rangle \\ &= \frac{2D\gamma^2\alpha^2\tau}{\left(1-\alpha\right)^2}\left[(l-k) - \frac{2\alpha}{1-\alpha^2}\left(1-\alpha^{l-k}\right)\right], \quad (3.12)\end{aligned}$$

with k and l integer numbers defined such that $(k-1)\tau < t_1 \leq k\tau$ and $(l-1)\tau < t_2 \leq l\tau$ and the force kick correlations

$$\begin{aligned}\langle \tilde{\mathrm{F}}(n\tau)\tilde{\mathrm{F}}(m\tau)\rangle &= \frac{1}{\tau^2}\sum_{i=1}^{\infty}\sum_{j=1}^{\infty}\left(\frac{\lambda\tau}{\gamma}\right)^{i+j} \int_{(n-i)\tau}^{(n-i+1)\tau} \mathrm{d}t' \int_{(m-j)\tau}^{(m-j+1)\tau} \mathrm{d}t'' \langle \mathrm{f}(t')\mathrm{f}(t'')\rangle \\ &= \frac{2D\gamma^2}{\tau}\sum_{i=1}^{\infty}\sum_{j=1}^{\infty}\alpha^{i+j}\delta_{n-i,m-j} = \frac{2D\gamma^2}{\tau}\alpha^{|n-m|}\frac{\alpha^2}{1-\alpha^2}\,. \quad (3.13)\end{aligned}$$

The third term is obtained analogously as

$$\begin{aligned}\int_{t_1}^{t_2} \mathrm{d}t' \int_{t_1}^{t_2} \mathrm{d}t'' \langle \mathrm{F_{fb}}(t')\mathrm{f}(t'')\rangle &= \sum_{n=k}^{l-1}\sum_{i=1}^{\infty}\alpha^i \int_{t_1}^{t_2} \mathrm{d}t'' \int_{(n-i)\tau}^{(n-i+1)\tau} \mathrm{d}t' \,\langle \mathrm{f}(t')\mathrm{f}(t'')\rangle \\ &= \frac{2D\gamma^2\alpha}{1-\alpha}\left[\left(1-\alpha^{l-k}\right)\left(k\tau - t_1 - \frac{\tau}{1-\alpha}\right) + (l-k)\,\tau\right]. \quad (3.14)\end{aligned}$$

Setting $t_1 = t'$ and $t_2 = t'+t$, the solution for the mean square displacement, eq. (3.10), then reads

$$\begin{aligned}\left\langle \left(x(t'+t)-x(t')\right)^2\right\rangle =& 2Dt + 2D\frac{\alpha\left(2-\alpha\right)}{\left(1-\alpha\right)^2}(l-k)\tau \\ &- \frac{4D\alpha}{\left(1-\alpha\right)^2}\left[\tau - \left(1-\alpha\right)\left(1-\alpha^2\right)\left(k\tau - t'\right)\right]\frac{1-\alpha^{l-k}}{1-\alpha^2}\,. \quad (3.15)\end{aligned}$$

From this solution, we can differentiate the passive diffusion term, an additional diffusion-like term and an exponential term that can also be written as

$$\alpha^{l-k} = \mathrm{sgn}(\alpha^{l-k})\mathrm{e}^{(l-k)\ln|\alpha|} = \mathrm{sgn}(\alpha^{l-k})\mathrm{e}^{-(l-k)\tau/\tau_\alpha}\,. \quad (3.16)$$

This term thus decays on the time scale

$$\tau_\alpha = -\tau/\ln|\alpha| \tag{3.17}$$

and is associated with a loss of persistence in the forces, see eq. (3.13). The effect can be understood in the following way: A large displacement in the position between times $(n-1)\tau$ and $n\tau$ leads to a strong force kick at time $n\tau^-$, resulting in a large displacement of the position at time $(n+1)\tau$ compared to time $n\tau$ before the kick. The effect exponentially decreases on the time scale τ_α. The MSD bears a similarity to the one for a microswimmer, eq. (1.5), where diffusion in the swimming direction leads to a similar exponentially decaying term. The main difference between the two cases is that here, the time scale on which the decay takes place is connected to the strength of the driving force. Additionally, the leading order correction in the forces is linear and the effect of the feedback potential may lead to both an increase or a decrease in the mean square displacement depending on its sign. Interestingly, the mean square displacement not only depends on the time difference t and the number of feedback potential updates $l-k$ but also on the distance of the reference time t' to the next update time of the potential at $k\tau$. Therefore, the noise-averaged MSD $\langle(x(t'+t)-x(t'))^2\rangle$ is not identical to the time-averaged MSD $\langle(x(t'+t)-x(t'))^2\rangle_{t'}$ which is obtained for an additional average over t'. Thus, for a measurement of the MSD care needs to be taken in defining the measured quantity.

Examples of the mean square displacement in the case of attractive ($\alpha<0$) and repulsive forces ($\alpha>0$) are given in Fig. 3.1, illustrating the effect of the time offset $\Delta t' = k\tau - t'$. On time scales $t < \Delta t'$ the particle shows diffusion with diffusion constant D. Taking an average over the time-offset $\Delta t'$ in eq. (3.15) results in an effective short-time diffusion coefficient D_s given by

$$\frac{D_\mathrm{s}}{D} = \frac{1}{1-\alpha^2}\,, \tag{3.18}$$

that is unequal to the freely-diffusing case. This can be seen as an artifact of the force-kick description. At medium and long times, the behavior depends on the sign of the feedback potential. For a repulsive potential, the effective propulsion away from the former position leads to a $\propto t^2$ regime in the MSD and a long-time diffusion coefficient D_L which is higher than the free diffusion coefficient ($D_\mathrm{L} > D$). For attractive feedback potentials, the effect of the potential draws the particle back to its past position leading to a reduction in the MSD with minima at $t \approx 2n\tau$. The long time behavior is diffusive again, now with a diffusion coefficient $D_\mathrm{L} < D$. The diffusive regime at long times is in both cases caused by the loss of persistence in the forces and the long-time diffusion coefficient D_L is given by

$$\frac{D_\mathrm{L}}{D} = \lim_{t\to\infty}\frac{1}{2t}\langle(x(t'+t)-x(t'))^2\rangle = \frac{1}{(1-\alpha)^2}\,. \tag{3.19}$$

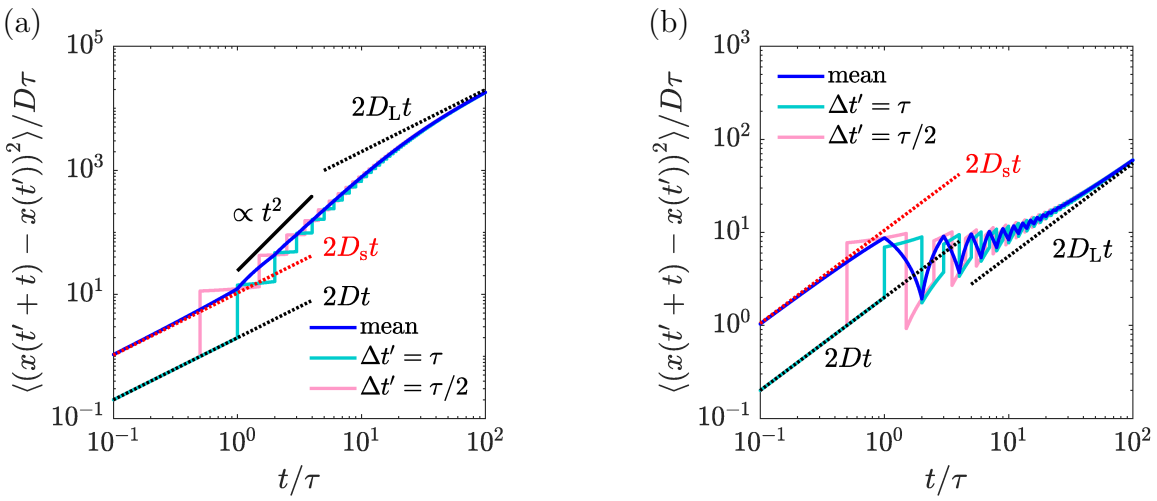

Figure 3.1: Analytic solution for force kicks with (a) $\alpha = 0.9$ and (b) $\alpha = -0.9$. Results are shown for different values of the time offset to the next feedback update $\Delta t'$ as well as the case of taking a mean over $\Delta t'$. The repulsive feedback potential ($\alpha > 0$) leads to a propulsion of the particle and a $\propto t^2$ behavior for medium times. The long-time diffusion coefficient is increased compared to the freely diffusing case. The attractive feedback potential ($\alpha < 0$) leads to oscillations of period 2τ. The long-time diffusion coefficient is decreased. The α-dependence of the effective short- and long-time diffusion coefficients is shown in Fig. 3.2.

Results for this quantity are shown in Fig. 3.2. The lowest order contribution of the programming potential to the long-time diffusion is linear

$$\frac{D_\mathrm{L}}{D} \approx 1 + 2\alpha\,. \tag{3.20}$$

The minimal value for the long-time diffusion is obtained in the case $\alpha = -1$, for which the particle is completely pushed back to its past position a time τ prior to the actual time. It might seem counter-intuitive at first that despite the full return to the old position, the diffusion coefficient is still non-zero. This is due to the fact that even though we do return to the previous position, this former position also proceeds in time. Effectively, the particle can move only half the distance it normally would, reducing the effective long-time diffusion coefficient to

$$\lim_{\alpha\to-1} \frac{D_\mathrm{L}(\alpha)}{D} = \frac{1}{4}\,. \tag{3.21}$$

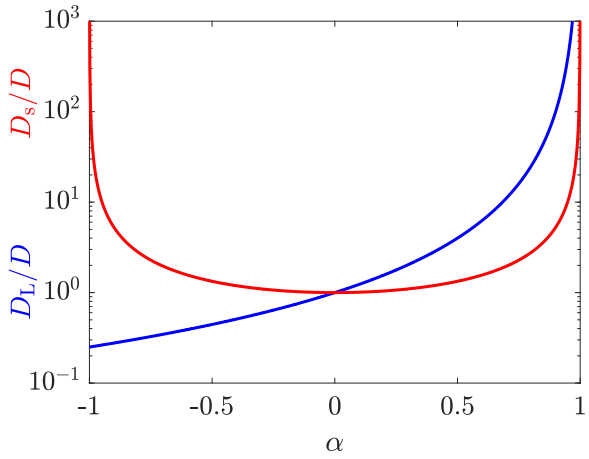

Figure 3.2: Long-time diffusion coefficient D_L and effective short-time diffusion coefficient D_s for harmonic force kicks. The long-time diffusion coefficient has a minimum value of $D_\mathrm{L} = 1/4$ at $\alpha = -1$ and diverges for $\alpha = 1$. The effective short-time diffusion coefficient D_s, resulting as an artifact of the description via force kicks, diverges for $|\alpha| = 1$.

Continuous forces with discrete update times

Next, a harmonic feedback potential with discrete update times is considered. The forces in this case are given by

$$\mathrm{F_{fb}}(t) = \lambda \left[x(t) - x((k-2)\tau)\right] . \tag{3.22}$$

for a time interval $(k-1)\tau < t \leq k\tau$ with an integer number k. The feedback forces are thus always present in this approximation, but the time shift between the actual position and the past position entering the feedback forces takes values between τ and 2τ. The equation of motion can be written in the form

$$\frac{\mathrm{d}x(t)}{\mathrm{d}t} = \frac{1}{\gamma}\mathrm{F_{fb}}\left(x(t) - x((k-2)\tau)\right) + \frac{1}{\gamma}\mathrm{f}(t) . \tag{3.23}$$

which is easily solvable, although the solution obtained from integration still depends on the previous positions of the particle:

$$\begin{aligned} x(t) =& \mathrm{e}^{\frac{\lambda}{\gamma}t} \int_{(k-1)\tau}^{t} \mathrm{d}t' \frac{\mathrm{f}(t')}{\gamma} \mathrm{e}^{-\frac{\lambda}{\gamma}t'} + x\left((k-1)\,\tau\right) \mathrm{e}^{\frac{\lambda}{\gamma}(t-(k-1)\tau)} \\ &+ x\left((k-2)\,\tau\right) \left(1 - \mathrm{e}^{\frac{\lambda}{\gamma}(t-(k-1)\tau)}\right) . \end{aligned} \tag{3.24}$$

Here, we assume the particle to have been at rest at $x = 0$ up to time $t = 0$ and the

equation is solved recursively to obtain

$$\begin{aligned} x(t) =& \mathrm{e}^{\frac{\lambda}{\gamma}t} \int_{(k-1)\tau}^{t} \mathrm{d}t' \frac{\mathrm{f}(t')}{\gamma} \mathrm{e}^{-\frac{\lambda}{\gamma}t'} \\ &+ \sum_{n=0}^{k-2} c_n \int_{(k-n-2)\tau}^{(k-n-1)\tau} \mathrm{d}t' \frac{\mathrm{f}(t')}{\gamma} \mathrm{e}^{-\frac{\lambda}{\gamma}t'} \mathrm{e}^{-\frac{\lambda}{\gamma}t} \\ &+ \sum_{n=0}^{k-3} c_n \int_{(k-n-3)\tau}^{(k-n-2)\tau} \mathrm{d}t' \frac{\mathrm{f}(t')}{\gamma} \mathrm{e}^{-\frac{\lambda}{\gamma}t'} \mathrm{e}^{-\frac{\lambda}{\gamma}(k-2)\tau} \left(1 - \mathrm{e}^{\frac{\lambda}{\gamma}(t-(k-1)\tau)}\right) \end{aligned} \tag{3.25}$$

where

$$\begin{aligned} c_n &= \frac{\mathrm{e}^{-n\frac{\lambda}{\gamma}\tau}}{2 - \mathrm{e}^{\frac{\lambda}{\gamma}\tau}} \left(1 - \left(\mathrm{e}^{\frac{\lambda}{\gamma}\tau} - 1\right)^{n+1}\right) \\ &= \frac{\mathrm{e}^{-n\alpha}}{2 - \mathrm{e}^{\alpha}} \left(1 - (\mathrm{e}^{\alpha} - 1)^{n+1}\right) . \end{aligned} \tag{3.26}$$

for $n \geq 0$ and $c_n = 0$ for $n < 0$. Further, $\alpha = \lambda\tau/\gamma$ as defined before. In this case, sensible choices for α need to fulfill $\mathrm{e}^{\alpha} < 2$ as otherwise the contributions due to previous times become larger with farther distance in time. The MSD for a particle moving under the influence of the feedback potential can then be obtained as

$$\left\langle (x(t'+t) - x(t'))^2 \right\rangle = \left\langle (x(t'+t))^2 \right\rangle + \left\langle (x(t'))^2 \right\rangle - 2\langle x(t'+t)x(t') \rangle . \tag{3.27}$$

The cross correlation term $\langle x(t_2)x(t_1)\rangle$ with $(k-1)\tau < t_1 \leq k\tau$ and $(l-1)\tau < t_2 \leq l\tau$ and $t_1 \leq t_2$ is given by

$$\begin{aligned} \langle x(t_2)x(t_1)\rangle / (D\tau) = -\frac{1}{\alpha} \mathrm{e}^{\alpha(t_2-t_1)/\tau} \Bigg[& \left(1 - \mathrm{e}^{-2\alpha\Delta t_1/\tau}\mathrm{e}^{2\alpha}\right) \delta_{kl} \\ &+ A(k-2, l-2) \left(1 - \mathrm{e}^{2\alpha}\right) \mathrm{e}^{-2\alpha\Delta t_1/\tau}\mathrm{e}^{2\alpha} \\ &+ A(k-3, l-2) \left(1 - \mathrm{e}^{2\alpha}\right) \mathrm{e}^{-\alpha\Delta t_1/\tau}\mathrm{e}^{2\alpha} \left(1 - \mathrm{e}^{-\alpha\Delta t_1/\tau}\mathrm{e}^{\alpha}\right) \\ &+ c_{l-k-1} \left(1 - \mathrm{e}^{-\alpha\Delta t_1/\tau}\mathrm{e}^{\alpha}\right) \Bigg] \\ &- \frac{1}{\alpha} \left(\mathrm{e}^{\alpha(l-k)} - \mathrm{e}^{\alpha(t_2-t_1)/\tau}\mathrm{e}^{-\alpha\Delta t_1/\tau}\mathrm{e}^{\alpha}\right) \Bigg[A(k-2, l-3) \left(1 - \mathrm{e}^{2\alpha}\right) \mathrm{e}^{-\alpha\Delta t_1/\tau} \\ &+ A(k-3, l-3) \left(1 - \mathrm{e}^{2\alpha}\right) \left(1 - \mathrm{e}^{-\alpha\Delta t_1/\tau}\mathrm{e}^{\alpha}\right) \\ &+ c_{l-k-2}\, \mathrm{e}^{-2\alpha} \left(1 - \mathrm{e}^{-2\alpha\Delta t_1/\tau}\mathrm{e}^{2\alpha}\right) \mathrm{e}^{\alpha\Delta t_1/\tau} \Bigg] . \end{aligned} \tag{3.28}$$

Here $\Delta t_1 = k\tau - t_1$ is the time offset between t_1 and the next potential update and

$$\begin{aligned} A(k,m) =& \sum_{n=0}^{k} c_n c_{n-k+m} \mathrm{e}^{2n\alpha} \\ =& \frac{\mathrm{e}^{-\alpha(m-k)}}{\left(\mathrm{e}^{\alpha}-2\right)^2} \Bigg\{ \frac{\left(\mathrm{e}^{\alpha}-1\right)^{2k+2}-1}{\left(\mathrm{e}^{\alpha}-2\right)\mathrm{e}^{\alpha}} \left(\mathrm{e}^{\alpha}-1\right)^{m-k+2} \\ & - \frac{\mathrm{e}^{\alpha}-1}{\mathrm{e}^{\alpha}-2} \left[\left(\mathrm{e}^{\alpha}-1\right)^{k+1}-1\right] \left[1+\left(\mathrm{e}^{\alpha}-1\right)^{m-k}\right] + k + 1 \Bigg\} . \end{aligned} \tag{3.29}$$

The necessary terms in eq. (3.27) can then be obtained for $t_1 = t_2 = t + t'$ for the first, $t_1 = t_2 = t'$ for the second and $t_1 = t$, $t_2 = t' + t$ for the third term. In particular, the MSD with respect to the resting position is given at the renewal times $k\tau$ (where $k = 0, 1, 2, \ldots$) by,

$$\begin{aligned} &\langle x(k\tau)^2 \rangle / (D\tau) \\ &\quad = \frac{1}{\alpha} \frac{\mathrm{e}^{2\alpha}-1}{\left(\mathrm{e}^{\alpha}-2\right)^2} \left[\frac{\left(\mathrm{e}^{\alpha}-1\right)^2}{\left(\mathrm{e}^{\alpha}-2\right)\mathrm{e}^{\alpha}} \left(\left(\mathrm{e}^{\alpha}-1\right)^{2k} - 1 \right) - 2 \frac{\mathrm{e}^{\alpha}-1}{\mathrm{e}^{\alpha}-2} \left(\left(\mathrm{e}^{\alpha}-1\right)^{k} - 1 \right) + k \right] . \end{aligned} \tag{3.30}$$

Note that as for the kicked case, eq. (3.28) depends not only on the time difference $t_2 - t_1$ as well as the number of potential renewals $(k - l)$ during that time, but also on the offset to the next renewal point of the potential. For measurements of the MSD, the resulting curve will thus vary depending on the protocol used, see Fig. 3.3. Qualitatively the same MSD behavior is retrieved as for the kicked case, i.e., for a repulsive potential propulsion ($\propto t^2$) is found at medium times with an increased long-time diffusion coefficient D_L, while an attractive potential leads to oscillations and a decreased long-time diffusion coefficient, see also Fig. 3.3. Additionally, in contrast to the previously-discussed kicked case, this description does not lead to the artifact of an increased short-time diffusion coefficient.

The long-time diffusion coefficient only depends on the normalized strength of the external potential α and is given by

$$\frac{D_\mathrm{L}}{D} = \frac{\mathrm{e}^{2\alpha}-1}{2\alpha\left(2-\mathrm{e}^{\alpha}\right)^2} . \tag{3.31}$$

Its dependence on the feedback strength α is shown in Fig. 3.4. For small feedback forcing the expression can be approximated as

$$\frac{D_\mathrm{L}}{D} \approx 1 + 3\alpha \tag{3.32}$$

such that the leading order correction is linear. However, even in this limit the result does not agree with the previous approximation of force kicks, see eq. (3.20).

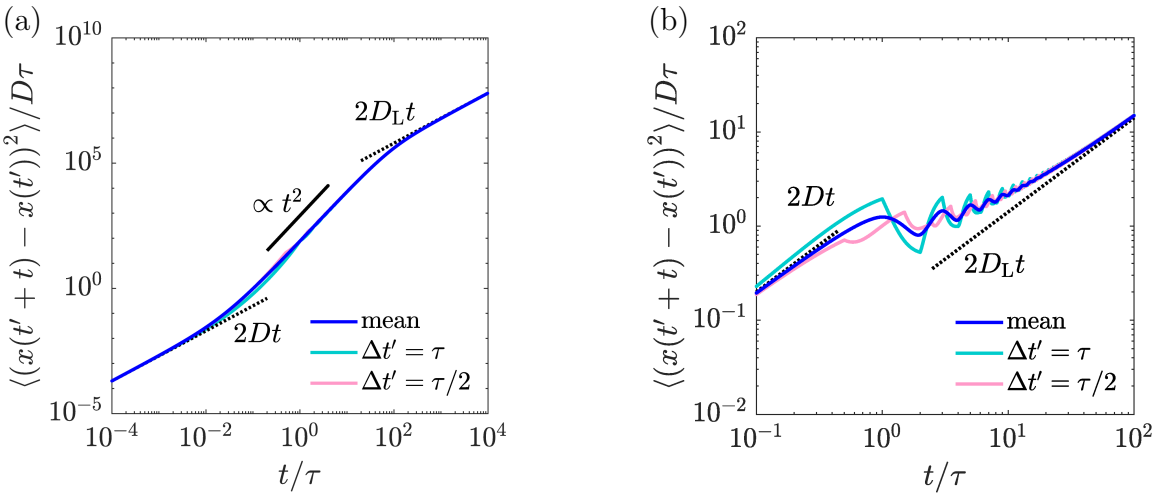

Figure 3.3: Analytic result for harmonic feedback forces with discrete update times with (a) $\alpha = 0.68$ and (b) $\alpha = -2.0$ for different values of the time offset $\Delta t'$. The reference time t' is chosen large enough such that effects of the initial resting condition have subsided.

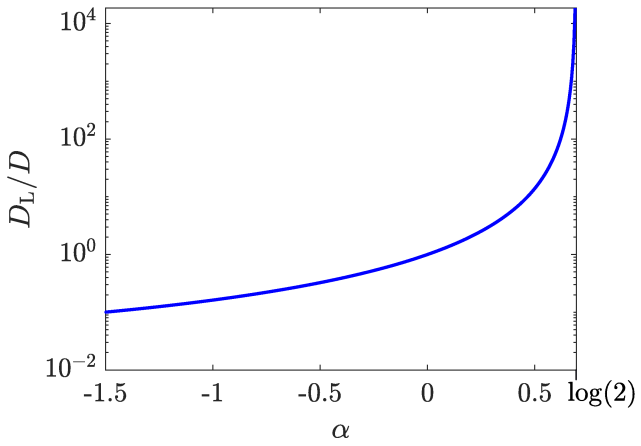

Figure 3.4: Long-time diffusion coefficient D_{L} for a harmonic potential with discrete feedback update times. The long-time diffusion coefficient vanishes for high negative values of α and diverges at $\mathrm{e}^{\alpha} = 2$.

Continuous forces with continuous update times

Finally, the exact equation with the feedback forces

$$\mathrm{F}_{\mathrm{fb}}(x(t) - x(t-\tau)) = \lambda\,[x(t) - x(t-\tau)] \tag{3.33}$$

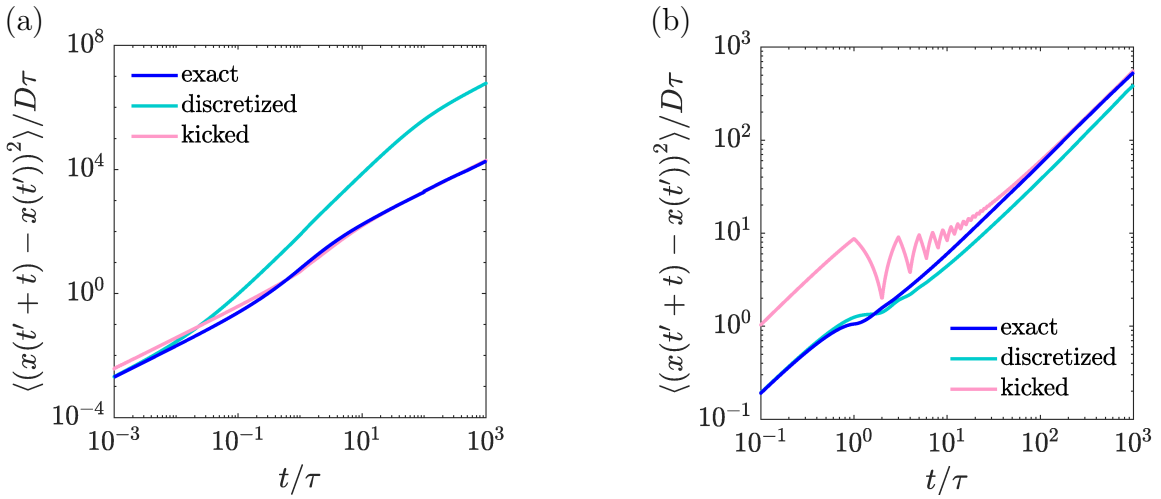

Figure 3.5: Results for (a) $\alpha = 0.68$ and (b) $\alpha = -0.9$ for the different approximation schemes compared to the exact numerical solution. The qualitative behavior is covered correctly by both approximation schemes apart from the oscillation period in the case of attractive potentials. The long-time diffusion in the exact case matches the approximation of force kicks.

is considered, for which the resulting equation of motion is given by

$$\gamma \frac{\mathrm{d}x(t)}{\mathrm{d}t} = \lambda \left[x(t) - x(t-\tau)\right] + \mathrm{f}(t)\,. \tag{3.34}$$

The mean square displacement is determined numerically by integration of eq. (3.34). The result is shown in Fig. 3.5 and compared to the previous approximative cases. The qualitative behavior is captured by both approximative scheme. There is, however, a difference in the oscillatory behavior for attractive potentials: While discretized schemes show oscillations with period 2τ, the exact equation leads to oscillatory behavior of period τ. This can be understood quite easily on the basis of the underlying equation. Starting at a position x_0 at an update time of the potential, the corresponding potential drawing the particle back to this position is introduced after a delay time $t = \tau$. In the discretized case, the same potential is kept until $t = 2\tau$, after which the feedback potential is updated, drawing the particle away from the starting position such that the MSD increases again. The first minimum in the MSD is then given for $t \approx 2\tau$. Contrarily, for the continuous case, the corresponding feedback potential is also introduced at $t = \tau$ but is immediately updated, drawing the particle away from the starting position for $t > \tau$. The first minimum is then given for $t \approx \tau$.

Furthermore, a quantitative comparison reveals that the approximation of discretized update times leads to a significant overestimation of the propulsion strength in the repulsive case. Additionally, this approximation is unable to correctly capture the long time diffusive behavior regardless of the nature of the feedback. Contrarily, the

force-kick picture leads to abnormal behavior with respect to short-time diffusion and overestimates the amplitude of the oscillations in the attractive case. However, the long time diffusive behavior matches the exact results. In fact, the solution in the case of force kicks is the same as integrating the exact equation with a time step τ, which can be seen from the definition of the forces and the additivity of the Brownian noise. Because of the scalability of the potential, there exists no inherent length-scale in the system. At sufficiently long times, the length-scale can thus be chosen such, that the displacement within a delay time is small on this relative scale. Therefore, the exact solution is retrieved and the long-time diffusion coefficient in the exact case is given by

$$\frac{D_\mathrm{L}}{D} = \frac{1}{(1-\alpha)^2}\,, \tag{3.35}$$

as in the kicked case, with the constraint $|\alpha| < 1$.

3.1.2 Gaussian feedback potential

As a more realistic version of a feedback potential, a Gaussian form is considered. This potential gives a more realistic description as it does not continually grow stronger at farther distances. The effect of the feedback potential is then spatially localized.

Continuous forces with continuous update times

The feedback potential in this case is given by

$$V_\mathrm{fb}(r) = A\mathrm{e}^{-\frac{r^2}{2b^2}}\,, \tag{3.36}$$

which is also assumed in the following Section, Publication II, for the many-particle case. The force follows as

$$\mathbf{F}_\mathrm{fb}(\mathbf{r}(t)-\mathbf{r}(t-\tau)) = \frac{A}{b^2}\left(\mathbf{r}(t)-\mathbf{r}(t-\tau)\right)\,\mathrm{e}^{-\frac{(\mathbf{r}(t)-\mathbf{r}(t-\tau))^2}{2b^2}}\,, \tag{3.37}$$

which can be approximated by harmonic forces of strength $\lambda = A/b^2$ for small delay times τ and large widths b of the Gaussian. The system is solved numerically with the Brownian time $\tau_b = b^2/D$ as the time unit and b as the length scale. The potential strength A is normalized to the thermal energy k_BT. The effect of the feedback potential on the dynamics of a single particle is investigated, which is described by eq. (3.1). The result is shown in Fig. 3.6 and matches qualitatively with the previously discussed harmonic feedback. Note however, that the system dynamics is no longer simply dependent on the product of the potential amplitude and the delay time. The amount of decrease or increase in the long-time diffusion coefficient D_L depends on both, the strength of the potential A and the feedback delay time τ, independently,

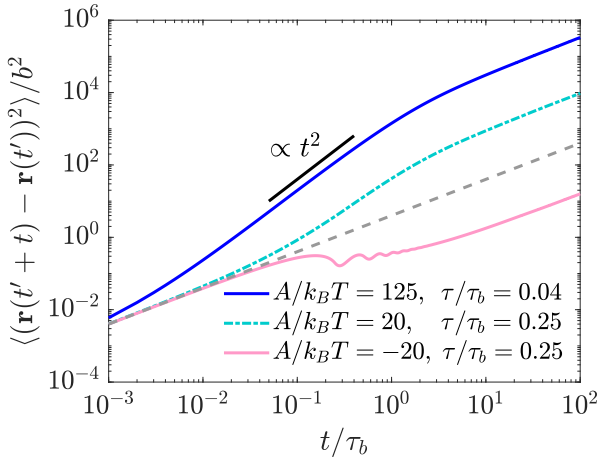

Figure 3.6: MSD for two cases of a repulsive ($A/k_BT = 20$, $A/k_BT = 125$ with $A\tau/k_BT\tau_b = 5$) and an attractive ($A/k_BT = -20$) feedback potential. The case of vanishing potential ($A/k_BT = 0$) is also shown for comparison (gray dashed line).

see Fig. 3.7. The first dependence is obvious as A sets the strength of the force acting on the particles. The dependence on τ can be understood by first considering the two limits of small and large τ. For small τ the particles are always close to their past position and, due to the Gaussian form of the feedback potential, the forces are small. In particular, for the limit $\tau \to 0$ the potential force vanishes and $D_\mathrm{L} = D$. On the other hand, for large τ the probability to be close to the past position, i.e., within the range of the feedback potential, is small. The effect of the potential thus reduces for large τ. In between the two limits, we observe an extremum in the long-time diffusion coefficient with respect to the delay time τ. Here, the maximum in the repulsive case occurs at smaller delay times than the minimum in the attractive potential.

For the repulsive potential case, an estimate of the effective particle propulsion velocity can be obtained. At high feedback strength A the noise term in the one-dimensional version of eq. (3.1) can be neglected. Determining a solution meeting the fix point condition $\frac{\mathrm{d}x}{\mathrm{d}t} = v_\mathrm{fp} = \text{const.}$, results in a predicted velocity

$$v_\mathrm{fp} = \frac{b}{\tau}\sqrt{2\ln\left(\frac{A\tau}{\gamma b^2}\right)}\,. \tag{3.38}$$

In the opposite limit of small potential amplitude, the displacement in the feedback-force is dominated by diffusion and $r - r' \approx \sqrt{2D\tau}$ in eq. (3.1) such that

$$v_\mathrm{sa} = \frac{A\sqrt{2D\tau}}{\gamma b^2}\mathrm{e}^{-\frac{D\tau}{b^2}} \propto A\,. \tag{3.39}$$

These limits are shown in Fig. 3.8 in comparison to the numerical result for the velocity. In particular for small values of τ, the predicted fix point velocity is in good agreement with the numerical results.

Collective effects, that arise if this repulsive Gaussian feedback potential is introduced onto a colloidal suspension, are discussed in the following Section, Publication II.

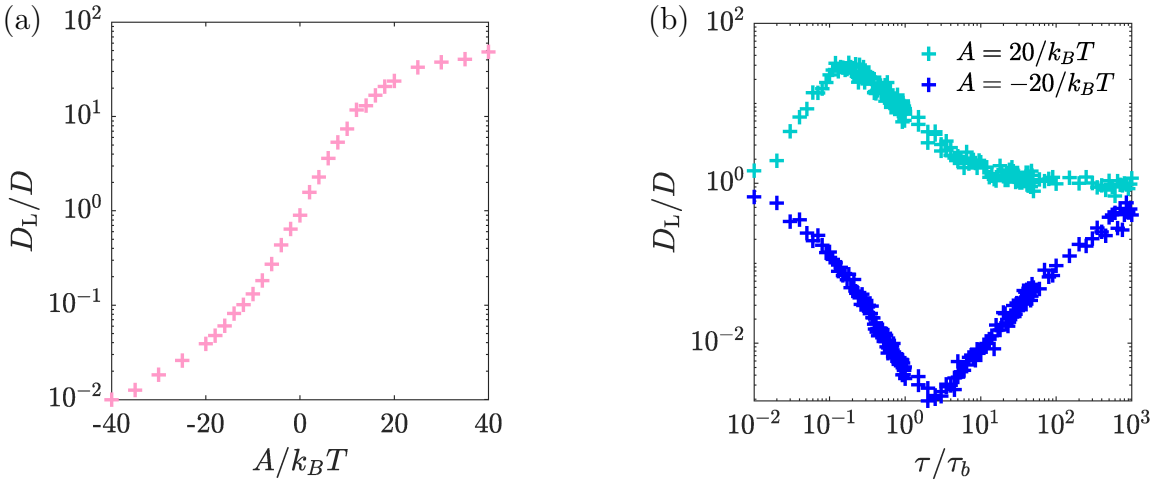

Figure 3.7: Long-time diffusion coefficient (a) for variation of the potential strength A where $\tau = 0.25$ and (b) different delay times τ. Diffusion is enhanced for repulsive and decreased for attractive potentials with an extremum at medium delay times.

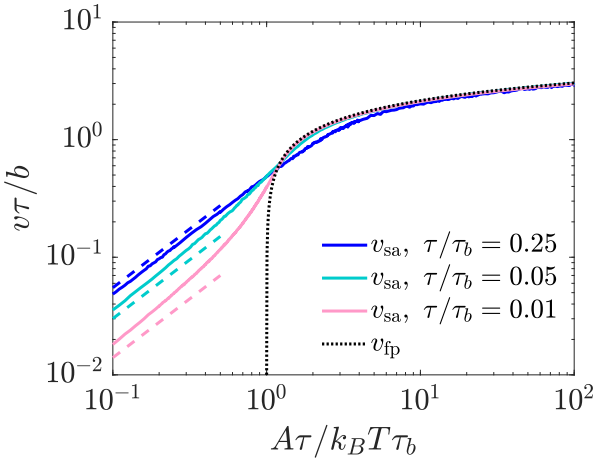

Figure 3.8: Numerical results for particle velocity (solid curves), as a function of potential amplitude A, for different values of the delay time τ. The corresponding small amplitude limits v_{sa} are indicated by dashed lines of the corresponding color. Appropriate scaling leads to coinciding curves for large A in accordance with the expected fix point velocity v_{fp}.

Publication II Traveling band formation in feedback-driven colloids

S. Tarama, S. U. Egelhaaf, H. Löwen
Traveling band formation in feedback-driven colloids,
Phys. Rev. E **100**, 022609 (2019),
published by *American Physical Society*.

Digital Object Identifier (DOI): 10.1103/PhysRevE.100.022609

Link to version of record:
https://journals.aps.org/pre/pdf/10.1103/PhysRevE.100.022609

Statement of contribution

S.U.E. and H.L. have developed the project. I have implemented the BD Simulation code and DDFT calculation and produced and analyzed the data under the supervision of H.L. I have created all figures and a first draft of the paper which was revised with the help of H.L. and S.U.E. All authors have contributed to interpreting the simulation results.

Copyright and license notice

PHYSICAL REVIEW E **100**, 022609 (2019)

Traveling band formation in feedback-driven colloids

Sonja Tarama,[1,*] Stefan U. Egelhaaf,[2] and Hartmut Löwen[1]

[1]*Institute for Theoretical Physics II: Soft Matter, Heinrich Heine University Düsseldorf, Universitätsstraße 1, D-40225 Düsseldorf, Germany*

[2]*Condensed Matter Physics Laboratory, Heinrich Heine University Düsseldorf, Universitätsstraße 1, D-40225 Düsseldorf, Germany*

(Received 18 April 2019; published 30 August 2019)

Using simulation and theory we study the dynamics of a colloidal suspension in two dimensions subject to a time-delayed repulsive feedback that depends on the positions of the colloidal particles. The colloidal particles experience an additional potential that is a superposition of repulsive potential energies centered around the positions of all the particles a delay time ago. Here we show that such a feedback leads to self-organization of the particles into traveling bands. The width of the bands and their propagation speed can be tuned by the delay time and the range of the imposed repulsive potential. The emerging traveling band behavior is observed in Brownian dynamics computer simulations as well as microscopic dynamic density functional theory. Traveling band formation also persists in systems of finite size leading to rotating traveling waves in the case of circularly confined systems.

DOI: 10.1103/PhysRevE.100.022609

I. INTRODUCTION

Non-equilibrium systems subject to a feedback potential have been studied extensively in recent times [1–10]. Due to the feedback used, e.g., to stabilize dynamics [10–14] or structure [8,15], the system dynamics becomes history dependent. The feedback can be realized through external programming of a laser trap [8,16–22] or, more naturally, may arise in autochemotactic particles, i.e., if the particles themselves are part of the production mechanism of the chemical substance they react to. In particular, examples of the latter include biological systems such as bacteria [23,24] and army ants [25], as well as synthetic microswimmers such as active colloidal particles [26–32] or self-propelling droplets [33,34].

In the context of many-particle systems, the topic of pattern formation [35–41] is of central interest. In particular, the Ginzburg-Landau [42–45] and Swift-Hohenberg equations [46] are widely used to study pattern formation. Most of these studies present a coarse-grained treatment using effective continuum theories but do not resolve the individual particles. One pattern which is commonly observed in many different systems is traveling waves or moving bands of particles. Examples include actin waves formed in the biological actin-myosin systems [47–49], metachronal waves in cilia arrays [50], the patterning in systems of active agents under various settings [40,51–56], the formation of bands in passive colloidal suspensions driven by ac [57,58] or dc [59–64] fields, and phase separating mixtures [40,65,66]. Recent work on pattern forming systems also considers the effect of time-delayed feedback using continuum theories [44,67–69].

In this paper, we present a study of feedback-driven colloidal particles as an example of a feedback system of discrete components considered on the fundamental particle level. In our model, the particles are subjected to a feedback potential driving them away from their previous positions. Using Brownian dynamics computer simulations and dynamical density functional theory [70–75], we show that this repulsive feedback leads to self-organization of the particles into a moving band structure reminiscent of a traveling wave. Remarkably, this ordering takes place despite the absence of any attractive interactions in the system, for which static band formation is known to occur [76,77]. The width of the bands and their propagation speed can be tuned by the delay time and the range of the imposed repulsive delay potential. Finally, we demonstrate that traveling band formation also persists under strong confinement, leading, in circularly confined systems, to globally rotating and spiraling bands [78].

Our model can be realized in experiments for colloidal suspensions. The suspensions can be exposed to a potential energy landscape using optical fields which are programed via a feedback loop [20,79,80]. Typically the colloids are attracted towards the intensity maximum of the optical field. However, by inverting the intensity landscape a repulsion is achieved, in which case the particles are driven away from the dark regions.

The paper is organized as follows: In the following section we introduce the underlying Langevin equation including a delay term [81–88] describing the dynamics of the system. We continue with presenting our simulation results in Sec. III. A prediction of the observed traveling wave formation is derived from dynamic density functional theory in Sec. IV. Subsequently, we consider confinement effects in Sec. V. Finally, we conclude with a summary of our main findings and an outlook to possible extensions of the system in Sec. VI.

II. MODEL AND BROWNIAN DYNAMICS COMPUTER SIMULATIONS

The Brownian dynamics of N colloidal particles in two spatial dimensions is described by their time-dependent positions $\mathbf{r}_i(t)$ $(i = 1, \ldots, N)$ and governed by the following

*sonja.tarama@hhu.de

Langevin equation:

$$\gamma \frac{d\mathbf{r}_i}{dt} = \mathbf{f}_i(t) + \sum_{j=1}^{N} \mathbf{F}(\mathbf{r}_i(t) - \mathbf{r}_j(t-\tau)) + \sum_{\substack{j=1 \\ j\neq i}}^{N} \mathbf{F}_{\mathrm{Yuk}}(\mathbf{r}_i(t) - \mathbf{r}_j(t)), \quad (1)$$

which can be viewed as a force balance equation. The left-hand side of Eq. (1) contains the Stokes drag force with γ denoting the friction coefficient. The Gaussian random force $\mathbf{f}_i(t)$ mimics the collision of the particle with solvent molecules. This stochastic force is characterized by its first two moments $\langle \mathbf{f}_i(t)\rangle = 0$ and $\langle \mathbf{f}_i(t) \otimes \mathbf{f}_j(t')\rangle = 2D\gamma^2 \mathbb{1}\delta(t-t')\delta_{ij}$, where D is the short-time diffusion coefficient of the particles, $\delta(t)$ is the Dirac delta function, and δ_{ij} denotes the Kronecker delta. The important new ingredients in Eq. (1) are the feedback forces $\mathbf{F}(\mathbf{r}_i(t) - \mathbf{r}_j(t-\tau))$. These forces are evaluated at distances between the actual position $\mathbf{r}_i(t)$ of particle i and the *former* positions $\mathbf{r}_j(t-\tau)$ of the other particles j (where the special case $i = j$ is included). Here, τ is the time difference, which we refer to as the *delay time* of the feedback.

We derive $\mathbf{F}(\mathbf{r})$ from a potential $V_{\mathrm{fb}}(r)$ as

$$\mathbf{F}(\mathbf{r}) = -\nabla_{\mathbf{r}} V_{\mathrm{fb}}(r)$$

and assume for simplicity a Gaussian form

$$V_{\mathrm{fb}}(r) = A \exp\left(-\frac{r^2}{2b^2}\right), \quad (2)$$

characterized by an energy amplitude A and a range b. The Gaussian potential form is a good approximation for optical systems such as optical tweezers and occurs naturally for autochemotactic particles [31]. Here, we confine ourselves to the case of repulsive feedback potentials such that the energy amplitude $A > 0$ is positive and the special case $A = 0$ serves as an equilibrium reference case. For $A > 0$, all particles are driven away from the past positions of all particles including their own.

Finally, the equations of motion include direct particle-particle interaction forces

$$\mathbf{F}_{\mathrm{Yuk}}(\mathbf{r}) = -\nabla_{\mathbf{r}} \Phi(r) \quad (3)$$

via a repulsive Yukawa pair potential

$$\Phi(r) = \frac{V_0}{r} \exp(-\kappa r) \quad (4)$$

involving an inverse range κ and an amplitude V_0.

We perform Brownian dynamics simulations with a square simulation box of length L and periodic boundary conditions with $N = 6400$ particles. Some of the simulations were repeated in a rectangular box, in order to obtain stable traveling bands. This was necessary because at the onset of the formation of traveling bands, the band stability is highly dependent on the commensurability of the box size and the preferred wavelength. Possible wavelengths in the finite system are restricted to those being commensurate with the periodic boundaries, which thus requires the system length to be adjusted. The equation for the particle positions, Eq. (1), is integrated using an explicit Euler scheme with a finite time step of $\Delta t = 10^{-4}\tau_0$, where $\tau_0 = b^2/D$ denotes the Brownian time scale.

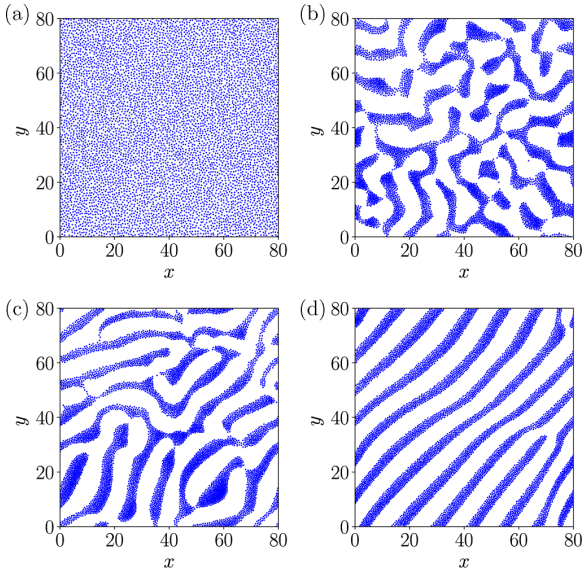

FIG. 1. Formation of bands. The plots show snapshots of the system at times (a) $t = 0$, (b) $t = 10$, (c) $t = 50$, and (d) $t = 100$ for the case of a strong feedback potential ($A = 20$). Separation into crowded and empty regions is followed by the formation of bands.

In the following, lengths are normalized to the feedback potential range b and times to the Brownian time $\tau_0 = b^2/D$. Energies are given in terms of the thermal energy $k_BT \equiv D\gamma$. In order to keep the set of parameters limited, we maintain $V_0 = 60\, bk_BT$, $\kappa = 4.5/b$, and $\tau = 0.25\,\tau_0$ constant in our units. Furthermore, we use a number density $\rho_0 = N/L^2 = 1/b^2$. The units are dropped hereafter for ease of notation. We use the feedback amplitude A as a control parameter and investigate the change in the system structure and dynamics as a function of it.

Our simulation protocol is as follows: First, the system is equilibrated without any feedback potential (corresponding to a two-dimensional pure Yukawa system [89]), after which the positions are recorded for updating the feedback potential. We define $t = 0$ as the time at which the feedback potential is first introduced into the system. Subsequently, the relaxation of the system is monitored for a long time, several hundreds of time units.

III. SIMULATION RESULTS

A. Band formation

Figure 1 shows a typical instance of system relaxation in the case of strong feedback potentials. The initial equilibrated homogeneous fluid state in Fig. 1(a) spontaneously separates into two regions which are either empty or crowded (i.e., exhibiting a high density of particles). This demixed state coarsens further as a function of time into a configuration of system-spanning straight bands at long times, resembling those observed in mixtures of particles subjected to bidisperse

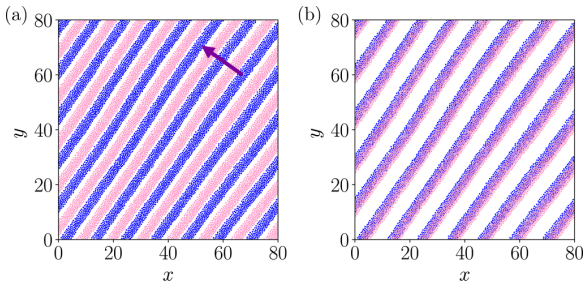

FIG. 2. Particle positions at times $t = 500$ (blue/dark) and (a) $t = 500.25$ and (b) $t = 500.5$ (pink/light) for feedback amplitude $A = 20$. The particles move approximately one bandwidth in the normal direction within a feedback time $\tau = 0.25$. The direction of movement is indicated by the arrow in (a).

Magnus forces [90]. The width of the formed bands depends on the specific parameters of the particle repulsion and the feedback potential as well as the delay time τ. In particular, no band formation is observed for very small delay times, in which case the feedback potential can be understood as modified direct interactions between the particles, while larger delay times lead to an increase in the time scale on which band formation takes place. The orientation of the bands is tilted relative to the quadratic box with the angle depending on the initial configuration as well as the commensurability of the wavelength and the box size. The commensurability condition leads to a finite set of possible orientations for the bands while the initialization determines which of these is realized.

The emerging bands are observed to move collectively along the normal of their interfaces. The empty regions are found at the former particle positions, i.e., the positions where the potential is inserted, suggesting that particles try to effectively avoid regions where they have been a time τ before. In more detail, the occurrence of the separation into empty and crowded regions can be explained in the following way: If in a disordered system as in Fig. 1(a) there are by chance more particles at a particular position at time t, the strong repulsive potential imposed at time $t + \tau$ leads to fewer particles at this position, which in turn leads to a small potential and more particles at time $t + 2\tau$. The feedback potential thus leads to a self-ordering and the particle distribution effectively changes between one state and its negative image with period 2τ. The easiest way to achieve this, namely, the one with the fewest collisions between the particles, is a collective movement into one direction as given for the moving lamellar phase seen in Fig. 2.

Based on the previous consideration, a band moves over its full periodicity λ_b during twice the delay time τ such that a scaling expression for the magnitude of the expected band velocity is obtained as

$$v_s = \frac{\lambda_b}{2\tau}. \tag{5}$$

Remarkably, knowledge of the static property, namely, the wavelength and orientation of the band structure, thus provides an estimate of the dynamics of the system, i.e., the band velocity. Likewise, determining the velocity of the bands for a given feedback time yields an approximative value for the band periodicity λ_b. Moreover, through a determination of the velocity and periodicity, the feedback time can be estimated, which, in particular in biological systems, might not be easily accessible otherwise.

The prediction for the band velocity obtained from the scaling expression can be compared to the simulation results. For the latter case, we use the systematic force

$$\mathbf{F}_i(t) = \left[\sum_{j=1}^{N} \mathbf{F}(\mathbf{r}_i(t) - \mathbf{r}_j(t-\tau)) + \sum_{\substack{j=1 \\ j\neq i}}^{N} \mathbf{F}_{\mathrm{Yuk}}(\mathbf{r}_i(t) - \mathbf{r}_j(t)) \right] \tag{6}$$

acting on particle i at time t to define an instantaneous drift velocity

$$\mathbf{v}_i(t) = \frac{\mathbf{F}_i(t)}{\gamma} \tag{7}$$

of this particle. From this expression, the mean global drift velocity $\mathbf{v}$ is then obtained by averaging over all particles as

$$\mathbf{v} = \frac{1}{N} \sum_{i=1}^{N} \langle \mathbf{v}_i(t') \rangle , \tag{8}$$

where

$$\langle B(t') \rangle = \frac{1}{T} \int_{t_0}^{t_0+T} dt' B(t') \tag{9}$$

denotes an average taken over time t' for an observable $B(t')$. The time t_0 is bigger than a typical relaxation time of the system and T is the width of the time window over which the average is performed. Here, we use $t_0 = 500$ and $T = 500$. In the ordered band state the mean drift velocity equals the velocity of the bands. The comparison between the two velocities is shown in the next section as a function of the feedback potential amplitude A [Fig. 7].

B. Dependence on the feedback strength

The system shows different structuring depending on the amplitude of the applied feedback potential A. The patterns are shown in Fig. 3 with the color code indicating the drift velocity directions of the individual particles. As a general result, we find that the average of these velocities, the mean drift velocity $\mathbf{v}$, is typically normal to the band direction.

With respect to potential strength A, we observe that, while for small $A \lesssim 1$ [Fig. 3(a)], diffusion prevents any structure formation, higher potential amplitudes lead to patterning [Fig. 3(b)] and, for even larger potential strength, to the formation of a band structure. The necessary potential amplitude for pattern formation can be estimated by considering at which point the feedback force $\mathbf{F}$ becomes comparable to the interparticle repulsion force $\mathbf{F}_{\mathrm{Yuk}}$. From the condition $\mathbf{F}^2 = \mathbf{F}^2_{\mathrm{Yuk}}$, we find that $A \approx 6$, which is in reasonable agreement with the simulation results which indicate the start of band formation

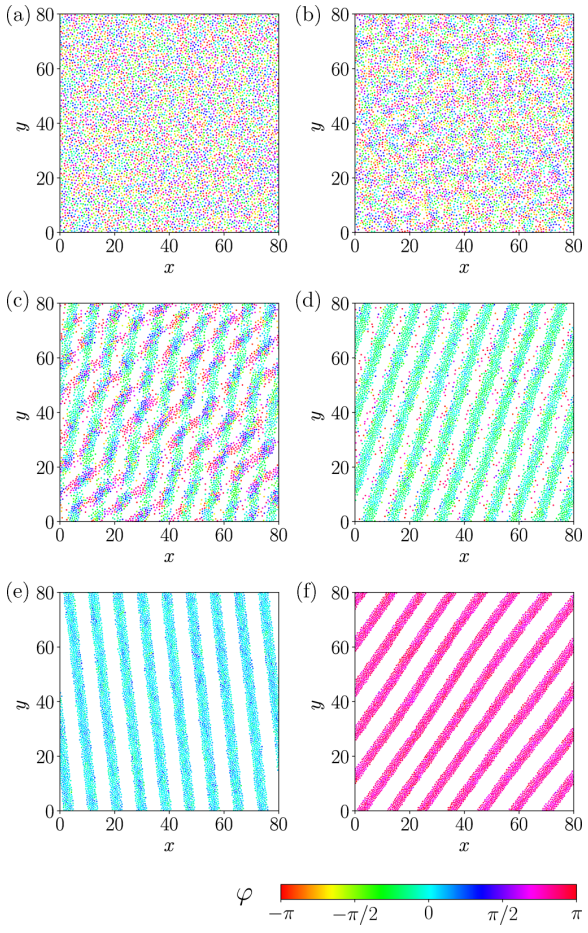

FIG. 3. System snapshots for feedback potential strengths (a) $A = 1$, (b) $A = 5$, (c) $A = 6$, (d) $A = 6.5$, (e) $A = 10$, and (f) $A = 20$ after $t = 500$. A band pattern is formed initially for sufficiently high strengths of the feedback potential. The direction of motion of the particles is extracted from the individual drift velocities $\mathbf{v}_i(t) = |\mathbf{v}_i|(\cos\varphi_i, \sin\varphi_i)$ and the angle φ_i is indicated by color.

at $5 \leqslant A^* \leqslant 6$. Close to this threshold, the band state can be constituted of two distinct band orientations [Fig. 3(c)]. Further increasing the potential leads to a single band orientation with a considerable number of particles traveling in the opposite direction [Fig. 3(d)]. At even higher potentials [Figs. 3(e) and 3(f)], the system forms stable bands with all particles moving as part of the bands into the same direction.

We have checked the system for hysteretic behavior via additional simulations. For a finite system, a small hysteresis effect is observed in forming the bands, which appears to be due to the finite system size and the prescribed periodic boundary conditions.

The density distribution within the bands ρ_b can be determined by changing to a co-moving frame. Taking an average along the band tangential, the density only depends on the position s in the drift direction $\hat{\mathbf{e}}_\mathrm{v}$,

$$\rho_\mathrm{b}(s) = \left\langle \sum_{i=1}^{N} \delta(s - \mathbf{r}_i(t') \cdot \hat{\mathbf{e}}_\mathrm{v}) \right\rangle. \tag{10}$$

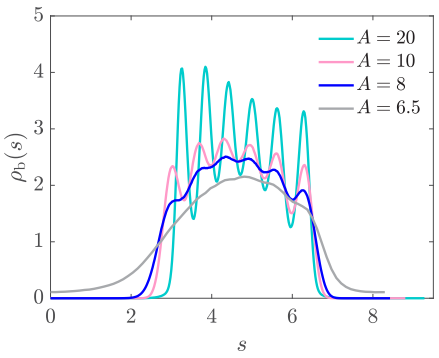

FIG. 4. Density profile $\rho_\mathrm{b}(s)$ of the bands in the co-moving frame, as a function of the position s in the band drift direction for different feedback potential strengths A.

One period of these profiles is shown in Fig. 4, revealing an increasing layering of particles for strong feedback amplitudes and hence an increasing internal order of the bands.

In the following, the formed patterns are explored in more detail via the structure factor, defined by

$$S(\mathbf{k}) = \left\langle \frac{1}{N} \sum_{i,j=1}^{N} e^{-i\mathbf{k}(\mathbf{r}_i(t') - \mathbf{r}_j(t'))} \right\rangle. \tag{11}$$

Figure 5 shows $S(\mathbf{k})$ for the cases shown in Fig. 3 as a function of the components of the wave vector $\mathbf{k} = (k_x, k_y)$. The outer black ring corresponds to the mean particle distance. For higher potential, its radius is shifted away from the equilibrium value $2\pi\rho_0^{1/2}$ towards higher wave numbers, indicating that the mean distance between particles in the band structure is considerably smaller than the one in the homogeneous system without the feedback potential.

Further, the inner black ring first appearing in Fig. 5(b) represents the ordering due to the feedback potential. With respect to the feedback potential strength A, different stages of ordering are observed at this wave number which we denote by k^*. First, for small potentials, directionally independent patterning at $k^* \approx 0.82$ is found [Fig. 5(b)], which for stronger amplitudes develops a directional dependence with two preferred band orientations [Fig. 5(c)]. While medium potentials [Figs. 5(c) and 5(d)] still show some remainder of the initial orientationally independent ordering, indicated by the light gray ring at k^*, this feature disappears at large feedback potential strength A [Figs. 5(e) and 5(f)]. For strong feedback A, only a single band orientation is found. For large potential amplitudes [Figs. 5(d)–5(f)], the nonsinusoidal form of the density profile, visualized in Fig. 4, is reflected in higher harmonics which lead to additional peaks at multiples of k^* in the structure factor. For easier comparison, the azimuthal average $S(k)$ is shown in Fig. 6 for different feedback strengths A, illustrating the shift in the mean particle distance as well as the growth of the new wave number k^* and its higher harmonics.

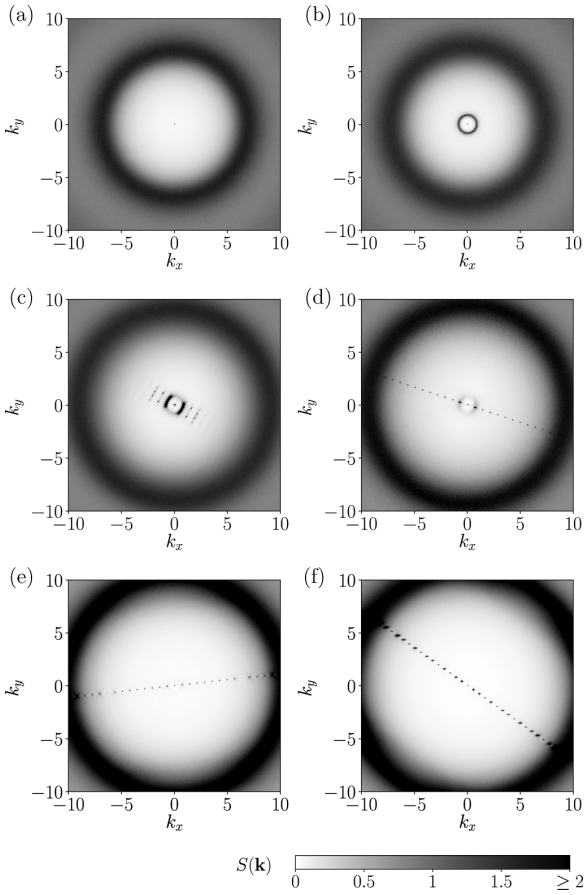

FIG. 5. Two-dimensional structure factor $S(\mathbf{k})$ for the systems of Fig. 3, i.e., for feedback amplitude (a) $A = 1$, (b) $A = 5$, (c) $A = 6$, (d) $A = 6.5$, (e) $A = 10$, and (f) $A = 20$. The outer black ring corresponds to the mean particle distance, the inner black ring, visible in (b)–(d), to patterning at the wave number k^*. The system transitions from directionally homogeneous patterning at wave number k^* to preferred orientations between $A = 5$ and 6.

Extracting the wavelength of the band pattern from the structure factor $S(k)$ allows for a comparison between the estimated value of the band velocity obtained from the scaling expression introduced in the previous section and the simulation results. The prediction for the band velocity according to the scaling expression v_s, given by Eq. (5), and the simulation results for the magnitude v of the global drift velocity $\mathbf{v}$, defined by Eq. (8), are shown in Fig. 7. Above a threshold value $5 \leqslant A^* \leqslant 6$, v increases sharply. For high feedback amplitudes A it saturates to a value that depends on the specific choice of the remaining potential parameters as well as the delay time τ. The agreement between the theoretical prediction and the simulation results is acceptable but not exact. The reason for the discrepancy is that the bands filled with particles and the empty spaces in between are not exactly equal in width, a consequence of the feedback force pushing the particles from behind. The difference in width is also visible in Fig. 2. The length traveled by the bands is thus

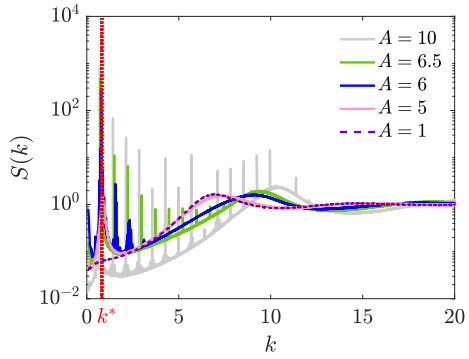

FIG. 6. Azimuthally averaged structure factor $S(k)$ for different values of the feedback potential strength A. The structure factor shows the appearance of a new structure of wave number $k^* \approx 0.82$ in the system, corresponding to the wavelength of the traveling bands. For stronger potentials additional peaks appear at multiples of this wave number indicating higher harmonics.

overestimated when using half the wavelength of the band structure instead of the width of the bands, leading to a slightly higher predicted velocity for the present parameters.

For the individual particles, the directed drift motion becomes visible in the mean-squared displacement (MSD), which we define by

$$\Delta(t) = \left\langle \frac{1}{N} \sum_{i=1}^{N} (\mathbf{r}_i(t'+t) - \mathbf{r}_i(t'))^2 \right\rangle. \tag{12}$$

The MSD changes qualitatively with the onset of the traveling wave instability: Increasing A over the threshold value for band formation changes the long-time behavior from diffusive ($\propto t$) to a directed drift motion ($\propto t^2$), similar to what is found for active (self-propelled) Brownian particles [26,91] (see Fig. 8). Thus, the feedback potential effectively provides a source of self-propulsion.

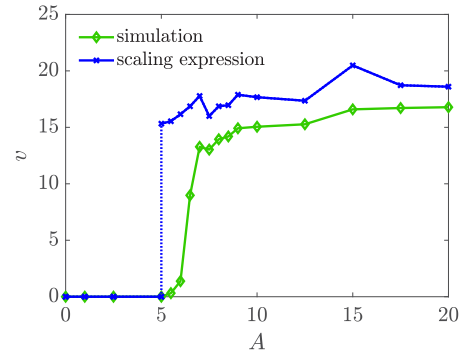

FIG. 7. Mean drift velocity obtained from simulations [Eq. (8)] compared to the band velocity predicted via the scaling expression [Eq. (5)]. For the latter, the wavelength $\lambda_b = 2\pi/k^*$ is a necessary input; its value is extracted from the structure factor obtained through simulations.

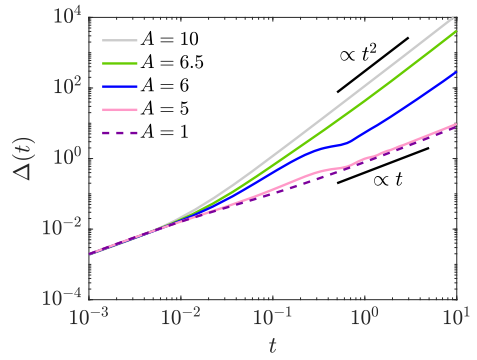

FIG. 8. MSD $\Delta(t)$ for different values of the feedback potential strength A. Within the time window considered, the long-time MSD changes from diffusive to ballistic behavior.

IV. DYNAMICAL DENSITY FUNCTIONAL THEORY

The previously observed values for the potential strength A^* and wave number k^* characterizing the onset of the pattern formation instability are now derived from microscopic dynamic density functional theory (DDFT). The theory requires the particle interactions as the only input.

DDFT is based on the Smoluchowski equation [92] corresponding to the Langevin equation (1). The equivalent time-delayed Smoluchowski equation is known for the one-particle case [3,86–88,93,94] and is briefly discussed in Sec. IV A. Subsequently, this single-particle case is extended to the case of many particles (in Sec. IV B) and the approximations used to obtain a self-contained DDFT equation are introduced in Sec. IV C. Finally, the system's stability against traveling waves is investigated within DDFT in Sec. IV D and the obtained predictions are compared to the simulation results in Sec. IV E.

A. One-particle time-delayed Smoluchowski equation

To determine the time-delayed Smoluchowski equation equivalent to Eq. (1), we first revisit the case of just a single feedback-driven particle. In [93], the Smoluchowski equation corresponding to a time-delayed Langevin equation was derived. Equations (1), (12), and (14) of this work are relevant here and are reproduced below for the case of a constant noise amplitude. Specifically, in [93] it was shown that a time-delayed Langevin equation of the form

$$\frac{\partial}{\partial t}X(t) = h(X(t), X(t-\tau)) + \sqrt{2D}\,\Gamma(t)\,, \tag{13}$$

for a general state variable $X(t)$ subject to a Gaussian noise $\Gamma(t)$, defined by $\langle\Gamma(t)\rangle = 0$ and $\langle\Gamma(t)\Gamma(t')\rangle = \delta(t-t')$, is equivalent to the Smoluchowski equation

$$\frac{\partial}{\partial t}w(x,t|x_\tau,t_\tau)|_{t_\tau=t-\tau} = \hat{L}(x,\nabla_x,x_\tau)w(x,t|x_\tau,t_\tau) \tag{14}$$

with

$$\hat{L}(x,\nabla_x,x_\tau) = -\frac{\partial}{\partial x}h(x,x_\tau) + D\frac{\partial^2}{\partial x^2}\,. \tag{15}$$

Here, the conditional probability $w(x,t|x_\tau,t_\tau)$ gives the probability for the system to be in state x at time t, under the condition that it was in state x_τ at time $t_\tau = t-\tau$. The time derivative on the left-hand side of Eq. (14) only acts on t but not t_τ. The one-particle equivalent of our Eq. (1) is contained in this solution by identifying the actual and the time-shifted system states x and x_τ with the particle positions $\mathbf{r}$ and $\mathbf{r}_\tau$. We set $h(\mathbf{r},\mathbf{r}_\tau) = F(\mathbf{r},\mathbf{r}_\tau)/\gamma$ for which

$$\hat{L}(\mathbf{r},\nabla,\mathbf{r}_\tau) = -\frac{1}{\gamma}\nabla F(\mathbf{r},\mathbf{r}_\tau) + D\Delta, \tag{16}$$

where Δ denotes the Laplace operator. The Smoluchowski equation then reads

$$\left.\frac{\partial w(\mathbf{r},t|\mathbf{r}_\tau,t_\tau)}{\partial t}\right|_{t_\tau=t-\tau} = \frac{1}{\gamma}\nabla[k_BT\nabla - \mathbf{F}(\mathbf{r},\mathbf{r}_\tau)]w(\mathbf{r},t|\mathbf{r}_\tau,t_\tau)\,. \tag{17}$$

From this equation, the joint probability $w(\mathbf{r},t;\mathbf{r}_\tau,t_\tau) = w(\mathbf{r},t|\mathbf{r}_\tau,t_\tau)w(\mathbf{r}_\tau,t_\tau)$ is obtained by multiplication with $w(\mathbf{r}_\tau,t_\tau)$ as

$$\left.\frac{\partial w(\mathbf{r},t;\mathbf{r}_\tau,t_\tau)}{\partial t}\right|_{t_\tau=t-\tau} = \frac{1}{\gamma}\nabla[k_BT\nabla - \mathbf{F}(\mathbf{r},\mathbf{r}_\tau)]w(\mathbf{r},t;\mathbf{r}_\tau,t_\tau)\,. \tag{18}$$

Finally, integration over the past position $\mathbf{r}_\tau$ yields an expression for the probability $w(\mathbf{r},t) = \int d\mathbf{r}_\tau\, w(\mathbf{r},t;\mathbf{r}_\tau,t_\tau)$ to find a particle at $\mathbf{r}$ at time t without specifying its past position [3,86–88,93,94]; i.e., it leads from the joint probability to have a particle at position $\mathbf{r}$ at time t and at position $\mathbf{r}_\tau$ at time t_τ to one for the joint probability to have a particle at position $\mathbf{r}$ at time t and at any position at time t_τ. The resulting probability $w(\mathbf{r},t)$ is then no longer dependent on the past time t_τ and its time evolution is given by

$$\frac{\partial w(\mathbf{r},t)}{\partial t} = D\Delta w(\mathbf{r},t) - \frac{1}{\gamma}\int d\mathbf{r}_\tau\,\nabla\mathbf{F}(\mathbf{r},\mathbf{r}_\tau)w(\mathbf{r},t;\mathbf{r}_\tau,t_\tau)\,. \tag{19}$$

B. Extension to the many-particle case

We now return to the original problem of finding a Smoluchowski equation equivalent to Eq. (1). In this case, the system state $X(t)$ is given by a set of particle positions which should still obey Eq. (14). The many-body conditional probability density $w(\mathbf{r}^N,t|\mathbf{r}^N_\tau,t_\tau)$ to have N particles at positions $\mathbf{r}^N = \mathbf{r}_1,\ldots,\mathbf{r}_N$ at time t under the condition that the previous corresponding positions were $\mathbf{r}^N_\tau = \mathbf{r}_{\tau_1},\ldots,\mathbf{r}_{\tau_N}$ at time $t_\tau = t-\tau$ is thus given by

$$\left.\frac{\partial w(\mathbf{r}^N,t|\mathbf{r}^N_\tau,t_\tau)}{\partial t}\right|_{t_\tau=t-\tau} = \frac{1}{\gamma}\sum_{i=1}^{N}\nabla_i\left[k_BT\nabla_i - \left(-\nabla_i U_{\rm tot}(\mathbf{r}^N,\mathbf{r}^N_\tau)\right)\right]w\left(\mathbf{r}^N,t|\mathbf{r}^N_\tau,t_\tau\right). \tag{20}$$

Here, the gradient or divergence ∇_i indicates differentiation with respect to $\mathbf{r}_i$. The forces on the particles are expressed as potential gradients $-\nabla_i U_{\mathrm{tot}}(\mathbf{r}^N, \mathbf{r}_\tau^N)$ with the derivative in this term only intended to act on U_{tot} and not on $w(\mathbf{r}^N, t|\mathbf{r}_\tau^N, t_\tau)$. The potential includes the direct pair interaction potential between the particles, Φ, and a contribution due to the feedback potential, V_{fb}:

$$U_{\mathrm{tot}}\big(\mathbf{r}^N, \mathbf{r}_\tau^N\big) = \frac{1}{2}\sum_{\substack{i,\,j=1\\ i\neq j}}^{N} \Phi(|\mathbf{r}_i - \mathbf{r}_j|) + \sum_{i,j=1}^{N} V_{\mathrm{fb}}(|\mathbf{r}_i - \mathbf{r}_{\tau_j}|)\,. \tag{21}$$

Analogously to the one-particle case, multiplication of Eq. (20) with the probability $w(\mathbf{r}_\tau^N, t_\tau)$ to have had N particles at the positions $\mathbf{r}_\tau^N$ at time t_τ leads to an equation for the joint probability $w(\mathbf{r}^N, t; \mathbf{r}_\tau^N, t_\tau) = w(\mathbf{r}^N, t|\mathbf{r}_\tau^N, t_\tau) w(\mathbf{r}_\tau^N, t_\tau)$, given by

$$\left.\frac{\partial w\big(\mathbf{r}^N, t; \mathbf{r}_\tau^N, t_\tau\big)}{\partial t}\right|_{t_\tau = t-\tau} = \frac{1}{\gamma}\sum_{i=1}^{N} \nabla_i\big[k_B T \nabla_i + \big(\nabla_i U_{\mathrm{tot}}(\mathbf{r}^N, \mathbf{r}_\tau^N)\big)\big] w\big(\mathbf{r}^N, t; \mathbf{r}_\tau^N, t_\tau\big). \tag{22}$$

Integration over the past positions $\mathbf{r}_\tau^N$ yields an equation for the probability density solely dependent on the set of current positions $\mathbf{r}^N$ given by

$$w(\mathbf{r}^N, t) = \int d\mathbf{r}_{\tau_1} \cdots \int d\mathbf{r}_{\tau_N} w\big(\mathbf{r}^N, t; \mathbf{r}_\tau^N, t_\tau\big)\,. \tag{23}$$

Performing the integration, the potential term in Eq. (22),

$$\int d\mathbf{r}_{\tau_1} \cdots \int d\mathbf{r}_{\tau_N} U_{\mathrm{tot}}\big(\mathbf{r}^N, \mathbf{r}_\tau^N\big) w\big(\mathbf{r}^N, t; \mathbf{r}_\tau^N, t_\tau\big) = \int d\mathbf{r}_{\tau_1} \cdots \int d\mathbf{r}_{\tau_N} U_{\mathrm{tot}}\big(\mathbf{r}^N, \mathbf{r}_\tau^N\big) w\big(\mathbf{r}^N, t\big|\mathbf{r}_\tau^N, t_\tau\big) w\big(\mathbf{r}_\tau^N, t_\tau\big), \tag{24}$$

cannot be traced back to a simple expression due to the fact that both $U_{\mathrm{tot}}(\mathbf{r}^N, \mathbf{r}_\tau^N)$ and $w(\mathbf{r}^N, t|\mathbf{r}_\tau^N, t_\tau)$ depend on the previous particle positions $\mathbf{r}_\tau^N$. Intuitively, this can be understood as being due to the coupling of $U_{\mathrm{tot}}(\mathbf{r}^N, \mathbf{r}_\tau^N)$ to the particle trajectories. This renders the reduction of the potential to a single value at the current position impossible. The many-particle equivalent of Eq. (19) obtained from integration of Eq. (22) thus reads

$$\frac{\partial w(\mathbf{r}^N, t)}{\partial t} = D\sum_{i=1}^{N} \Delta_i w(\mathbf{r}^N, t) + \frac{1}{\gamma}\int d\mathbf{r}_{\tau_1} \cdots \int d\mathbf{r}_{\tau_N} \sum_{i=1}^{N} \nabla_i w\big(\mathbf{r}^N, t; \mathbf{r}_\tau^N, t_\tau\big) \nabla_i U_{\mathrm{tot}}\big(\mathbf{r}^N, \mathbf{r}_\tau^N\big)\,. \tag{25}$$

Next, we define the one- and two-particle densities, ρ and $\rho^{(2)}$, as well as the time-shifted two-particle density, $\rho_{\mathrm{s}}^{(2)}$, via

$$\rho(\mathbf{r}_1, t) = N\int d\mathbf{r}_2 \cdots \int d\mathbf{r}_N \int d\mathbf{r}_{\tau_1} \cdots \int d\mathbf{r}_{\tau_N}\; w\big(\mathbf{r}^N, t; \mathbf{r}_\tau^N, t_\tau\big), \tag{26}$$

$$\rho^{(2)}(\mathbf{r}_1, \mathbf{r}_2, t) = N(N-1)\int d\mathbf{r}_3 \cdots \int d\mathbf{r}_N \int d\mathbf{r}_{\tau_1} \cdots \int d\mathbf{r}_{\tau_N}\; w\big(\mathbf{r}^N, t; \mathbf{r}_\tau^N, t_\tau\big), \tag{27}$$

$$\begin{aligned}\rho_{\mathrm{s}}^{(2)}(\mathbf{r}_1, t; \mathbf{r}_\tau, t_\tau) = {} & N\int d\mathbf{r}_2 \cdots \int d\mathbf{r}_N \int d\mathbf{r}_{\tau_1} \cdots \int d\mathbf{r}_{\tau_N}\; w\big(\mathbf{r}^N, t; \mathbf{r}_\tau^N, t_\tau\big)\delta(\mathbf{r}_\tau - \mathbf{r}_{\tau_1}) \\ & + N(N-1)\int d\mathbf{r}_2 \cdots \int d\mathbf{r}_N \int d\mathbf{r}_{\tau_1} \cdots \int d\mathbf{r}_{\tau_N}\; w\big(\mathbf{r}^N, t; \mathbf{r}_\tau^N, t_\tau\big)\delta(\mathbf{r}_\tau - \mathbf{r}_{\tau_2})\,.\end{aligned} \tag{28}$$

Here, the instantaneous densities $\rho(\mathbf{r}_1, t)$ and $\rho^{(2)}(\mathbf{r}_1, \mathbf{r}_2, t)$ do not depend on t_τ due to integration over the past positions $\mathbf{r}_\tau^N$. Furthermore, note that $\rho_{\mathrm{s}}^{(2)}(\mathbf{r}_1, t; \mathbf{r}_\tau, t_\tau)$ includes a self-term (first part) as well as a term due to other particles (second part) such that the resultant two-particle density is defined as the probability to find one particle at $\mathbf{r}_1$ at time t and any particle (i.e., the same or another) at position $\mathbf{r}_\tau$ at time t_τ.

To obtain an equation for the evolution of the one-particle density, Eq. (25) is integrated with $N\int d\mathbf{r}_2 \cdots \int d\mathbf{r}_N$. Using the above definitions, this leads to the exact equation

$$\gamma\frac{\partial \rho(\mathbf{r}_1, t)}{\partial t} = k_B T \Delta_1 \rho(\mathbf{r}_1, t) + \int d\mathbf{r}_2 \nabla_1 \rho^{(2)}(\mathbf{r}_1, \mathbf{r}_2, t) \nabla_1 \Phi(|\mathbf{r}_1 - \mathbf{r}_2|) + \int d\mathbf{r}_\tau \nabla_1 \rho_{\mathrm{s}}^{(2)}(\mathbf{r}_1, t; \mathbf{r}_\tau, t_\tau) \nabla_1 V_{\mathrm{fb}}(|\mathbf{r}_1 - \mathbf{r}_\tau|)\,. \tag{29}$$

It is worth mentioning that the last term, i.e., the interaction via the feedback potential, is similar to the preceding one, meaning that it takes the same form as a pair potential. The two terms differ in that the feedback does not act between positions at the same time but positions at time t and previous ones at time t_τ. Also, the last

term includes a self-term which is not present in the direct interactions.

C. Derivation of the DDFT equation

Starting from the many-body time-delayed Smoluchowski equation [Eq. (29)], which is stochastically equivalent to the Langevin equation [Eq. (1)], we construct a dynamical density functional theory (DDFT) [72]. The DDFT is then used in the next section to investigate the stability of the homogeneous density state against wave formation.

Equation (29) is exact but not self-contained as it includes the instantaneous and the time-shifted two-particle density. To obtain a closed equation, we first rewrite the direct interaction potential using the adiabatic approximation of DDFT,

$$\int d\mathbf{r}_2 \rho^{(2)}(\mathbf{r}_1,\mathbf{r}_2)\nabla_1\Phi(|\mathbf{r}_1-\mathbf{r}_2|) = -k_BT\rho(\mathbf{r}_1)\nabla_1 c^{(1)}(\mathbf{r}_1), \tag{30}$$

which expresses the particle interaction forces via the direct correlation function $c^{(1)}(\mathbf{r})$. The latter is related to the excess free energy, i.e., the nonideal part of the free energy, $\mathcal{F}_{\rm exc}$, by

$$c^{(1)}(\mathbf{r}) = -\frac{1}{k_BT}\frac{\delta\mathcal{F}_{\rm exc}[\rho(\mathbf{r})]}{\delta\rho(\mathbf{r})} \tag{31}$$

in equilibrium. The adiabatic approximation assumes the same relation in nonequilibrium.

Second, it is necessary to focus on the time-shifted two-particle density. In fact, even for the noninteracting particle case ($\Phi = 0$) this term leads to a hierarchy of equations whose solution is not at all trivial and subject to current research [3,86–88,93,94]. Here, we use the mean-field-like approximation

$$\begin{aligned}\rho_{\rm s}^{(2)}(\mathbf{r}_1,t;\mathbf{r}_\tau,t_\tau) &\approx \rho(\mathbf{r}_1,t)\rho(\mathbf{r}_\tau,t_\tau)\\ &= \rho(\mathbf{r}_1,t)\rho(\mathbf{r}_\tau,t-\tau).\end{aligned} \tag{32}$$

At this point, we are thus neglecting the correlations between the present and past positions of the particles. The description is then equivalent to having particles move in an effective external potential

$$\bar{V}_{\rm fb}(\mathbf{r}^N,t) = \int d\mathbf{r}_\tau \rho(\mathbf{r}_\tau,t-\tau)V_{\rm fb}(|\mathbf{r}-\mathbf{r}_\tau|), \tag{33}$$

which is obtained through a convolution of the time-shifted one-particle density with the feedback potential $V_{\rm fb}$. This is a crude approximation for systems where the different sets of actual particle paths are important and the one-particle density is not sufficient to describe the system. It should, however, be decent if we are close to a homogeneous state due to a small amplitude of the feedback potential or if we consider only a small perturbation to this state, as done in the next section. Such a homogeneous reference state is expected to lose its memory of the specific realization of past positions on the time scale $1/D\rho_0$, i.e., the time needed for particles to diffuse the mean interparticle distance. However, this approximation is in particular *not* well justified for dilute feedback systems or very short delay times $\tau \ll 1/D\rho_0$.

Finally, inserting the above approximations into Eq. (29), a self-contained approximative equation for the one-particle density is obtained:

$$\begin{aligned}\gamma\frac{\partial\rho(\mathbf{r},t)}{\partial t} &= k_BT\Delta\rho(\mathbf{r},t) - k_BT\nabla\rho(\mathbf{r})\nabla c^{(1)}(\mathbf{r})\\ &\quad + \nabla\rho(\mathbf{r},t)\nabla\int d\mathbf{r}_\tau\rho(\mathbf{r}_\tau,t-\tau)V_{\rm fb}(|\mathbf{r}-\mathbf{r}_\tau|).\end{aligned} \tag{34}$$

D. Linear stability analysis

Next, the effect of a small perturbation $\rho_{\rm p}(\mathbf{r},t)$ on a homogeneous state of constant density ρ_0 is investigated with

$$\rho(\mathbf{r},t) = \rho_0 + \rho_{\rm p}(\mathbf{r},t) \tag{35}$$

being the space- and time-dependent density. We expand the direct correlation function $c^{(1)}(\mathbf{r})$ about the bulk fluid value ρ_0 up to linear order,

$$\begin{aligned}c^{(1)}(\mathbf{r}) &\approx c_0^{(1)} + \int d\mathbf{r}_2 \left.\frac{\delta c^{(1)}(\mathbf{r})}{\delta\rho(\mathbf{r}_2)}\right|_{\rho_0}\rho_{\rm p}(\mathbf{r}_2,t)\\ &= c_0^{(1)} + \int d\mathbf{r}_2\, c^{(2)}(|\mathbf{r}-\mathbf{r}_2|;\rho_0)\rho_{\rm p}(\mathbf{r}_2,t),\end{aligned} \tag{36}$$

with the direct pair-correlation function

$$c^{(2)}(|\mathbf{r}-\mathbf{r}_2|;\rho_0) = -\frac{1}{k_BT}\left.\frac{\delta^2\mathcal{F}_{\rm exc}[\rho(\mathbf{r})]}{\delta\rho(\mathbf{r}_2)\delta\rho(\mathbf{r})}\right|_{\rho_0} \tag{37}$$

and insert this expression into Eq. (34). Linearization of the result in the perturbation density $\rho_{\rm p}(\mathbf{r},t)$ and nondimensionalization yields the equation

$$\begin{aligned}\frac{\partial\tilde{\rho}(\mathbf{k},t)}{\partial t} &= -k^2[\tilde{\rho}(\mathbf{k},t) - \rho_0\,\tilde{\rho}(\mathbf{k},t)\tilde{c}(k;\rho_0)\\ &\quad + \rho_0\,\tilde{\rho}(\mathbf{k},t-\tau)\tilde{V}_{\rm fb}(k)],\end{aligned} \tag{38}$$

where $\tilde{\rho}(\mathbf{k},t)$ indicates the Fourier transform of $\rho_{\rm p}(\mathbf{r},t)$, $\tilde{c}(k;\rho_0)$ the one of $c^{(2)}(|\mathbf{r}-\mathbf{r}_2|;\rho_0)$, and $\tilde{V}_{\rm fb}$ the one of the feedback potential.

Taking the ansatz for a wave solution of wave vector $\mathbf{k}$ and amplitude ε,

$$\rho_{\rm p}(\mathbf{r},t) = \varepsilon\, e^{i\mathbf{k}\mathbf{r}}e^{\lambda t}, \tag{39}$$

and inserting it into Eq. (38), we obtain the dispersion relation

$$\lambda = -k^2[1-\rho_0\,\tilde{c}(k;\rho_0) + \rho_0\,e^{-\lambda\tau}\tilde{V}_{\rm fb}(k)]. \tag{40}$$

The solution for λ can be separated into a real part α describing the growth of the perturbation and an imaginary part ω giving the angular frequency of the traveling wave as

$$\lambda(k) = \alpha(k) + i\omega(k). \tag{41}$$

This gives the two equations

$$\begin{aligned}\alpha(k) &= -k^2[1-\rho_0\,\tilde{c}(k;\rho_0) + \rho_0\,e^{-\alpha(k)\tau}\cos(\omega(k)\tau)\tilde{V}_{\rm fb}(k)],\\ \omega(k) &= k^2\rho_0\,e^{-\alpha(k)\tau}\sin(\omega(k)\tau)\tilde{V}_{\rm fb}(k),\end{aligned} \tag{42}$$

which implicitly define the solution. Since $\tilde{c}(k;\rho_0)$ for the equilibrium bulk fluid is required here as an input, we use a reference simulation without the feedback potential to obtain $\tilde{c}(k;\rho_0)$ which is related to the structure factor of the system

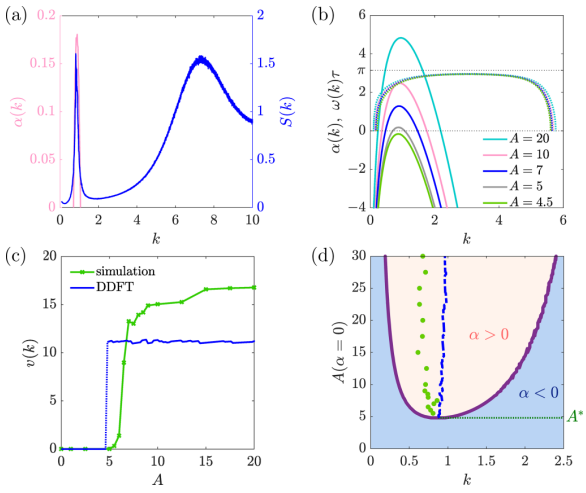

FIG. 9. Prediction of the instability using DDFT: (a) Simulation result for structure factor $S(k)$ and DDFT prediction for the growth rate $\alpha(k)$ for $A = 5$. (b) Growth rate $\alpha(k)$ and angular frequency $\omega(k)$ for different strengths of the feedback potential. Solid lines give values for α, dotted ones those for $\omega\tau$. (c) Comparison between DDFT prediction of band velocity and simulation results. (d) Stability curve giving the wave-number-dependent value of A for which the growth factor α changes from negative to positive. The minimal value of A, for which an $\alpha = 0$ exists, is denoted by $A^* \approx 4.8$. The green dots show the wave number at which patterning was observed in the simulations. The blue dashed line shows the maximally unstable wavelength according to the DDFT prediction.

by [95]

$$\tilde{c}(k;\rho_0) = \rho_0\left(1 - \frac{1}{S(k)}\right). \tag{43}$$

E. DDFT results and comparison to simulations

Results for $\alpha(k)$ and $\omega(k)$ are shown in Fig. 9. Figure 9(a) displays the range of unstable wave numbers defined via a positive $\alpha(k)$ and puts these into relation to the structure factor $S(k)$. Indeed, the maximally unstable wave number, i.e., the wave number at which $\alpha(k)$ has its maximum, coincides with the structural bandwidth characterized by k^*.

Figure 9(b) shows the full dispersion $\alpha(k)$ and $\omega(k)$ for various A. The range of unstable wave numbers is zero below the transition ($A < 4.8$) and increases with the feedback amplitude A above it. From the frequency $\omega(k)$, close to the transition, the phase velocity of the imposed wave is determined by $\omega(k)/k$. At $k = k^*$ this phase velocity should be close to the band velocity v such that the band velocity predicted by the theory is

$$v = \frac{\omega(k^*)}{k^*}. \tag{44}$$

According to Eqs. (5) and (44) we obtain an approximative phase shift of $\omega(k^*)\tau = \pi$ within the delay time. In fact, Fig. 9(b) reveals that the phase shift $\omega(k^*)\tau$ is close to π but deviations appear due to the approximative nature of Eq. (5). The phase shift $\omega(k^*)\tau$ is close to the ideal value π for any k close to the maximally unstable wave vector with discrepancies indicating that the wave does not change exactly between a pattern and its negative image after a delay time τ.

The theoretical prediction of the band velocity is compared to the simulation data in Fig. 9(c) and reasonable agreement is found with respect to onset and magnitude of the velocity as a function of the feedback potential amplitude A.

Figure 9(d) illustrates the stability in the plane defined by the wave number k and the feedback amplitude A. There is a separatrix distinguishing a stable [$\alpha(k) < 0$] from an unstable [$\alpha(k) > 0$] regime. The instability occurs beyond a critical amplitude $A^* \approx 4.8$ with an instability wave number $k^* = 0.87$. The DDFT prediction for the critical amplitude $A^* \approx 4.8$ compares favorably with the simulation results of $5 \leqslant A^* \leqslant 6$ which documents the predictive power of the microscopic theory. Deviations may be due to the approximative pair correlation function entering as an input for the nonequilibrium steady state or due to the adiabatic approximation.

In the unstable regime, $\alpha(k) > 0$, the maximally unstable wave number, i.e., the one with the fastest growth rate, is shown by the blue dashed line in Fig. 9(d). This prediction can be compared to the actual band wave number k^* found in the simulations shown as green dots. While at the onset of the transition these two wave numbers are very close [see also Fig. 9(a)], they exhibit a different trend for increasing A indicating that nonlinear effects play a larger role away from criticality.

V. CIRCULAR CONFINEMENT

In the case of periodic boundary conditions as discussed in Sec. III the commensurability of the box size and the (projected) wavelength effectively constrains the possible band orientations. Inversely, this constraint may affect the actually realized wavelength as certain combinations of orientation and wavelength that fit well with the box size may be preferred. In the following, we aim to investigate this effect in more detail by confining the system to a prescribed geometry. We choose a circular confinement which is imposed onto the system by an external potential $\Phi_c(r)$ which is radially symmetric. The potential is soft but diverges at a distance $r = R$ from the center such that a circular confinement is realized. We choose the external potential form

$$\Phi_c(r) = \frac{V_0}{R - r}\, e^{-\kappa(R-r)} \tag{45}$$

and fix the radius to $R \approx 45\,b$ such that the density $\rho_0 = N/\pi R^2 = 1/b^2$ with $N = 6400$ is the same as in the previous case.

Representative snapshots of the system for different feedback potential amplitudes A are shown in Fig. 10. Band formation is found as for the nonconfined case, with the pattern reaching further inwards if the feedback potential strength is increased. This is because the confining boundaries set a preferred band orientation and thus facilitate the formation of a traveling wave along the boundary. Due to the circular form of the confining potential, the bands are now forced into a rotational motion. Moreover, the circular geometry does not allow parallel wavefronts with a constant separation running from the boundary to the center. Thus, defects are

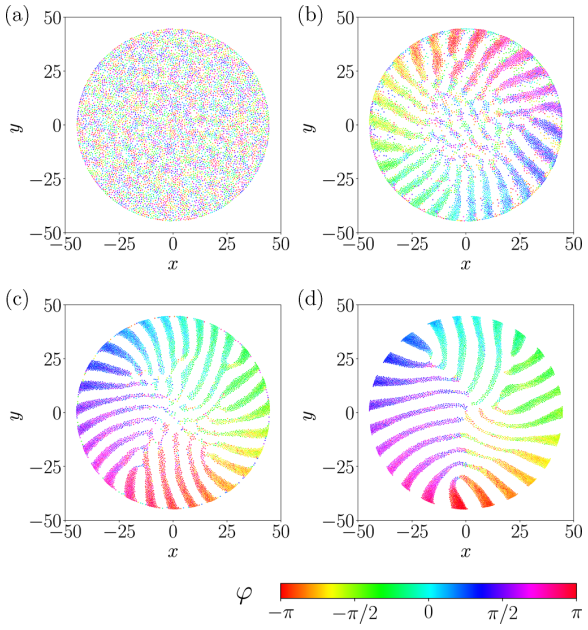

FIG. 10. Particle positions for potential strength (a) $A = 5.5$, (b) $A = 7$, (c) $A = 10$, and (d) $A = 20$ at time $t = 500$. The color code is the same as used in Fig. 3 and indicates the direction of movement of the particles.

unavoidable. At low and intermediate feedback potentials the formed pattern is approximately rotationally symmetric with respect to the center but not very well ordered. In contrast, at high values of A, the waves are well established and have an about constant wavelength. However, to allow for this arrangement, a separation into domains of different band orientation with a complicated topology at the center is required and observed.

To further examine the system response in this case, we consider the time-averaged radial density profile

$$\rho_c(r) = \left\langle \sum_{i=1}^{N} \delta\big(\mathbf{r} - \mathbf{r}_i(t')\big) \right\rangle, \tag{46}$$

which by symmetry depends only on the radial distance r to the center. Next, we also define a time-averaged angular drift velocity profile $\omega_c(r)$:

$$\omega_c(r) = \hat{\mathbf{e}}_z \cdot \left\langle \sum_{i=1}^{N} \frac{\mathbf{r}_i(t') \times \mathbf{v}_i(t')}{\mathbf{r}_i^2(t')} \delta\big(\mathbf{r} - \mathbf{r}_i(t')\big) \right\rangle \frac{1}{\rho_c(r)}, \tag{47}$$

where $\hat{\mathbf{e}}_z$ is the unit vector perpendicular to the plane of motion. The profile $\omega_c(r)$ likewise depends on the radial distance to the center only. Figure 11 shows results for the density profile $\rho_c(r)$ and the angular velocity $\omega_c(r)$. For growing feedback potential strength A, an accumulation of particles near the system boundary is observed as signaled by a peak in the density profile close to the wall accompanied by a (relative) depletion of particles near the center. This effect has also been found for self-propelled particles in circular confinement [96,97] and can qualitatively be understood here on similar

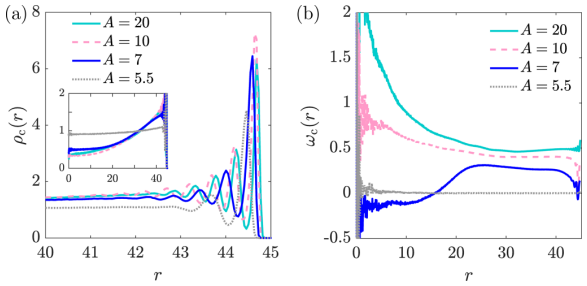

FIG. 11. (a) Radial density profile $\rho_c(r)$ and (b) angular drift velocity profile $\omega_c(r)$. In (b) the sign has been adjusted such that $\omega_c(r)$ takes a positive value for the particles in the bands (i.e., in the range $r \approx 20 - 40$). The feedback potential leads to a density accumulation at the system boundary and a rotational motion around the center.

grounds as suggested by the MSD (Fig. 8) which resembles active Brownian particles. The difference between the two cases is that here, the individual particle velocity is typically directed tangentially to the wall. Therefore, in the feedback case the accumulation is driven by wall curvature and larger A enhances the wall accumulation effect. In contrast, in the active particle case it is driven by persistence in the otherwise unconstrained propulsion direction.

Considering the angular velocity, we find that for small feedback potentials it is almost zero at all distances r from the center. Increasing A leads to the formation of a two-layer state with the inner part revolving in the *opposite* direction to the outer one, signaled by a sign change in ω_c. The continuous change in ω_c with distance r is consistent with a motion spiraling outwards. At even higher values of A, this feature disappears and all particles rotate like a rigid body with a constant joint angular velocity apart from some remaining distance dependence in the central part of the profile. Thus, the slope of ω_c is negative, implying a motion which is spiraling inwards. Furthermore, close to the wall, particles move in the opposite direction to the bands or at least significantly more slowly than the band. This is especially observed for intermediate feedback strengths, signaled by a dip in the angular velocity to values below zero. This effect is interpreted as an escape of particles from the ideal bands induced by wall curvature, leading to counterpropagating particles which are visible in the system snapshots of Figs. 10(b) and 10(c). It vanishes again for strong feedback strengths [see Fig. 10(d)].

For high feedback potential amplitude, the emergence of domains with different band orientations is observed. These domains are separated by grain boundaries which, interestingly, are neither static nor co-rotating with the same mean angular speed as the particles. Instead, they rotate with a considerably slower angular speed albeit in the same direction. This is documented in Fig. 12, where typical system snapshots are shown during one full but slow rotation of the system grain boundaries. Four boundaries separating different domains are indicated in Fig. 12.

The angular position of the grain boundaries as a function of time is shown in Fig. 13. Their angular positions change approximately linearly in time. A linear fit yields an average

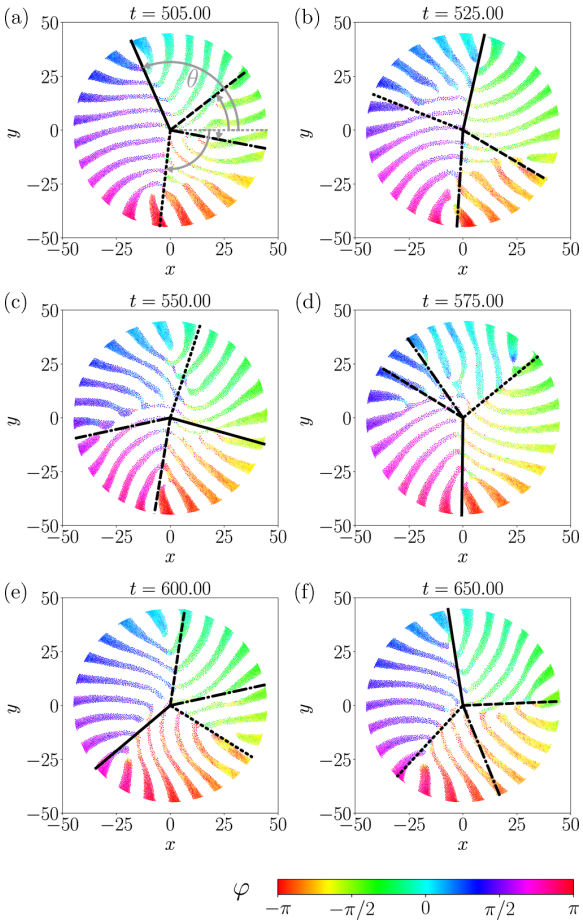

FIG. 12. Snapshots for potential amplitude $A = 20$ for approximately one full rotation of the slow domain boundaries which occurs over a time of about 150. As in Fig. 3, colors indicate the direction of the particle drift velocity. The phase boundaries between the different domains are also indicated as black lines. Their movement with respect to time is measured by the angles θ [indicated in (a)] and plotted in Fig. 13.

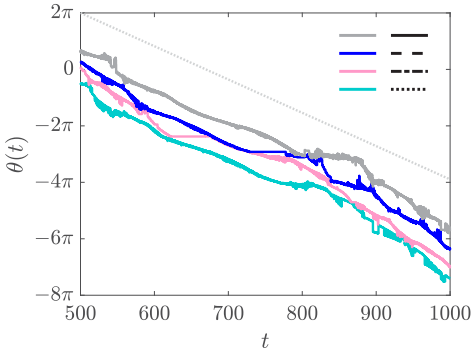

FIG. 13. Time dependence of the angular position θ of the grain boundaries indicated by the black lines in Fig. 12. For better visibility, the positions of the different grain boundaries are distinguished by color. The corresponding line styles of the boundaries indicated in Fig. 12 are shown in the legend. The mean angular velocity of the grains is indicated by the dotted line.

rotation speed of the grains of $\omega_g \approx -0.04$ for the system of Fig. 10(d), i.e., for a feedback amplitude of $A = 20$. This is one order of magnitude smaller than the mean particle angular velocity, which is $\omega_c \approx -0.5$ in the outermost part of the cavity [see Fig. 11(b)]. We speculate that the slower grain boundary speed is related to the group velocity of propagating bands in the bulk which is also much smaller than the phase velocity. In fact, from Fig. 9(b), the group velocity $d\omega(k)/dk|_{k=k^*}$ is only 13% of the phase velocity $\omega(k^*)/k^*$ at the wave number k^* for the given potential strength ($A = 20$).

To summarize, the feedback-driven suspension forms moving bands also under circular confinement. Due to the impenetrability of the walls, the band velocity has to be tangential to the wall; i.e., the band lamellas must be oriented perpendicular to the wall if the bands move along the normal of their interface as in the unconstrained case. While confinement to a straight (i.e., uncurved) slit geometry supports band formation perpendicular to the walls by imposing a preferred band orientation (data not shown), wall curvature destabilizes such bands due to the incompatibility with straight bands. Since the constraint of perpendicularity cannot be sustained for a *straight* band along a *curved* wall, the bands must either bend or change their width as a function of radial distance to the center such that $\lambda_b \equiv \lambda_b(r)$. Furthermore, as in the periodic boundary case, the fixed length of the circumference also poses a commensurability constraint for the band wavelength. However, this second constraint is weakened due to the grain boundaries. For the large feedback strengths considered here, the system exhibits tilted band formation. Dynamically this implies that spiraling waves are formed for which both inward and outward orientation are observed. In particular, particles near the curved wall cannot accommodate their individual motion with the global band motion and depending on A are either left behind or propagate faster [see Fig. 11(b)]. As a further important consequence, the convex curvature of the boundary leads to a significant particle accumulation near the wall and a depletion from the system center. The latter constitutes a natural source of disorder as topologically the cavity can never fulfill the constraints of curved bands meeting in the center. Instead the center becomes a nucleation point for grains with different band orientations. For strong feedback strengths, these grains co-rotate with much smaller angular velocities than that of the individual bands.

VI. CONCLUSIONS

We have shown that subjecting colloidal particles to a repulsive feedback potential dependent on their previous positions can lead to pattern formation. For a sufficiently strong repulsive potential, we have found a transition to a traveling band phase which can be predicted by a linear stability analysis of dynamical density functional theory. Under circular confinement, the transition persists but becomes more complex, exhibiting wall accumulation of particles, spiraling patterns, and creation of banded domains. Our

findings can be verified in experiments by using colloids in an external light field [17–21] or employing autochemotactic particles [33,34].

Future work can be performed along the following directions: First, it is worth considering an *attractive* feedback potential with a negative amplitude $A < 0$. For attractive feedback, particles tend to stay at their previous positions. Starting from an initial homogeneous system, this leads to the formation of particle clusters accompanied by a slowing down of the dynamics and to subsequent coarsening. The emerging structures are expected to be similar to those found in phase separation [98]. It would thus be interesting to identify and compare the scaling laws for the mean cluster size as a function of time in different regimes for various system parameters.

Second, while our scenario will not qualitatively change for other types of soft repulsion between the particles, a long-ranged attraction [76,77] in the interparticle forces can give rise to equilibrium gas-liquid phase separation [99] with a critical point. If a repulsive feedback potential is applied, there is competition between bulk phase separation and band formation which may lead to interesting new structures.

Third, if one considers higher particle densities or lower temperature than in this paper, the equilibrium two-dimensional Yukawa system exhibits freezing into a hexatic or hexagonal crystalline phase [100]. Applying a repulsive feedback is then expected to lead to the formation of traveling crystalline bands ("solids"), the detailed structure of which still has to be worked out. The density increase in the bands induced by the feedback will additionally support and enhance traveling crystal formation. Thus, it is expected that the phase boundary will depend on the amplitude A. Dynamical density functional theory can in principle be applied to describe crystallization in nonequilibrium [101,102].

Fourth, active particles in feedback potentials present a rich playground to investigate further complex collective effects due to competition between activity and feedback forces. Even in the absence of feedback the collective behavior of active particles is rich [103] and it remains to be explored how swarming [104] and motility-induced phase separation [105] compete with feedback potentials. Again dynamical density functional theory can be employed for an appropriate instability analysis [106].

Last, possible future work should also include extending the system presented here to three dimensions and considering the effect of more complex confining geometries [107], for example, nonconvex walls and moving boundaries. Likewise, multiple (competing) [108] or more complex [44,109] feedback terms can be considered. The latter may also take a density-dependent form, thus describing quorum sensing [20].

ACKNOWLEDGMENTS

We thank W. Zimmermann, B. Liebchen, C. Hoell, and M. Tarama for helpful discussions. We gratefully acknowledge financial support by the DFG Grants No. LO 418/19-1 and No. EG 269/6-1.

[1] L. Granger, L. Dinis, J. M. Horowitz, and J. M. R. Parrondo, Europhys. Lett. **115**, 50007 (2016).
[2] S. A. M. Loos, R. Gernert, and S. H. L. Klapp, Phys. Rev. E **89**, 052136 (2014).
[3] S. A. M. Loos and S. H. L. Klapp, Phys. Rev. E **96**, 012106 (2017).
[4] S. A. M. Loos and S. H. L. Klapp, Sci. Rep. **9**, 2491 (2019).
[5] B. von Lospichl and S. H. L. Klapp, Phys. Rev. E **98**, 042605 (2018).
[6] B. J. Lopez, N. J. Kuwada, E. M. Craig, B. R. Long, and H. Linke, Phys. Rev. Lett. **101**, 220601 (2008).
[7] R. Gernert and S. H. L. Klapp, Phys. Rev. E **92**, 022132 (2015).
[8] P. Popli, S. Ganguly, and S. Sengupta, Soft Matter **14**, 104 (2018).
[9] Y. Yang and M. A. Bevan, ACS Nano **12**, 10712 (2018).
[10] K. Lichtner and S. H. L. Klapp, Europhys. Lett. **92**, 40007 (2010).
[11] K. Pyragas, Phys. Lett. A **170**, 421 (1992).
[12] P. Hövel and E. Schöll, Phys. Rev. E **72**, 046203 (2005).
[13] A. E. Cohen, Phys. Rev. Lett. **94**, 118102 (2005).
[14] Y. Jun and J. Bechhoefer, Phys. Rev. E **86**, 061106 (2012).
[15] U. Khadka, V. Holubec, H. Yang, and F. Cichos, Nat. Commun. **9**, 3864 (2018).
[16] V. Blickle and C. Bechinger, Nat. Phys. **8**, 143 (2011).
[17] R. D. L. Hanes, M. C. Jenkins, and S. U. Egelhaaf, Rev. Sci. Instrum. **80**, 083703 (2009).
[18] F. Evers, R. D. L. Hanes, C. Zunke, R. F. Capellmann, J. Bewerunge, C. Dalle-Ferrier, M. C. Jenkins, I. Ladadwa, A. Heuer, R. Castañeda-Priego, and S. U. Egelhaaf, Eur. Phys. J.: Spec. Top. **222**, 2995 (2013).
[19] J. Bewerunge and S. U. Egelhaaf, Phys. Rev. A **93**, 013806 (2016).
[20] T. Bäuerle, A. Fischer, T. Speck, and C. Bechinger, Nat. Commun. **9**, 3232 (2018).
[21] P. Jones, O. Marag, and G. Volpe, *Optical Tweezers: Principles and Applications* (Cambridge University Press, Cambridge, UK, 2015).
[22] K. Nishizawa, M. Bremerich, H. Ayade, C. F. Schmidt, T. Ariga, and D. Mizuno, Sci. Adv. **3**, e1700318 (2017).
[23] J. Adler, Science **153**, 708 (1966).
[24] E. F. Keller and L. A. Segel, J. Theor. Biol. **30**, 235 (1971).
[25] I. D. Couzin and N. R. Franks, Proc. R. Soc. London Ser. B **270**, 139 (2003).
[26] C. Bechinger, R. Di Leonardo, H. Löwen, C. Reichhardt, G. Volpe, and G. Volpe, Rev. Mod. Phys. **88**, 045006 (2016).
[27] B. Liebchen, D. Marenduzzo, I. Pagonabarraga, and M. E. Cates, Phys. Rev. Lett. **115**, 258301 (2015).
[28] B. Liebchen, M. E. Cates, and D. Marenduzzo, Soft Matter **12**, 7259 (2016).
[29] B. Liebchen, D. Marenduzzo, and M. E. Cates, Phys. Rev. Lett. **118**, 268001 (2017).
[30] S. Saha, R. Golestanian, and S. Ramaswamy, Phys. Rev. E **89**, 062316 (2014).

[31] A. Sengupta, S. van Teeffelen, and H. Löwen, Phys. Rev. E **80**, 031122 (2009).
[32] A. Sengupta, T. Kruppa, and H. Löwen, Phys. Rev. E **83**, 031914 (2011).
[33] C. Jin, C. Krüger, and C. C. Maass, Proc. Natl. Acad. Sci. USA **114**, 5089 (2017).
[34] C. Jin, B. V. Hokmabad, K. A. Baldwin, and C. C. Maass, J. Phys. Condens. Matter **30**, 054003 (2018).
[35] M. Cross and H. Greenside, *Pattern Formation and Dynamics in Nonequilibrium Systems* (Cambridge University Press, Cambridge, UK, 2009).
[36] M. C. Cross and P. C. Hohenberg, Rev. Mod. Phys. **65**, 851 (1993).
[37] G. Gonnella, E. Orlandini, and J. M. Yeomans, Phys. Rev. Lett. **78**, 1695 (1997).
[38] R. Zakine, J.-B. Fournier, and F. van Wijland, Phys. Rev. Lett. **121**, 028001 (2018).
[39] B. Chacko, C. Chalmers, and A. J. Archer, J. Chem. Phys. **143**, 244904 (2015).
[40] A. Krekhov, V. Weith, and W. Zimmermann, Phys. Rev. E **88**, 040302(R) (2013).
[41] E. Lushi, R. E. Goldstein, and M. J. Shelley, Phys. Rev. E **98**, 052411 (2018).
[42] I. S. Aranson and L. Kramer, Rev. Mod. Phys. **74**, 99 (2002).
[43] D. Puzyrev, S. Yanchuk, A. G. Vladimirov, and S. V. Gurevich, SIAM J. Appl. Dyn. Syst. **13**, 986 (2014).
[44] M. Ciszak, C. Mayol, C. R. Mirasso, and R. Toral, Phys. Rev. E **92**, 032911 (2015).
[45] H. Emmerich, H. Löwen, R. Wittkowski, T. Gruhn, G. I. Tóth, G. Tegze, and L. Gránásy, Adv. Phys. **61**, 665 (2012).
[46] J. Swift and P. C. Hohenberg, Phys. Rev. A **15**, 319 (1977).
[47] G. Gerisch, T. Bretschneider, A. Müller-Taubenberger, E. Simmeth, M. Ecke, S. Diez, and K. Anderson, Biophys. J. **87**, 3493 (2004).
[48] T. Le Goff, B. Liebchen, and D. Marenduzzo, Phys. Rev. Lett. **117**, 238002 (2016).
[49] V. Schaller, C. Weber, C. Semmrich, E. Frey, and A. R. Bausch, Nature (London) **467**, 73 (2010).
[50] J. Elgeti and G. Gompper, Proc. Natl. Acad. Sci. USA **110**, 4470 (2013).
[51] T. Vicsek, A. Czirók, E. Ben-Jacob, I. Cohen, and O. Shochet, Phys. Rev. Lett. **75**, 1226 (1995).
[52] H. Chaté, F. Ginelli, G. Grégoire, and F. Raynaud, Phys. Rev. E **77**, 046113 (2008).
[53] A. M. Menzel and H. Löwen, Phys. Rev. Lett. **110**, 055702 (2013).
[54] L. Ophaus, S. V. Gurevich, and U. Thiele, Phys. Rev. E **98**, 022608 (2018).
[55] H. Reinken, S. Heidenreich, M. Bär, and S. H. L. Klapp, New J. Phys. **21**, 013037 (2019).
[56] S. K. Schnyder, J. J. Molina, Y. Tanaka, and R. Yamamoto, Sci. Rep. **7**, 5163 (2017).
[57] T. Vissers, A. van Blaaderen, and A. Imhof, Phys. Rev. Lett. **106**, 228303 (2011).
[58] A. Wysocki and H. Löwen, Phys. Rev. E **79**, 041408 (2009).
[59] J. Dzubiella, G. P. Hoffmann, and H. Löwen, Phys. Rev. E **65**, 021402 (2002).
[60] C. Reichhardt and C. J. Olson Reichhardt, Phys. Rev. E **75**, 040402(R) (2007).
[61] M. Ikeda, H. Wada, and H. Hayakawa, Europhys. Lett. **99**, 68005 (2012).
[62] C. Reichhardt, J. Thibault, S. Papanikolaou, and C. J. O. Reichhardt, Phys. Rev. E **98**, 022603 (2018).
[63] C. Reichhardt and C. J. O. Reichhardt, Soft Matter **14**, 490 (2018).
[64] J. Dzubiella and H. Löwen, J. Phys. Condens. Matter **14**, 9383 (2002).
[65] T. Okuzono and T. Ohta, Phys. Rev. E **64**, 045201(R) (2001).
[66] T. Okuzono and T. Ohta, Phys. Rev. E **67**, 056211 (2003).
[67] S. V. Gurevich, Phys. Rev. E **87**, 052922 (2013).
[68] F. Tabbert, C. Schelte, M. Tlidi, and S. V. Gurevich, Phys. Rev. E **95**, 032213 (2017).
[69] S. V. Gurevich and R. Friedrich, Phys. Rev. Lett. **110**, 014101 (2013).
[70] U. M. B. Marconi and P. Tarazona, J. Chem. Phys. **110**, 8032 (1999).
[71] U. M. B. Marconi and P. Tarazona, J. Phys. Condens. Matter **12**, A413 (2000).
[72] A. J. Archer and R. Evans, J. Chem. Phys. **121**, 4246 (2004).
[73] P. Español and H. Löwen, J. Chem. Phys. **131**, 244101 (2009).
[74] R. Evans, M. Oettel, R. Roth, and G. Kahl, J. Phys. Condens. Matter **28**, 240401 (2016).
[75] R. Wittkowski and H. Löwen, Mol. Phys. **109**, 2935 (2011).
[76] C. J. Olson Reichhardt, C. Reichhardt, and A. R. Bishop, Phys. Rev. E **82**, 041502 (2010).
[77] H. J. Zhao, V. R. Misko, and F. M. Peeters, New J. Phys. **14**, 063032 (2012).
[78] H. Wioland, F. G. Woodhouse, J. Dunkel, J. O. Kessler, and R. E. Goldstein, Phys. Rev. Lett. **110**, 268102 (2013).
[79] M. Leyman, F. Ogemark, J. Wehr, and G. Volpe, Phys. Rev. E **98**, 052606 (2018).
[80] F. A. Lavergne, H. Wendehenne, T. Bäuerle, and C. Bechinger, Science **364**, 70 (2019).
[81] T. Ohira and T. Yamane, Phys. Rev. E **61**, 1247 (2000).
[82] T. Ohira and T. Hosaka, Artif. Life Rob. **9**, 194 (2005).
[83] T. Ohira and J. Milton, *Delay Differential Equations: Recent Advances and New Directions* (Springer, Boston, 2009), pp. 1–31.
[84] S. Trimper and K. Zabrocki, Phys. Lett. A **331**, 423 (2004).
[85] M. Le Berre, E. Ressayre, A. Tallet, and Y. Pomeau, Phys. Rev. A **41**, 6635 (1990).
[86] S. Guillouzic, I. L'Heureux, and A. Longtin, Phys. Rev. E **59**, 3970 (1999).
[87] F. Atay, *Complex Time-Delay Systems: Theory and Applications, Understanding Complex Systems* (Springer, Berlin, 2010).
[88] S. A. M. Loos and S. H. L. Klapp, arXiv:1903.02322.
[89] H. Löwen, J. Phys. Condens. Matter **4**, 10105 (1992).
[90] C. J. O. Reichhardt and C. Reichhardt, Phys. Rev. E **99**, 012606 (2019).
[91] J. R. Howse, R. A. L. Jones, A. J. Ryan, T. Gough, R. Vafabakhsh, and R. Golestanian, Phys. Rev. Lett. **99**, 048102 (2007).
[92] J. Dhont, *An Introduction to Dynamics of Colloids*, Studies in Interface Science Vol. 2 (Elsevier Science, Amsterdam, 1996).
[93] T. D. Frank, Phys. Rev. E **71**, 031106 (2005).
[94] T. D. Frank, Phys. Rev. E **72**, 011112 (2005).
[95] J. Hansen and I. McDonald, *Theory of Simple Liquids* (Elsevier Science, Amsterdam, 1990).

[96] F. Smallenburg and H. Löwen, Phys. Rev. E **92**, 032304 (2015).
[97] T. Jamali and A. Naji, Soft Matter **14**, 4820 (2018).
[98] H. Tanaka, J. Phys. Condens. Matter **12**, R207 (2000).
[99] G. A. Vliegenthart and H. N. W. Lekkerkerker, J. Chem. Phys. **112**, 5364 (2000).
[100] S. C. Kapfer and W. Krauth, Phys. Rev. Lett. **114**, 035702 (2015).
[101] S. van Teeffelen, C. N. Likos, and H. Löwen, Phys. Rev. Lett. **100**, 108302 (2008).
[102] U. Zimmermann, F. Smallenburg, and H. Löwen, J. Phys. Condens. Matter **28**, 244019 (2016).
[103] J. U. Klamser, S. C. Kapfer, and W. Krauth, Nat. Commun. **9**, 5045 (2018).
[104] J. Elgeti, R. G. Winkler, and G. Gompper, Rep. Prog. Phys. **78**, 056601 (2015).
[105] M. E. Cates and J. Tailleur, Annu. Rev. Condens. Matter Phys. **6**, 219 (2015).
[106] A. M. Menzel, A. Saha, C. Hoell, and H. Löwen, J. Chem. Phys. **144**, 024115 (2016).
[107] K. Beppu, Z. Izri, J. Gohya, K. Eto, M. Ichikawa, and Y. T. Maeda, Soft Matter **13**, 5038 (2017).
[108] A. Ahlborn and U. Parlitz, Phys. Rev. E **72**, 016206 (2005).
[109] V. Pyragas and K. Pyragas, Phys. Lett. A **382**, 574 (2018).

Chapter 4

Concluding remarks

Colloidal suspensions, comprised of mesoscopic particles suspended in a liquid, are highly sensitive to the application of external fields. Here, the effect of two different kinds of external potentials has been investigated.

First, a colloidal capacitor analogue was considered in Chapter 2 (Publication I). In this case, the colloidal suspension is confined to a narrow slit between two capacitor plates which is only a few colloidal radii in width. For this configuration, the system response to the application of a strong electric alternating voltage was studied. A resonance effect was observed in which the impedance of the system shows a minimum with respect to the driving frequency of the electric voltage. This occurs as a consequence of field-induced ion condensation at the capacitor plates and the resulting coherent motion of the condensed ions upon a variation of the field. The resonance frequency depends on the system width and can thus be tuned by changing the distance between the capacitor plates. The effect may be exploited in the design of micro-scale capacitive devices. Moreover, future studies should consider refinements to the model, including incorporating the effect of remaining counterions [289] as well as polarization [290] and reorientation [291] effects in the background liquid. The hydrodynamic flows caused by the movement of the suspended colloids [292] and the detailed effect of the capacitor plates [293] also require additional attention.

Second, a feedback potential, for which the applied potential depends on the system history, was considered in Chapter 3. For this type of potential, it was shown that attractive potential forms can lead to a reduction in the mean square displacement (MSD) while repulsive potentials give rise to behavior reminiscent of self-propulsion. The presented analytical results for the one-particle case can be used as a valuable reference for experiments. These can be realized, e.g., by the use of holographic optical tweezers [169], which is currently underway through a collaboration with our experimental Soft Matter department.

Furthermore, as a collective effect, self-organization into traveling bands was observed for repulsive potentials in Chapter 3 (Publication II). This is particularly interesting as the considered system included neither attractive interactions that may lead to particle bands [294] nor direction-dependent potentials that prescribe a traveling direction [161, 295]. Instead, the band formation takes place autonomously

via spontaneous separation into high-potential areas that are void of particles and low-potential areas that are crowded with them. The traveling direction results by growth of local oriented regions until a single orientation prevails. The ordering takes place under spontaneous breaking of symmetry, thus suggesting a way that direction-independent interactions can result in directed collective motion. This many-particle case may also be of relevance for autochemotactic particles in biological systems. In these systems, more complex responses to the system state may emerge, leading to effects such as quorum sensing [140]. Future work could therefore focus on the introduction of more complicated coupling algorithms [140, 296] and multiple competing feedback terms [297]. Also, for biological microswimmers the competition between a feedback interaction and self-propulsion may be an interesting next step to investigate. Furthermore, higher densities leading to traveling crystal phases can be discussed. The presented framework of dynamic density functional theory (DDFT) can be used as a starting point for these investigations. In fact, a DDFT has already been formulated for microswimmers including hydrodynamic effects [202, 203, 272] which could be combined with the theory presented here to obtain a corresponding description. Additionally, the discrete, particle-based approach of our simulations complements existing continuum approaches to feedback systems [298, 299].

In conclusion, the responsiveness of colloidal suspensions to external fields can be exploited to adjust the system behavior in a desired way. Furthermore, feedback effects constitute the foundation on which intelligent materials can be constructed. To study such effects, feedback-driven colloids present an ideal model system.

Bibliography

[1] R. Jones. *Soft Condensed Matter*. Oxford Master Series in Physics, (Oxford University Press, Oxford, UK 2002).

[2] M. Doi. *Soft Matter Physics*, (Oxford University Press, Oxford, UK 2013).

[3] I. Hamley. *Introduction to Soft Matter: Synthetic and Biological Self-Assembling Materials*, (John Wiley and Sons, Chichester, UK 2013).

[4] S. R. Nagel. *Experimental soft-matter science*. Rev. Mod. Phys. **89**, 025002 (2017).

[5] J. van der Gucht. *Grand Challenges in Soft Matter Physics*. Front. Phys. **6**, 87 (2018).

[6] P.-G. de Gennes. *Soft Matter (Nobel Lecture)*. Angew. Chem., Int. Ed. **31**, 842 (1992).

[7] M. Doi and S. Edwards. *The Theory of Polymer Dynamics*, (Clarendon Press, Oxford, UK 1988).

[8] R. G. Winkler. *Semiflexible Polymers in Shear Flow*. Phys. Rev. Lett. **97**, 128301 (2006).

[9] P. N. Pusey and W. van Megen. *Phase behaviour of concentrated suspensions of nearly hard colloidal spheres*. Nature **320**, 340 (1986).

[10] F. Parisse and C. Allain. *Drying of Colloidal Suspension Droplets: Experimental Study and Profile Renormalization*. Langmuir **13**, 3598 (1997).

[11] J. Barrat and J. Hansen. *Basic Concepts for Simple and Complex Liquids*, (Cambridge University Press, Cambridge, UK 2003).

[12] D. Chelazzi, R. Giorgi and P. Baglioni. *Microemulsions, Micelles, and Functional Gels: How Colloids and Soft Matter Preserve Works of Art*. Angew. Chem., Int. Ed. **57**, 7296 (2018).

[13] N. A. Peppas and A. R. Khare. *Preparation, structure and diffusional behavior of hydrogels in controlled release*. Adv. Drug Deliv. Rev. **11**, 1 (1993).

[14] I. Y. Galaev and B. Mattiasson. *'Smart' polymers and what they could do in biotechnology and medicine*. Trends Biotechnol. **17**, 335 (1999).

[15] J. A. Burdick and W. L. Murphy. *Moving from static to dynamic complexity in hydrogel design*. Nat. Commun. **3**, 1269 (2012).

[16] W. Richtering and B. R. Saunders. *Gel architectures and their complexity.* Soft Matter **10**, 3695 (2014).

[17] M. Shibayama, X. Li and T. Sakai. *Gels: From Soft Matter to BioMatter.* Ind. Eng. Chem. Res. **57**, 1121 (2018).

[18] J. L. Barrat, W. Gotze and A. Latz. *The liquid-glass transition of the hard-sphere system.* J. Phys. Condens. Matter **1**, 7163 (1989).

[19] K. Binder, J. Horbach, H. Knoth and P. Pfleiderer. *Computer simulation of molten silica and related glass forming fluids: recent progress.* J. Phys. Condens. Matter **19**, 205102 (2007).

[20] J.-L. Barrat, J. Baschnagel and A. Lyulin. *Molecular dynamics simulations of glassy polymers.* Soft Matter **6**, 3430 (2010).

[21] E. Zaccarelli, S. M. Liddle and W. C. K. Poon. *On polydispersity and the hard sphere glass transition.* Soft Matter **11**, 324 (2015).

[22] K. M. Yamada and R. Mayor. *Editorial overview: Cell dynamics in development, tissue remodelling, and cancer.* Curr. Opin. Cell Biol. **42**, iv (2016).

[23] S. K. Schnyder, J. J. Molina, Y. Tanaka and R. Yamamoto. *Collective motion of cells crawling on a substrate: roles of cell shape and contact inhibition.* Sci. Rep. **7**, 5163 (2017).

[24] M. Tarama and R. Yamamoto. *Mechanics of Cell Crawling by Means of Force-free Cyclic Motion.* J. Phys. Soc. Jpn. **87**, 044803 (2018).

[25] A. Goychuk, D. B. Brückner, A. W. Holle, J. P. Spatz, C. P. Broedersz and E. Frey. *Morphology and Motility of Cells on Soft Substrates.* arXiv:1808.00314 (2018).

[26] C. S. Harwood, K. Fosnaugh and M. Dispensa. *Flagellation of Pseudomonas putida and analysis of its motile behavior.* J. Bacteriol. **171**, 4063 (1989).

[27] M. Hintsche, V. Waljor, R. Großmann, M. J. Kühn, K. M. Thormann, F. Peruani and C. Beta. *A polar bundle of flagella can drive bacterial swimming by pushing, pulling, or coiling around the cell body.* Sci. Rep. **7**, 16771 (2017).

[28] B. ten Hagen, S. van Teeffelen and H. Löwen. *Brownian motion of a self-propelled particle.* J. Phys. Condens. Matter **23**, 194119 (2011).

[29] M. E. Cates. *Diffusive transport without detailed balance in motile bacteria: does microbiology need statistical physics?* Rep. Prog. Phys. **75**, 042601 (2012).

[30] S. Sareh, J. Rossiter, A. Conn, K. Drescher and R. E. Goldstein. *Swimming like algae: biomimetic soft artificial cilia.* J. Royal Soc. Interface **10**, 20120666 (2013).

[31] A. M. Menzel. *Tuned, driven, and active soft matter.* Phys. Rep. **554**, 1 (2015).

[32] C. Bechinger, R. Di Leonardo, H. Löwen, C. Reichhardt, G. Volpe and G. Volpe. *Active particles in complex and crowded environments.* Rev. Mod. Phys. **88**, 045006 (2016).

[33] J. Schwarz-Linek, J. Arlt, A. Jepson, A. Dawson, T. Vissers, D. Miroli, T. Pilizota, V. A. Martinez and W. C. Poon. *Escherichia coli as a model active colloid: A practical introduction.* Colloids Surf. B **137**, 2 (2016).

[34] Y. Yang, J. Elgeti and G. Gompper. *Cooperation of sperm in two dimensions: Synchronization, attraction, and aggregation through hydrodynamic interactions.* Phys. Rev. E **78**, 061903 (2008).

[35] M. Kumar and A. M. Ardekani. *Effect of external shear flow on sperm motility.* Soft Matter **15**, 6269 (2019).

[36] C. N. Likos. *Effective interactions in soft condensed matter physics.* Phys. Rep. **348**, 267 (2001).

[37] H. Löwen. *Colloidal soft matter under external control.* J. Phys. Condens. Matter **13**, R415 (2001).

[38] W. M. Winslow. *Induced Fibration of Suspensions.* J. Appl. Phys. **20**, 1137 (1949).

[39] T. C. Halsey. *Electrorheological Fluids.* Science **258**, 761 (1992).

[40] W. Wen, X. Huang and P. Sheng. *Electrorheological fluids: structures and mechanisms.* Soft Matter **4**, 200 (2008).

[41] Y. D. Liu and H. J. Choi. *Electrorheological fluids: smart soft matter and characteristics.* Soft Matter **8**, 11961 (2012).

[42] J. Rabinow. *The magnetic fluid clutch.* Electr. Eng. **67**, 1167 (1948).

[43] J. P. McTague. *Magnetoviscosity of Magnetic Colloids.* J. Chem. Phys. **51**, 133 (1969).

[44] D. J. Klingenberg. *Magnetorheology: Applications and challenges.* AIChE J. **47**, 246 (2001).

[45] J. de Vicente, D. J. Klingenberg and R. Hidalgo-Alvarez. *Magnetorheological fluids: a review.* Soft Matter **7**, 3701 (2011).

[46] A. Milecki and M. Hauke. *Application of magnetorheological fluid in industrial shock absorbers.* Mech. Syst. Signal. Process. **28**, 528 (2012).

[47] M. Zrínyi, L. Barsi and A. Büki. *Ferrogel: A new magneto-controlled elastic medium.* Polym. Gels Networks **5**, 415 (1997).

[48] A. Y. Zubarev. *Effect of chain-like aggregates on ferrogel magnetodeformation.* Soft Matter **9**, 4985 (2013).

[49] P. Cremer, H. Löwen and A. M. Menzel. *Superelastic stress–strain behavior in ferrogels with different types of magneto-elastic coupling.* Phys. Chem. Chem. Phys. **18**, 26670 (2016).

[50] T. Sun, X. Gong, W. Jiang, J. Li, Z. Xu and W. Li. *Study on the damping properties of magnetorheological elastomers based on cis-polybutadiene rubber.* Polym. Test. **27**, 520 (2008).

[51] H. Deng, X. Gong and L. Wang. *Development of an adaptive tuned vibration absorber with magnetorheological elastomer.* Smart Mater. Struct. **15**, N111 (2006).

[52] R. L. Snyder, V. Q. Nguyen and R. V. Ramanujan. *Design parameters for magneto-elastic soft actuators.* Smart Mater. Struct. **19**, 055017 (2010).

[53] Y. Osada and D. De Rossi. *Polymer Sensors and Actuators.* Macromolecular Systems - Materials Approach, (Springer-Verlag, Berlin Heidelberg, DE 2000).

[54] M. Gandhi and B. Thompson. *Smart Materials and Structures*, (Springer Netherlands, Dordrecht, NL 1992).

[55] H. Abramovich. *Intelligent Materials and Structures.* De Gruyter Textbook, (De Gruyter, Berlin, DE 2016).

[56] C. Alvarez-Lorenzo and A. Concheiro (eds.). *Smart Materials for Drug Delivery.* Smart Materials Series, (RSC Publishing, Cambridge, UK 2013).

[57] M. Aguilar and J. Román. *Smart Polymers and their Applications.* Woodhead Publishing in Materials, (Woodhead Publishing, Sawston, UK 2014).

[58] Y.-Q. Liu, J.-N. Ma, Y. Liu, D.-D. Han, H.-B. Jiang, J.-W. Mao, C.-H. Han, Z.-Z. Jiao and Y.-L. Zhang. *Facile fabrication of moisture responsive graphene actuators by moderate flash reduction of graphene oxides films.* Opt. Mater. Express **7**, 2617 (2017).

[59] T. Jia, Y. Wang, Y. Dou, Y. Li, M. Jung de Andrade, R. Wang, S. Fang, J. Li, Z. Yu, R. Qiao, Z. Liu, Y. Cheng, Y. Su, M. Minary-Jolandan, R. H. Baughman, D. Qian and Z. Liu. *Moisture Sensitive Smart Yarns and Textiles from Self-Balanced Silk Fiber Muscles.* Adv. Funct. Mater. **29**, 1808241 (2019).

[60] G. Ju, M. Cheng and F. Shi. *A pH-responsive smart surface for the continuous separation of oil/water/oil ternary mixtures.* NPG Asia Materials **6**, e111 (2014).

[61] R. W. Whatmore. *Pyroelectric devices and materials.* Rep. Prog. Phys. **49**, 1335 (1986).

[62] M. J. Dapino. *Magnetostrictive Materials.* In *Encyclopedia of Smart Materials*, (John Wiley and Sons, New York, US 2002).

[63] P. W. Forsbergh. *Piezoelectricity, Electrostriction and Ferroelectricity.* In *Dielectrics / Dielektrika*, (Springer-Verlag OHG., Berlin · Göttingen · Heidelberg, DE 1956).

[64] I. Ahmed, H. Lin, L. Zou, Z. Li, A. L. Brody, I. M. Qazi, L. Lv, T. R. Pavase, M. U. Khan, S. Khan and L. Sun. *An overview of smart packaging technologies for monitoring safety and quality of meat and meat products.* Packag. Technol. Sci. **31**, 449 (2018).

[65] P. Müller and M. Schmid. *Intelligent Packaging in the Food Sector: A Brief Overview.* Foods **8**, 16 (2019).

[66] X. Qiu and S. Hu. *"Smart" Materials Based on Cellulose: A Review of the Preparations, Properties, and Applications.* Materials **6**, 738 (2013).

[67] R. P. Wool. *Self-healing materials: a review.* Soft Matter **4**, 400 (2008).

[68] E. B. Murphy and F. Wudl. *The world of smart healable materials.* Prog. Polym. Sci. **35**, 223 (2010).

[69] W. Binder. *Self-Healing Polymers: From Principles to Applications*, (Wiley-VCH, Weinheim, DE 2013).

[70] M. Hager, S. van der Zwaag and U. Schubert. *Self-healing Materials.* Adv. Polym. Sci., (Springer International Publishing, Basel, CH 2016).

[71] E. J. Markvicka, M. D. Bartlett, X. Huang and C. Majidi. *An autonomously electrically self-healing liquid metal-elastomer composite for robust soft-matter robotics and electronics.* Nat. Mater. **17**, 618 (2018).

[72] R. Hoogenboom. *Temperature-responsive polymers: properties, synthesis and applications.* In M. R. Aguilar and J. S. Román (eds.), *Smart Polymers and their Applications*, (Woodhead Publishing, Sawston, UK 2014).

[73] D. Canadinc, W. Trehern, J. Ma, I. Karaman, F. Sun and Z. Chaudhry. *Ultra-high temperature multi-component shape memory alloys.* Scr. Mater. **158**, 83 (2019).

[74] A. Deep, U. Chaudhary and V. Gupta. *Quorum sensing and bacterial pathogenicity: From molecules to disease.* J. Lab. Physicians **3**, 4 (2011).

[75] B. A. Doğaner, L. K. Yan and H. Youk. *Autocrine Signaling and Quorum Sensing: Extreme Ends of a Common Spectrum.* Trends Cell Biol. **26**, 262 (2016).

[76] B. Rémy, S. Mion, L. Plener, M. Elias, E. Chabrière and D. Daudé. *Interference in Bacterial Quorum Sensing: A Biopharmaceutical Perspective.* Front. Pharmacol. **9**, 203 (2018).

[77] M. B. Miller and B. L. Bassler. *Quorum Sensing in Bacteria.* Annu. Rev. Microbiol. **55**, 165 (2001).

[78] C. M. Waters and B. L. Bassler. *Quorum Sensing: Cell-to-Cell Communication in Bacteria.* Annu. Rev. Cell Dev. Biol. **21**, 319 (2005).

[79] A. Pai, Y. Tanouchi and L. You. *Optimality and robustness in quorum sensing (QS)-mediated regulation of a costly public good enzyme.* Proc. Natl. Acad. Sci. U.S.A. **109**, 19810 (2012).

[80] M. Abercrombie and J. E. Heaysman. *Observations on the social behaviour of cells in tissue culture: I. Speed of movement of chick heart fibroblasts in relation to their mutual contacts.* Exp. Cell Res. **5**, 111 (1953).

[81] R. Mayor and C. Carmona-Fontaine. *Keeping in touch with contact inhibition of locomotion.* Trends Cell Biol. **20**, 319 (2010).

[82] A. Roycroft and R. Mayor. *Molecular basis of contact inhibition of locomotion.* Cell. Mol. Life Sci. **73**, 1119 (2016).

[83] B. Stramer and R. Mayor. *Mechanisms and in vivo functions of contact inhibition of locomotion.* Nat. Rev. Mol. Cell Biol. **18**, 43 (2016).

[84] S. K. Schnyder, J. J. Molina and R. Yamamoto. *Control of cell colony growth by contact inhibition* arXiv:1810.00546 (2018).

[85] M. G. P. Stoker and H. Rubin. *Density Dependent Inhibition of Cell Growth in Culture.* Nature **215**, 171 (1967).

[86] M. G. P. Stoker. *Role of Diffusion Boundary Layer in Contact Inhibition of Growth.* Nature **246**, 200 (1973).

[87] A. I. McClatchey and A. S. Yap. *Contact inhibition (of proliferation) redux.* Curr. Opin. Cell Biol. **24**, 685 (2012).

[88] A. Sengupta, S. van Teeffelen and H. Löwen. *Dynamics of a microorganism moving by chemotaxis in its own secretion.* Phys. Rev. E **80**, 031122 (2009).

[89] J. E. Phillips and R. H. Gomer. *A secreted protein is an endogenous chemorepellant in Dictyostelium discoideum.* Proc. Natl. Acad. Sci. U.S.A. **109**, 10990 (2012).

[90] C. A. Parent and P. N. Devreotes. *A Cell's Sense of Direction.* Science **284**, 765 (1999).

[91] D. Drubin. *Cell polarity.* Frontiers in molecular biology, (Oxford University Press, Oxford, UK 2000).

[92] O. D. Weiner. *Regulation of cell polarity during eukaryotic chemotaxis: the chemotactic compass.* Curr. Opin. Cell Biol. **14**, 196 (2002).

[93] P. J. M. Van Haastert and P. N. Devreotes. *Chemotaxis: signalling the way forward.* Nat. Rev. Mol. Cell Biol. **5**, 626 (2004).

[94] M. Kollmann, L. Løvdok, K. Bartholomé, J. Timmer and V. Sourjik. *Design principles of a bacterial signalling network.* Nature **438**, 504 (2005).

[95] Y. Artemenko, T. J. Lampert and P. N. Devreotes. *Moving towards a paradigm: common mechanisms of chemotactic signaling in Dictyostelium and mammalian leukocytes.* Cell. Mol. Life Sci. **71**, 3711 (2014).

[96] R. M. Macnab and D. E. J. Koshland. *The gradient-sensing mechanism in bacterial chemotaxis.* Proc. Natl. Acad. Sci. U.S.A. **69**, 2509 (1972).

[97] S. M. Block, J. E. Segall and H. C. Berg. *Impulse responses in bacterial chemotaxis.* Cell **31**, 215 (1982).

[98] D. B. Dusenbery. *Spatial sensing of stimulus gradients can be superior to temporal sensing for free-swimming bacteria.* Biophys. J. **74**, 2272 (1998).

[99] G. H. Wadhams and J. P. Armitage. *Making sense of it all: bacterial chemotaxis.* Nat. Rev. Mol. Cell Biol. **5**, 1024 (2004).

[100] S. Chatterjee, R. A. da Silveira and Y. Kafri. *Chemotaxis when Bacteria Remember: Drift versus Diffusion.* PLOS Comput. Biol. **7**, 1 (2011).

[101] B. A. Camley, J. Zimmermann, H. Levine and W.-J. Rappel. *Emergent Collective Chemotaxis without Single-Cell Gradient Sensing.* Phys. Rev. Lett. **116**, 098101 (2016).

[102] B. A. Camley. *Collective gradient sensing and chemotaxis: modeling and recent developments.* J. Phys. Condens. Matter **30**, 223001 (2018).

[103] B. Cheng, R. de Lemos, P. Inverardi and J. Magee. *Software Engineering for Self-Adaptive Systems*, (Springer-Verlag, Berlin Heidelberg, DE 2009).

[104] D. Miyashiro, K. Shiba, T. Miyashita, S. A. Baba, M. Yoshida and S. Kamimura. *Chemotactic response with a constant delay-time mechanism in Ciona spermatozoa revealed by a high time resolution analysis of flagellar motility.* Biol. Open **4**, 109 (2015).

[105] J. E. Segall, S. M. Block and H. C. Berg. *Temporal comparisons in bacterial chemotaxis.* Proc. Natl. Acad. Sci. U.S.A. **83**, 8987 (1986).

[106] M. T. Keating and J. T. Bonner. *Negative chemotaxis in cellular slime molds.* J. Bacteriol. **130**, 144 (1977).

[107] R. Wedlich-Söldner and T. Betz. *Self-organization: the fundament of cell biology.* Philos. Trans. Royal Soc. B **373**, 20170103 (2018).

[108] T. Saha and M. Galic. *Self-organization across scales: from molecules to organisms.* Philos. Trans. Royal Soc. B **373**, 20170113 (2018).

[109] M. E. Cates and J. Tailleur. *Motility-Induced Phase Separation.* Annu. Rev. Condens. Matter Phys. **6**, 219 (2015).

[110] J. Elgeti, R. G. Winkler and G. Gompper. *Physics of microswimmers—single particle motion and collective behavior: a review.* Rep. Prog. Phys. **78**, 056601 (2015).

[111] W. B. Russel, D. A. Saville and W. R. Schowalter. *Colloidal Dispersions.* Cambridge Monographs on Mechanics, (Cambridge University Press, Cambridge, UK 1989).

[112] J. Dhont. *An Introduction to Dynamics of Colloids.* Studies in Interface Science, (Elsevier Science, Amsterdam, NL 1996).

[113] R. Brown. *XXVII. A brief account of microscopical observations made in the months of June, July and August 1827, on the particles contained in the pollen of plants; and on the general existence of active molecules in organic and inorganic bodies.* Philos. Mag. **4**, 161 (1828).

[114] H. Hamaker. *The London—van der Waals attraction between spherical particles.* Physica **4**, 1058 (1937).

[115] K. Kremer, M. O. Robbins and G. S. Grest. *Phase Diagram of Yukawa Systems: Model for Charge-Stabilized Colloids.* Phys. Rev. Lett. **57**, 2694 (1986).

[116] J.-P. Hansen and H. Löwen. *Effective Interactions Between Electric Double Layers.* Annu. Rev. Phys. Chem. **51**, 209 (2000).

[117] J. Hierrezuelo, A. Sadeghpour, I. Szilagyi, A. Vaccaro and M. Borkovec. *Electrostatic Stabilization of Charged Colloidal Particles with Adsorbed Polyelectrolytes of Opposite Charge.* Langmuir **26**, 15109 (2010).

[118] E. Verwey, J. Overbeek and K. van Nes. *Theory of the Stability of Lyophobic Colloids: The Interaction of Sol Particles Having an Electric Double Layer*, (Elsevier Publishing Company, New York, US 1948).

[119] B. Derjaguin and L. Landau. *Theory of the stability of strongly charged lyophobic sols and of the adhesion of strongly charged particles in solutions of electrolytes.* Acta Physicochim. URSS **14**, 633 (1941).

[120] T. Sato and R. Ruch. *Stabilization of colloidal dispersions by polymer adsorption.* Surfactant science series, (Marcel Dekker Inc, New York, US 1980).

[121] J. C. Crocker and D. G. Grier. *Microscopic measurement of the pair interaction potential of charge-stabilized colloid.* Phys. Rev. Lett. **73**, 352 (1994).

[122] E. Allahyarov, H. Löwen and S. Trigger. *Effective forces between macroions: The cases of asymmetric macroions and added salt.* Phys. Rev. E **57**, 5818 (1998).

[123] H. W. Walker and S. B. Grant. *Influence of surface charge and particle size on the stabilization of colloidal particles by model polyelectrolytes.* Colloids Surf. A. **135**, 123 (1998).

[124] R. Evans and D. H. Napper. *Steric stabilization I.* Kolloid-Zeitschrift und Zeitschrift für Polymere **251**, 409 (1973).

[125] C. P. Royall, M. E. Leunissen and A. van Blaaderen. *A new colloidal model system to study long-range interactions quantitatively in real space.* J. Phys. Condens. Matter **15**, S3581 (2003).

[126] S. K. Sainis, V. Germain, C. O. Mejean and E. R. Dufresne. *Electrostatic Interactions of Colloidal Particles in Nonpolar Solvents: Role of Surface Chemistry and Charge Control Agents.* Langmuir **24**, 1160 (2008).

[127] J. Hansen, P. N. Pusey, P. B. Warren, H. Löwen, E. Allahyarov, J. Dzubiella, C. V. Ferber, A. Jusufi, C. N. Likos and M. Heni. *Interactions and phase transitions of colloidal dispersions in bulk and at interfaces.* Philos. Trans. Royal Soc. A **359**, 909 (2001).

[128] H. Löwen. *Colloidal dispersions in external fields: recent developments.* J. Phys. Condens. Matter **20**, 404201 (2008).

[129] H. Löwen. *Introduction to colloidal dispersions in external fields.* Eur. Phys. J. Spec. Top. **222**, 2727 (2013).

[130] Y. L. Wu, D. Derks, A. van Blaaderen and A. Imhof. *Melting and crystallization of colloidal hard-sphere suspensions under shear.* Proc. Natl. Acad. Sci. U.S.A. **106**, 10564 (2009).

[131] T. Vissers, A. Wysocki, M. Rex, H. Löwen, C. P. Royall, A. Imhof and A. van Blaaderen. *Lane formation in driven mixtures of oppositely charged colloids.* Soft Matter **7**, 2352 (2011).

[132] M. Barrett, A. Deschner, J. P. Embs and M. C. Rheinstädter. *Chain formation in a magnetic fluid under the influence of strong external magnetic fields studied by small angle neutron scattering.* Soft Matter **7**, 6678 (2011).

[133] F. Evers, R. D. L. Hanes, C. Zunke, R. F. Capellmann, J. Bewerunge, C. Dalle-Ferrier, M. C. Jenkins, I. Ladadwa, A. Heuer, R. Castañeda-Priego and S. U. Egelhaaf. *Colloids in light fields: Particle dynamics in random and periodic energy landscapes.* Eur. Phys. J. Spec. Top. **222**, 2995 (2013).

[134] N. P. Barry and M. S. Bretscher. *Dictyostelium amoebae and neutrophils can swim.* Proc. Natl. Acad. Sci. U.S.A. **107**, 11376 (2010).

[135] K. Shiba, D. Shibata and K. Inaba. *Autonomous changes in the swimming direction of sperm in the gastropod Strombus luhuanus.* J. Exp. Biol. **217**, 986 (2014).

[136] D. L. Ringo. *Flagellar motion and fine structure of the flagellar apparatus in Chlamydomonas.* J. Cell Biol. **33**, 543 (1967).

[137] J. Hyams and G. Borisy. *Flagellar coordination in Chlamydomonas reinhardtii: isolation and reactivation of the flagellar apparatus.* Science **189**, 891 (1975).

[138] N. A. Whitehead, A. M. Barnard, H. Slater, N. J. Simpson and G. P. Salmond. *Quorum-sensing in Gram-negative bacteria.* FEMS Microbiol. Rev. **25**, 365 (2001).

[139] K. Papenfort and B. L. Bassler. *Quorum sensing signal-response systems in Gram-negative bacteria.* Nat. Rev. Microbiol. **14**, 576 (2016).

[140] T. Bäuerle, A. Fischer, T. Speck and C. Bechinger. *Self-organization of active particles by quorum sensing rules.* Nat. Commun. **9**, 3232 (2018).

[141] J. Zhao, D. Vollmer, H.-J. Butt and G. K. Auernhammer. *Localized instabilities of colloidal motion in ac electric field gradients.* J. Phys. Condens. Matter **20**, 404212 (2008).

[142] M. Ikeda, H. Wada and H. Hayakawa. *Instabilities and turbulence-like dynamics in an oppositely driven binary particle mixture.* EPL **99**, 68005 (2012).

[143] A. Bricard, J.-B. Caussin, D. Das, C. Savoie, V. Chikkadi, K. Shitara, O. Chepizhko, F. Peruani, D. Saintillan and D. Bartolo. *Emergent vortices in populations of colloidal rollers.* Nat. Commun. **6**, 7470 (2015).

[144] A. Erbe, M. Zientara, L. Baraban, C. Kreidler and P. Leiderer. *Various driving mechanisms for generating motion of colloidal particles.* J. Phys. Condens. Matter **20**, 404215 (2008).

[145] H. Löwen, T. Horn, T. Neuhaus and B. ten Hagen. *Two-dimensional colloidal mixtures in magnetic and gravitational fields.* Eur. Phys. J. Spec. Top. **222**, 2961 (2013).

[146] P. Dillmann, G. Maret and P. Keim. *Two-dimensional colloidal systems in time-dependent magnetic fields.* Eur. Phys. J. Spec. Top. **222**, 2941 (2013).

[147] M. C. Jenkins and S. U. Egelhaaf. *Colloidal suspensions in modulated light fields.* J. Phys. Condens. Matter **20**, 404220 (2008).

[148] G. Volpe, G. Volpe and S. Gigan. *Brownian Motion in a Speckle Light Field: Tunable Anomalous Diffusion and Selective Optical Manipulation.* Sci. Rep. **4**, 3936 (2014). Article.

[149] T. Sentjabrskaja, M. Laurati and S. U. Egelhaaf. *One- and two-component colloidal glasses under transient shear.* Eur. Phys. J. Spec. Top. **226**, 3023 (2017).

[150] S. Grandner and S. H. L. Klapp. *Freezing of charged colloids in slit pores.* J. Chem. Phys. **129**, 244703 (2008).

[151] A. Reinmüller, E. C. Oğuz, R. Messina, H. Löwen, H. J. Schöpe and T. Palberg. *Confined colloidal crystals in and out of equilibrium.* Eur. Phys. J. Spec. Top. **222**, 3011 (2013).

[152] D. Babič, C. Schmitt and C. Bechinger. *Colloids as model systems for problems in statistical physics.* Chaos **15**, 026114 (2005).

[153] C. Bechinger and E. Frey. *Phase behaviour of colloids in confining geometry.* J. Phys. Condens. Matter **13**, R321 (2001).

[154] A. D. Dinsmore, J. C. Crocker and A. G. Yodh. *Self-assembly of colloidal crystals.* Curr. Opin. Colloid Interface Sci. **3**, 5 (1998).

[155] M. E. Leunissen, C. G. Christova, A.-P. Hynninen, C. P. Royall, A. I. Campbell, A. Imhof, M. Dijkstra, R. van Roij and A. van Blaaderen. *Ionic colloidal crystals of oppositely charged particles.* Nature **437**, 235 (2005).

[156] A. van Blaaderen, M. Dijkstra, R. van Roij, A. Imhof, M. Kamp, B. W. Kwaadgras, T. Vissers and B. Liu. *Manipulating the self assembly of colloids in electric fields.* Eur. Phys. J. Spec. Top. **222**, 2895 (2013).

[157] J. Dobnikar, A. Snezhko and A. Yethiraj. *Emergent colloidal dynamics in electromagnetic fields.* Soft Matter **9**, 3693 (2013).

[158] C. Reichhardt and C. J. O. Reichhardt. *Velocity force curves, laning, and jamming for oppositely driven disk systems.* Soft Matter **14**, 490 (2018).

[159] A. Wysocki and H. Löwen. *Oscillatory driven colloidal binary mixtures: Axial segregation versus laning.* Phys. Rev. E **79**, 041408 (2009).

[160] E. V. Yakovlev, K. A. Komarov, K. I. Zaytsev, N. P. Kryuchkov, K. I. Koshelev, A. K. Zotov, D. A. Shelestov, V. L. Tolstoguzov, V. N. Kurlov, A. V. Ivlev and S. O. Yurchenko. *Tunable two-dimensional assembly of colloidal particles in rotating electric fields.* Sci. Rep. **7**, 13727 (2017).

[161] J. Dzubiella, G. P. Hoffmann and H. Löwen. *Lane formation in colloidal mixtures driven by an external field.* Phys. Rev. E **65**, 021402 (2002).

[162] C. Reichhardt, J. Thibault, S. Papanikolaou and C. J. O. Reichhardt. *Laning and clustering transitions in driven binary active matter systems.* Phys. Rev. E **98**, 022603 (2018).

[163] J. Dzubiella and H. Löwen. *Pattern formation in driven colloidal mixtures: tilted driving forces and re-entrant crystal freezing.* J. Phys. Condens. Matter **14**, 9383 (2002).

[164] A. Kaiser, A. Snezhko and I. S. Aranson. *Flocking ferromagnetic colloids.* Sci. Adv. **3** (2017).

[165] F. Smallenburg, H. R. Vutukuri, A. Imhof, A. van Blaaderen and M. Dijkstra. *Self-assembly of colloidal particles into strings in a homogeneous external electric or magnetic field.* J. Phys. Condens. Matter **24**, 464113 (2012).

[166] V. A. Froltsov, C. N. Likos and H. Löwen. *Colloids in inhomogeneous external magnetic fields: particle tweezing, trapping and void formation.* J. Phys. Condens. Matter **16**, S4103 (2004).

[167] D. G. Grier. *A revolution in optical manipulation.* Nature **424**, 810 (2003).

[168] R. W. Bowman and M. J. Padgett. *Optical trapping and binding.* Rep. Prog. Phys. **76**, 026401 (2013).

[169] P. Jones, O. Marag and G. Volpe. *Optical Tweezers: Principles and Applications*, (Cambridge University Press, Cambridge, UK 2015).

[170] R. D. L. Hanes and S. U. Egelhaaf. *Dynamics of individual colloidal particles in one-dimensional random potentials: a simulation study.* J. Phys. Condens. Matter **24**, 464116 (2012).

[171] R. D. L. Hanes, C. Dalle-Ferrier, M. Schmiedeberg, M. C. Jenkins and S. U. Egelhaaf. *Colloids in one dimensional random energy landscapes.* Soft Matter **8**, 2714 (2012).

[172] R. D. L. Hanes, M. Schmiedeberg and S. U. Egelhaaf. *Brownian particles on rough substrates: Relation between intermediate subdiffusion and asymptotic long-time diffusion.* Phys. Rev. E **88**, 062133 (2013).

[173] J. Bewerunge, A. Sengupta, R. F. Capellmann, F. Platten, S. Sengupta and S. U. Egelhaaf. *Colloids exposed to random potential energy landscapes: From particle number density to particle-potential and particle-particle interactions.* J. Chem. Phys. **145**, 044905 (2016).

[174] C. Bechinger, M. Brunner and P. Leiderer. *Phase Behavior of Two-Dimensional Colloidal Systems in the Presence of Periodic Light Fields.* Phys. Rev. Lett. **86**, 930 (2001).

[175] C. Dalle-Ferrier, M. Krüger, R. D. L. Hanes, S. Walta, M. C. Jenkins and S. U. Egelhaaf. *Dynamics of dilute colloidal suspensions in modulated potentials.* Soft Matter **7**, 2064 (2011).

[176] V. Blickle, T. Speck, L. Helden, U. Seifert and C. Bechinger. *Thermodynamics of a Colloidal Particle in a Time-Dependent Nonharmonic Potential.* Phys. Rev. Lett. **96**, 070603 (2006).

[177] S. Bianchi, R. Pruner, G. Vizsnyiczai, C. Maggi and R. Di Leonardo. *Active dynamics of colloidal particles in time-varying laser speckle patterns.* Sci. Rep. **6**, 27681 (2016).

[178] E. M. Purcell. *Life at low Reynolds number.* Am. J. Phys. **45**, 3 (1977).

[179] E. M. Purcell. *The efficiency of propulsion by a rotating flagellum.* Proc. Natl. Acad. Sci. U.S.A. **94**, 11307 (1997).

[180] C. Brennen and H. Winet. *Fluid Mechanics of Propulsion by Cilia and Flagella.* Annu. Rev. Fluid Mech. **9**, 339 (1977).

[181] M. Polin, I. Tuval, K. Drescher, J. P. Gollub and R. E. Goldstein. *Chlamydomonas Swims with Two "Gears" in a Eukaryotic Version of Run-and-Tumble Locomotion.* Science **325**, 487 (2009).

[182] P. Bayly, B. Lewis, E. Ranz, R. Okamoto, R. Pless and S. Dutcher. *Propulsive Forces on the Flagellum during Locomotion of Chlamydomonas reinhardtii.* Biophys. J. **100**, 2716 (2011).

[183] R. Dreyfus, J. Baudry, M. L. Roper, M. Fermigier, H. A. Stone and J. Bibette. *Microscopic artificial swimmers.* Nature **437**, 862 (2005).

[184] I. Buttinoni, J. Bialké, F. Kümmel, H. Löwen, C. Bechinger and T. Speck. *Dynamical Clustering and Phase Separation in Suspensions of Self-Propelled Colloidal Particles.* Phys. Rev. Lett. **110**, 238301 (2013).

[185] S. Herminghaus, C. C. Maass, C. Krüger, S. Thutupalli, L. Goehring and C. Bahr. *Interfacial mechanisms in active emulsions.* Soft Matter **10**, 7008 (2014).

[186] A. M. Maier, C. Weig, P. Oswald, E. Frey, P. Fischer and T. Liedl. *Magnetic Propulsion of Microswimmers with DNA-Based Flagellar Bundles.* Nano Lett. **16**, 906 (2016).

[187] M. Kaynak, A. Ozcelik, A. Nourhani, P. E. Lammert, V. H. Crespi and T. J. Huang. *Acoustic actuation of bioinspired microswimmers.* Lab Chip **17**, 395 (2017).

[188] A. Kaiser, H. H. Wensink and H. Löwen. *How to Capture Active Particles.* Phys. Rev. Lett. **108**, 268307 (2012).

[189] J. Palacci, S. Sacanna, A. P. Steinberg, D. J. Pine and P. M. Chaikin. *Living Crystals of Light-Activated Colloidal Surfers.* Science **339**, 936 (2013).

[190] X. Zheng, B. ten Hagen, A. Kaiser, M. Wu, H. Cui, Z. Silber-Li and H. Löwen. *Non-Gaussian statistics for the motion of self-propelled Janus particles: Experiment versus theory.* Phys. Rev. E **88**, 032304 (2013).

[191] A. Brown and W. Poon. *Ionic effects in self-propelled Pt-coated Janus swimmers.* Soft Matter **10**, 4016 (2014).

[192] K. Kroy, D. Chakraborty and F. Cichos. *Hot microswimmers.* Eur. Phys. J. Spec. Top. **225**, 2207 (2016).

[193] G. Volpe, I. Buttinoni, D. Vogt, H.-J. Kümmerer and C. Bechinger. *Microswimmers in patterned environments.* Soft Matter **7**, 8810 (2011).

[194] M. N. Popescu, W. E. Uspal and S. Dietrich. *Self-diffusiophoresis of chemically active colloids.* Eur. Phys. J. Spec. Top. **225**, 2189 (2016).

[195] C. Jin, C. Krüger and C. C. Maass. *Chemotaxis and autochemotaxis of self-propelling droplet swimmers.* Proc. Natl. Acad. Sci. U.S.A **114**, 5089 (2017).

[196] C. Jin, B. V. Hokmabad, K. A. Baldwin and C. C. Maass. *Chemotactic droplet swimmers in complex geometries.* J. Phys. Condens. Matter **30**, 054003 (2018).

[197] S. Babel, B. ten Hagen and H. Löwen. *Swimming path statistics of an active Brownian particle with time-dependent self-propulsion.* J. Stat. Mech.: Theory Exp. **2014**, P02011 (2014).

[198] B. ten Hagen, R. Wittkowski, D. Takagi, F. Kümmel, C. Bechinger and H. Löwen. *Can the self-propulsion of anisotropic microswimmers be described by using forces and torques?* J. Phys. Condens. Matter **27**, 194110 (2015).

[199] R. Aditi Simha and S. Ramaswamy. *Hydrodynamic Fluctuations and Instabilities in Ordered Suspensions of Self-Propelled Particles.* Phys. Rev. Lett. **89**, 058101 (2002).

[200] Y. Hatwalne, S. Ramaswamy, M. Rao and R. A. Simha. *Rheology of Active-Particle Suspensions.* Phys. Rev. Lett. **92**, 118101 (2004).

[201] A. Baskaran and M. C. Marchetti. *Statistical mechanics and hydrodynamics of bacterial suspensions.* Proc. Natl. Acad. Sci. U.S.A. **106**, 15567 (2009).

[202] A. M. Menzel, A. Saha, C. Hoell and H. Löwen. *Dynamical density functional theory for microswimmers.* J. Chem. Phys. **144**, 024115 (2016).

[203] C. Hoell, H. Löwen and A. M. Menzel. *Dynamical density functional theory for circle swimmers.* New J. Phys. **19**, 125004 (2017).

[204] T. Ishikawa. *Suspension biomechanics of swimming microbes.* J. Royal Soc. Interface **6**, 815 (2009).

[205] E. Lauga and T. R. Powers. *The hydrodynamics of swimming microorganisms.* Rep. Prog. Phys. **72**, 096601 (2009).

[206] K. Drescher, J. Dunkel, L. H. Cisneros, S. Ganguly and R. E. Goldstein. *Fluid dynamics and noise in bacterial cell–cell and cell–surface scattering.* Proc. Natl. Acad. Sci. U.S.A. **108**, 10940 (2011).

[207] M. N. Popescu, S. Dietrich, M. Tasinkevych and J. Ralston. *Phoretic motion of spheroidal particles due to self-generated solute gradients.* Eur. Phys. J. E **31**, 351 (2010).

[208] R. Palaparthi, D. T. Papageorgiou and C. Maldarelli. *Theory and experiments on the stagnant cap regime in the motion of spherical surfactant-laden bubbles.* J. Fluid Mech. **559**, 1 (2006).

[209] I. O. Götze and G. Gompper. *Mesoscale simulations of hydrodynamic squirmer interactions.* Phys. Rev. E **82**, 041921 (2010).

[210] L. Stricker. *Numerical simulation of artificial microswimmers driven by Marangoni flow.* J. Comput. Phys. **347**, 467 (2017).

[211] L. Tsimring, H. Levine, I. Aranson, E. Ben-Jacob, I. Cohen, O. Shochet and W. N. Reynolds. *Aggregation Patterns in Stressed Bacteria.* Phys. Rev. Lett. **75**, 1859 (1995).

[212] D. Woodward, R. Tyson, M. Myerscough, J. Murray, E. Budrene and H. Berg. *Spatio-temporal patterns generated by Salmonella typhimurium.* Biophys. J. **68**, 2181 (1995).

[213] R. Tyson, S. R. Lubkin and J. D. Murray. *A minimal mechanism for bacterial pattern formation.* Proc. Royal Soc. B **266**, 299 (1999).

[214] M. P. Brenner, L. S. Levitov and E. O. Budrene. *Physical Mechanisms for Chemotactic Pattern Formation by Bacteria.* Biophys. J. **74**, 1677 (1998).

[215] T. Curk, D. Marenduzzo and J. Dobnikar. *Chemotactic Sensing towards Ambient and Secreted Attractant Drives Collective Behaviour of E. coli.* PLOS ONE **8**, 1 (2013).

[216] B. Liebchen, D. Marenduzzo, I. Pagonabarraga and M. E. Cates. *Clustering and Pattern Formation in Chemorepulsive Active Colloids.* Phys. Rev. Lett. **115**, 258301 (2015).

[217] J. Agudo-Canalejo and R. Golestanian. *Active Phase Separation in Mixtures of Chemically Interacting Particles.* Phys. Rev. Lett. **123**, 018101 (2019).

[218] A. Bricard, J.-B. Caussin, N. Desreumaux, O. Dauchot and D. Bartolo. *Emergence of macroscopic directed motion in populations of motile colloids.* Nature **503**, 95 (2013).

[219] B. Liebchen, D. Marenduzzo and M. E. Cates. *Phoretic Interactions Generically Induce Dynamic Clusters and Wave Patterns in Active Colloids.* Phys. Rev. Lett. **118**, 268001 (2017).

[220] B. ten Hagen, F. Kümmel, R. Wittkowski, D. Takagi, H. Löwen and C. Bechinger. *Gravitaxis of asymmetric self-propelled colloidal particles.* Nat. Commun. **5**, 4829 (2014).

[221] A. F. Demirörs, M. T. Akan, E. Poloni and A. R. Studart. *Active cargo transport with Janus colloidal shuttles using electric and magnetic fields.* Soft Matter **14**, 4741 (2018).

[222] R. R. Bennett and R. Golestanian. *A steering mechanism for phototaxis in Chlamydomonas.* J. Royal Soc. Interface **12**, 20141164 (2015).

[223] S. Saha, R. Golestanian and S. Ramaswamy. *Clusters, asters, and collective oscillations in chemotactic colloids.* Phys. Rev. E **89**, 062316 (2014).

[224] Y. Dou and K. J. M. Bishop. *Autonomous navigation of shape-shifting microswimmers* arXiv:1908.05808 (2019).

[225] B. Liebchen and H. Löwen. *Synthetic Chemotaxis and Collective Behavior in Active Matter.* Acc. Chem. Res. **51**, 2982 (2018).

[226] H. Stark. *Artificial Chemotaxis of Self-Phoretic Active Colloids: Collective Behavior.* Acc. Chem. Res. **51**, 2681 (2018).

[227] E. Lushi, R. E. Goldstein and M. J. Shelley. *Nonlinear concentration patterns and bands in autochemotactic suspensions.* Phys. Rev. E **98**, 052411 (2018).

[228] F. D. C. Farrell, M. C. Marchetti, D. Marenduzzo and J. Tailleur. *Pattern Formation in Self-Propelled Particles with Density-Dependent Motility.* Phys. Rev. Lett. **108**, 248101 (2012).

[229] M. Rein, N. Heinß, F. Schmid and T. Speck. *Collective Behavior of Quorum-Sensing Run-and-Tumble Particles under Confinement.* Phys. Rev. Lett. **116**, 058102 (2016).

[230] R. Rijal, K. M. Consalvo, C. K. Lindsey and R. H. Gomer. *An endogenous chemorepellent directs cell movement by inhibiting pseudopods at one side of cells.* Mol. Biol. Cell **30**, 242 (2019).

[231] F. A. Lavergne, H. Wendehenne, T. Bäuerle and C. Bechinger. *Group formation and cohesion of active particles with visual perception–dependent motility.* Science **364**, 70 (2019).

[232] K. Anguige, J. King, J. Ward and P. Williams. *Mathematical modelling of therapies targeted at bacterial quorum sensing.* Math. Biosci. **192**, 39 (2004).

[233] C. K. Chun, E. A. Ozer, M. J. Welsh, J. Zabner and E. P. Greenberg. *Inactivation of a Pseudomonas aeruginosa quorum-sensing signal by human airway epithelia.* Proc. Natl. Acad. Sci. U.S.A. **101**, 3587 (2004).

[234] K. Vadakkan, A. A. Choudhury, R. Gunasekaran, J. Hemapriya and S. Vijayanand. *Quorum sensing intervened bacterial signaling: Pursuit of its cognizance and repression.* J. Genet. Eng. Biotechnol. **16**, 239 (2018).

[235] M. Abercrombie. *Contact inhibition and malignancy.* Nature **281**, 259 (1979).

[236] F. J. Cao, L. Dinis and J. M. R. Parrondo. *Feedback Control in a Collective Flashing Ratchet.* Phys. Rev. Lett. **93**, 040603 (2004).

[237] A. P. Bregulla, H. Yang and F. Cichos. *Stochastic Localization of Microswimmers by Photon Nudging.* ACS Nano **8**, 6542 (2014).

[238] A. E. Cohen and W. E. Moerner. *Method for trapping and manipulating nanoscale objects in solution.* Appl. Phys. Lett. **86**, 093109 (2005).

[239] Y. Jun and J. Bechhoefer. *Virtual potentials for feedback traps.* Phys. Rev. E **86**, 061106 (2012).

[240] F. Schwaiger, W. Zimmermann and W. Köhler. *Transient cage formation around hot gold colloids dispersed in polymer solutions.* J. Chem. Phys. **135**, 224905 (2011).

[241] M. Mijalkov, A. McDaniel, J. Wehr and G. Volpe. *Engineering Sensorial Delay to Control Phototaxis and Emergent Collective Behaviors.* Phys. Rev. X **6**, 011008 (2016).

[242] M. Leyman, F. Ogemark, J. Wehr and G. Volpe. *Tuning phototactic robots with sensorial delays.* Phys. Rev. E **98**, 052606 (2018).

[243] P. Popli, S. Ganguly and S. Sengupta. *Translationally invariant colloidal crystal templates.* Soft Matter **14**, 104 (2018).

[244] V. Blickle and C. Bechinger. *Realization of a micrometre-sized stochastic heat engine.* Nat. Phys. **8**, 143 (2011).

[245] R. D. L. Hanes, M. C. Jenkins and S. U. Egelhaaf. *Combined holographic-mechanical optical tweezers: Construction, optimization, and calibration.* Rev. Sci. Instrum. **80**, 083703 (2009).

[246] J. Bewerunge and S. U. Egelhaaf. *Experimental creation and characterization of random potential-energy landscapes exploiting speckle patterns.* Phys. Rev. A **93**, 013806 (2016).

[247] K. Nishizawa, M. Bremerich, H. Ayade, C. F. Schmidt, T. Ariga and D. Mizuno. *Feedback-tracking microrheology in living cells.* Sci. Adv. **3** (2017).

[248] A. E. Cohen. *Control of Nanoparticles with Arbitrary Two-Dimensional Force Fields.* Phys. Rev. Lett. **94**, 118102 (2005).

[249] K. Lichtner and S. H. L. Klapp. *Feedback-controlled transport in an interacting colloidal system.* EPL **92**, 40007 (2010).

[250] S. A. M. Loos, R. Gernert and S. H. L. Klapp. *Delay-induced transport in a rocking ratchet under feedback control.* Phys. Rev. E **89**, 052136 (2014).

[251] S. M. J. Khadem and S. H. L. Klapp. *Delayed feedback control of active particles: a controlled journey towards the destination.* Phys. Chem. Chem. Phys. **21**, 13776 (2019).

[252] K. Pyragas. *Continuous control of chaos by self-controlling feedback.* Phys. Lett. A **170**, 421 (1992).

[253] P. Hövel and E. Schöll. *Control of unstable steady states by time-delayed feedback methods.* Phys. Rev. E **72**, 046203 (2005).

[254] S. Trimper and K. Zabrocki. *Memory driven pattern formation.* Phys. Lett. A **331**, 423 (2004).

[255] U. Khadka, V. Holubec, H. Yang and F. Cichos. *Active particles bound by information flows.* Nat. Commun. **9**, 3864 (2018).

[256] E. Forgoston and I. B. Schwartz. *Delay-induced instabilities in self-propelling swarms.* Phys. Rev. E **77**, 035203 (2008).

[257] B. A. Rubik and D. E. Koshland. *Potentiation, desensitization, and inversion of response in bacterial sensing of chemical stimuli.* Proc. Natl. Acad. Sci. U.S.A. **75**, 2820 (1978).

[258] N. Van Kampen. *Stochastic Processes in Physics and Chemistry.* North-Holland Personal Library, (Elsevier Science, Amsterdam, NL 1992).

[259] F. Atay. *Complex Time-Delay Systems: Theory and Applications.* Understanding Complex Systems, (Springer-Verlag, Berlin Heidelberg, DE 2010).

[260] L. Giuggioli, T. J. McKetterick, V. M. Kenkre and M. Chase. *Fokker-Planck description for a linear delayed Langevin equation with additive Gaussian noise.* J. Phys. A **49**, 384002 (2016).

[261] S. A. M. Loos and S. H. L. Klapp. *Force-linearization closure for non-Markovian Langevin systems with time delay.* Phys. Rev. E **96**, 012106 (2017).

[262] S. A. M. Loos and S. H. L. Klapp. *Fokker–Planck Equations for Time-Delayed Systems via Markovian Embedding.* J. Stat. Phys. (2019, in print).

[263] T. D. Frank. *A Markov Approach to Nonlinear Multivariate Delay Systems with Noise.* Phys. Scr. **68**, 333 (2003).

[264] S. Guillouzic, I. L'Heureux and A. Longtin. *Small delay approximation of stochastic delay differential equations.* Phys. Rev. E **59**, 3970 (1999).

[265] T. D. Frank. *Delay Fokker-Planck equations, perturbation theory, and data analysis for nonlinear stochastic systems with time delays.* Phys. Rev. E **71**, 031106 (2005).

[266] U. M. B. Marconi and P. Tarazona. *Dynamic density functional theory of fluids.* J. Chem. Phys. **110**, 8032 (1999).

[267] U. M. B. Marconi and P. Tarazona. *Dynamic density functional theory of fluids.* J. Phys. Condens. Matter **12**, A413 (2000).

[268] A. J. Archer and R. Evans. *Dynamical density functional theory and its application to spinodal decomposition.* J. Chem. Phys. **121**, 4246 (2004).

[269] P. Español and H. Löwen. *Derivation of dynamical density functional theory using the projection operator technique.* J. Chem. Phys. **131**, 244101 (2009).

[270] M. Rex and H. Löwen. *Dynamical density functional theory for colloidal dispersions including hydrodynamic interactions.* Eur. Phys. J. E **28**, 139 (2009).

[271] H. Hansen-Goos and R. Roth. *Density functional theory for hard-sphere mixtures: the White Bear version mark II.* J. Phys. Condens. Matter **18**, 8413 (2006).

[272] C. Hoell, H. Löwen and A. M. Menzel. *Multi-species dynamical density functional theory for microswimmers: Derivation, orientational ordering, trapping potentials, and shear cells.* J. Chem. Phys. **151**, 064902 (2019).

[273] M. Rex, H. H. Wensink and H. Löwen. *Dynamical density functional theory for anisotropic colloidal particles.* Phys. Rev. E **76**, 021403 (2007).

[274] R. Wittkowski and H. Löwen. *Dynamical density functional theory for colloidal particles with arbitrary shape.* Mol. Phys. **109**, 2935 (2011).

[275] J. Hansen and I. McDonald. *Theory of Simple Liquids: with Applications to Soft Matter*, (Academic Press, Cambridge, US 2013).

[276] H. Löwen. *Density Functional Theory for Inhomogeneous Fluids: Statics, Dynamics, and Applications II.* In *3rd Warsaw School of Statistical Physics*, (Poland 2009).

[277] J. K. Percus. *Equilibrium state of a classical fluid of hard rods in an external field.* J. Stat. Phys. **15**, 505 (1976).

[278] J. K. Percus. *One-dimensional classical fluid with nearest-neighbor interaction in arbitrary external field.* J. Stat. Phys. **28**, 67 (1982).

[279] Y. Rosenfeld. *Free-energy model for the inhomogeneous hard-sphere fluid mixture and density-functional theory of freezing.* Phys. Rev. Lett. **63**, 980 (1989).

[280] R. Roth, R. Evans, A. Lang and G. Kahl. *Fundamental measure theory for hard-sphere mixtures revisited: the White Bear version.* J. Phys. Condens. Matter **14**, 12063 (2002).

[281] R. Roth. *Fundamental measure theory for hard-sphere mixtures: a review.* J. Phys. Condens. Matter **22**, 063102 (2010).

[282] A. J. Archer, B. Chacko and R. Evans. *The standard mean-field treatment of inter-particle attraction in classical DFT is better than one might expect.* J. Chem. Phys. **147**, 034501 (2017).

[283] D. Gillespie, W. Nonner and R. S. Eisenberg. *Coupling Poisson-Nernst-Planck and density functional theory to calculate ion flux.* J. Phys. Condens. Matter **14**, 12129 (2002).

[284] U. Küchler and B. Mensch. *Langevins stochastic differential equation extended by a time-delayed term.* Stoch. Stoch. Rep. **40**, 23 (1992).

[285] T. D. Frank and P. J. Beek. *Stationary solutions of linear stochastic delay differential equations: Applications to biological systems.* Phys. Rev. E **64**, 021917 (2001).

[286] T. J. McKetterick and L. Giuggioli. *Exact dynamics of stochastic linear delayed systems: Application to spatiotemporal coordination of comoving agents.* Phys. Rev. E **90**, 042135 (2014).

[287] H. R. Bailey and M. Z. Williams. *Some results on the differential-difference equation* $\dot{x}(t) = \sum_{i=0}^{N} A_i x(t - T_i)$. J. Math. Anal. Appl. **15**, 569 (1966).

[288] M. P. N. Juniper, R. Besseling, D. G. A. L. Aarts and R. P. A. Dullens. *Acousto-optically generated potential energy landscapes: Potential mapping using colloids under flow.* Opt. Express **20**, 28707 (2012).

[289] A. Oleksy and J.-P. Hansen. *Microscopic density functional theory of wetting and drying of a solid substrate by an explicit solvent model of ionic solutions.* Mol. Phys. **107**, 2609 (2009).

[290] G. Jeanmairet, N. Levy, M. Levesque and D. Borgis. *Molecular density functional theory of water including density–polarization coupling.* J. Phys. Condens. Matter **28**, 244005 (2016).

[291] E. Gongadze and A. Iglič. *Asymmetric size of ions and orientational ordering of water dipoles in electric double layer model - an analytical mean-field approach.* Electrochim. Acta **178**, 541 (2015).

[292] A. Wysocki and H. Löwen. *Effects of hydrodynamic interactions in binary colloidal mixtures driven oppositely by oscillatory external fields.* J. Phys. Condens. Matter **23**, 284117 (2011).

[293] J. Catalano and P. M. Biesheuvel. *AC-driven electro-osmotic flow in charged nanopores.* EPL **123**, 58006 (2018).

[294] C. J. Olson Reichhardt, C. Reichhardt and A. R. Bishop. *Structural transitions, melting, and intermediate phases for stripe- and clump-forming systems.* Phys. Rev. E **82**, 041502 (2010).

[295] C. Reichhardt and C. J. O. Reichhardt. *Velocity force curves, laning, and jamming for oppositely driven disk systems.* Soft Matter **14**, 490 (2018).

[296] M. Ciszak, C. Mayol, C. R. Mirasso and R. Toral. *Anticipated synchronization in coupled complex Ginzburg-Landau systems.* Phys. Rev. E **92**, 032911 (2015).

[297] A. Ahlborn and U. Parlitz. *Controlling dynamical systems using multiple delay feedback control.* Phys. Rev. E **72**, 016206 (2005).

[298] D. Puzyrev, S. Yanchuk, A. Vladimirov and S. Gurevich. *Stability of Plane Wave Solutions in Complex Ginzburg–Landau Equation with Delayed Feedback.* SIAM J. Appl. Dyn. Syst. **13**, 986 (2014).

[299] F. Tabbert, C. Schelte, M. Tlidi and S. V. Gurevich. *Delay-induced depinning of localized structures in a spatially inhomogeneous Swift-Hohenberg model.* Phys. Rev. E **95**, 032213 (2017).